Vangl2-Dependent Plasma Membrane Protrusion Behaviors Require an Intact Fibronectin Extracellular Matrix

By
Anna Mooney Love

A Dissertation Submitted in
Partial Fulfillment of the Requirements
for the Degree of Doctor of Molecular Biosciences

August 2018

Dr. Jason R. Jessen, Principal Investigator
Dr. David Nelson, Committee Chair
Dr. Matthew Elrod Erickson, Committee Member
Dr. Brian Robertson, Committee Member
Dr. Christopher Herlihy, Committee Member

Dedicated to my father William Coleman Mooney who arrived at his own finish line before I was able to arrive at mine.

Thanks to my husband Joseph Love for taking care of our daughter Willa Love during this process, and thanks to Willa Love for taking care of me.

Thanks to my mother Gail Mooney and grandmother Sissy Story for providing unbridled support.

Thanks to my brothers Bill Mooney, Jr. and Allen Mooney for getting on my nerves.

Thanks to my grandmother Jane Hanafee Mooney for making me strong.

Thanks to McCorry Street and the Barnett Family for raising me.

Additional thanks to those who helped shape the woman I have become, including: Louise and Winston Davison, Liz Headrick, The DeGeorge Family, and all my pals.

Acknowledgements

I acknowledge the support and mentorship provided by my principal investigator, Jason R. Jessen. I acknowledge the graduate research assistantship I received during my tenure in the Jessen lab.

I acknowledge the laughs, emotional support, and technical assistance provided by my lab mates and colleagues: Dianna J. Prince, Paola Molina, Anna O. Parnell, and Kishan Patel.

I acknowledge the technical support and guidance provided by Tammy N. Jessen.

I acknowledge the guidance provided by my dissertation committee members: David Nelson, Brian Robertson, Christopher Herlihy, and Matthew Elrod Erickson.

I acknowledge my former mentor and principal investigator responsible for my love of research and questions Ngee Sing Chong.

Funding

This study was funded by a grant from the National Institutes of Health (GM102356 to J.R.J.). Certain equipment items used to conduct this research were provided by Middle Tennessee State University. I acknowledge support from the molecular biosciences Ph.D. program and the biology department.

Abstract

Vang-Like 2 (Vangl2), a key player in the planar cell polarity (PCP) pathway, regulates collective and directed cell migration in zebrafish gastrulae. *vangl2* mutant zebrafish embryos exhibit a strong convergence and extension phenotype, characterized by a shortened and broadened body axis. To date, Vangl2's role in developing plasma membrane protrusions, including lamellipodia-like large protrusions and filopodia, is unclear. Previous works claim loss of Vangl2 results in decreased fibronectin extracellular matrix (ECM), while loss of Glypican4, a PCP protein thought to be working in opposition to Vangl2, causes increased fibronectin ECM. We aim to establish the role of Vangl2 and fibronectin ECM in membrane-protrusive activity. We report *vangl2* mutant cells produce excess unpolarized membrane protrusions, while *glypican4* mutant cells do not. Our data indicate non-canonical Wnt/Glypican4 signaling inhibits membrane protrusion polarization but minimally affects cell trajectory directness and protrusion quantity. Further, Vangl2 and its binding partner, Prickle1a, regulate membrane protrusion quantity, polarization, and productivity. Protein localization confocal imaging studies indicate Vangl2 accumulates in newly developing large membrane protrusions. Similar to *vangl2* mutant cells, *fibronectin* morphant cells exhibit loss of cell trajectory directness, increased numbers of membrane protrusions, and decreased large protrusion polarity. Additionally, Vangl2 fails to effectively localize to the cell surface in *fibronectin* morphant embryos. Injecting *fibronectin* mRNA into *vangl2* mutant embryos rescues membrane protrusion and cell trajectory defects but does not correct cellular length-width ratios, mediolateral cell alignment, or the embryonic convergence and extension

phenotype. Our work establishes cell-matrix interactions are integral for Vangl2-dependent membrane protrusion activities in migrant zebrafish gastrula cells.

Table of Contents

List of Figures…… **x**

List of Tables…….. **xv**

Table of Abbreviations……. **xvi**

Chapter 1: Introduction……... **1**

1.1 Cell Movements of the Zebrafish Gastrula……... **3**

1.2 Planar Cell Polarity…… **6**

1.3 Why is planar cell polarity important?..... **13**

1.4 Membrane Protrusions…….. **14**

1.5 Fibronectin Extracellular Matrix…….. **18**

1.6 Dissertation Goal…… **23**

Chapter 2: The Planar Cell Polarity Proteins, Vangl2 and Glypican4, Differentially Regulate Membrane Protrusion Formation…….. **24**

2.1 Introduction…… **24**

2.2 Results…….. **26**

2.3 Conclusion…….. **41**

Chapter 3: *vangl2* mRNA-Injected and *prickle1a* Morphant Ectodermal Cells Present Membrane Protrusion Defects…….. **44**

3.1 Introduction…… **44**

3.2 Results…….. **46**

3.3 Conclusion…….. **56**

Chapter 4: Vangl2 Localizes in Erupting Large Membrane Protrusions……. 59

4.1 Introduction…….…….. 59

4.2 Results……. 60

4.3 Conclusion…….. 74

Chapter 5: Loss of Fibronectin Disrupts Membrane Protrusion Formation and Polarization and *fibronectin* mRNA Injection Rescues the *vangl2* Mutant Membrane Protrusion Phenotype……. 76

5.1 Introduction…… 76

5.2 Results…….. 79

5.3 Conclusion……..... 92

Chapter 6: Vangl2 Cell Surface Localization Requires a Fibronectin Extracellular Matrix…….……. 95

6.1 Introduction…… 95

6.2 Results…….. 95

6.3 Conclusion……...……... 102

Chapter 7: Fibronectin Knockdown in *vangl2* Mutant Embryos…….…. 104

7.1 Introduction…… 104

7.2 Results…….. 104

7.3 Conclusion…….. 107

Chapter 8: Materials and Methods…….. 110

8.1 Zebrafish Lines and Husbandry…… 110

8.2 Morpholinos, Synthetic mRNA, and Embryo Microinjection…….. 110

8.3 Whole-Mount *in situ* Hybridization, Immunofluorescence, and Antibodies…… 112

8.4 Embryo Protein Extraction, Western Blot, and Antibodies……. 113

8.5 Microscopic Imaging…….. 114

8.6 Quantitation of Cell Shape, Alignment, Velocity, and Directness…….. 114

8.7 Analysis of Membrane Protrusions…….. 115

8.8 GFP-VANGL2 and Vangl2 Localization…….. 115

8.9 Statistics……... 117

Chapter 9: Discussion……..……. 118

9.1 Vangl2 and Glypican4 Differentially Regulate Membrane-Protrusive Activity…… 119

9.2 Vangl2 Overexpression and *prickle1a* Morphant Ectodermal Cells Exhibit Membrane Protrusion Defects……. 121

9.3 Vangl2 Asymmetrically Localizes in Erupting Large Membrane Protrusions…… 123

9.4 Fibronectin is Integral to Vangl2-Dependent Membrane-Protrusive Activity…… 126

References…….. 129

List of Figures

Figure 1 Convergence and Extension Movements…… 2

Figure 2 Cell Movements during Zebrafish Gastrulation…… 4

Figure 3 Vertebrate Planar Cell Polarity Pathway…….….. 8

Figure 4 Planar Cell Polarity Mutant Phenotypes…… 12

Figure 5 Filopodia and Large Membrane Protrusion ……. 17

Figure 6 Fibronectin in PCP Mutants…….. 20

Figure 7 Fibronectin Protein in PCP Mutants…….…… 21

Figure 8 Loss of Fibronectin in Wild-Type Zebrafish Embryos……. 22

Figure 9 Wild-Type, *vangl2* Mutant, and *glypican4* Mutant Cell Micrographs…. 27

Figure 10 *vangl2* Mutant Ectodermal Cells Exhibit Increased Filopodia…….. 28

Figure 11 *vangl2* Mutant Ectodermal Cells Exhibit Increased Large Membrane Protrusions……..… 29

Figure 12 *vangl2* Morphant Ectodermal Cells Exhibit Mild Membrane Protrusion Defects at Mid-Gastrulation (80% Epiboly)…….. 31

Figure 13 Planar Polarized Membrane Protrusions in Wild-Type versus PCP Mutant Cells…… 32

Figure 14 Large Membrane Protrusion Distributions in PCP Mutant Ectodermal Cells…… 34

Figure 15 Large Membrane Protrusion Productivity in PCP Mutant Ectodermal Cells…… 36

Figure 16 Trajectory Plots and Loss of Directness in PCP Mutant Ectodermal Cells…… 37

Figure 17 Large Membrane Protrusion Productivity Enhancement in PCP Mutant Ectodermal Cells…… 39

Figure 18 PCP Mutant Ectodermal Cells Present Hallmarks of PCP……. 40

Figure 19 Convergence and Extension Phenotypes in *prickle1a* Morphant Embryos and Embryos with Vangl2 Overexpression…….. 45

Figure 20 *vangl2* mRNA Validation…….. 47

Figure 21 Vangl2 Overexpression Causes Increased Membrane-Protrusive Activity……... 48

Figure 22 Loss of Prickle1a Causes Increased Membrane-Protrusive Activity….. 50

Figure 23 Decreased Polarized Membrane Protrusions in *vangl2*-Injected Embryos…….. 51

Figure 24 Decreased Polarized Membrane Protrusions in *prickle1a* Morphant Embryos……... 52

Figure 25 Defective Cell Migration and PCP in *vangl2*-Injected Embryos…… 54

Figure 26 Defective Cell Migration and PCP in *prickle1a* Morphant Embryos…. 55

Figure 27 Confocal Micrographs of Wild-Type Ectodermal Cells ……. 61

Figure 28 Anteroposterior Axis GFP-VANGL2 Fluorescence Intensity Plot Profile…….……. 62

Figure 29 GFP-VANGL2 is not Enriched at Anterior or Posterior Membranes... 64

Figure 30 Dorsoventral Axis GFP-VANGL2 Fluorescence Intensity Plot Profile…… 64

Figure 31 GFP-VANGL2 Symmetry at Dorsoventral Membranes……..... 65

Figure 32 Time-Lapse Micrographs Illustrating Large Membrane Protrusion Phases……..……. 67

Figure 33 Plot Profile for Large Membrane Protrusion Development Phases... 68

Figure 34 GFP-VANGL2 Enrichment in Eruption Phase Large Membrane Protrusions…….……. 69

Figure 35 GFP-VANGL2 Localization Normalizes in Extension Phase Large Membrane Protrusions……..……. 70

Figure 36 GFP-VANGL2 Enrichment in Protrusive Cellular Domains…..…… 72

Figure 37 Polarized and Non-Polarized Large Protrusions Exhibit Symmetrical GFP-VANGL2 Distribution……. 73

Figure 38 Fibronectin Extracellular Matrix in Tailbud Stage Wild-Type Embryo…….. 77

Figure 39 Tailbud Stage *fibronectin* (*fn1a/1b*) Morphant Embryo Convergence and Extension Phenotype……. 79

Figure 40 Confocal Micrographs of Wild-Type Embryos Injected with *fibronectin* (*fn1/1b*) Morpholinos……... 80

Figure 41 *fibronectin* (*fn1a/1b*) Morphant Embryos Produce Increased Membrane Protrusions…… 81

Figure 42 *fibronectin* (*fn1a/1b*) Morphant Embryos Exhibit Decreased Large Membrane Protrusion Polarity…… 83

Figure 43 *fibronectin* (*fn1a/1b*) Morphant Embryos Present PCP Defects…… 84

Figure 44 Confocal Micrographs of Fibronectin (fn) Expression in *fibronectin* (*fn1a/1b*) mRNA-Injected Wild-Type and *vangl2* Mutant Embryos……... 86

Figure 45 Fibronectin Rescues Membrane Protrusion Formation in *vangl2* Mutant Ectodermal Cells……. 89

Figure 46 Fibronectin Rescues Large Membrane Protrusion Polarization in *vangl2* Mutant Ectodermal Cells……..… 91

Figure 47 Fibronectin Fails to Rescue PCP Defects in *vangl2* Mutant Embryos 96

Figure 48 Confocal Micrographs of Cytoplasmic Vangl2 Localization during Early Gastrulation…… 97

Figure 49 Plot Profiles of Cytoplasmic Vangl2 Localization during Early Gastrulation……..... 98

Figure 50 Cell Surface Translocation of Vangl2 Disruption in *fibronectin* (*fn1a/1b*) Morphant Ectdoermal Cells……... 99

Figure 51 Plot Profiles Illustrating Disrupted Cell Surface Translocation of Vangl2 in *fibronectin* (*fn1a/1b*) Morphant Ectodermal Cells……... 100

Figure 52 Cell Surface Translocation of Vangl2 Disruption in *fibronectin* (*fn1a/1b*) Morphant Mesodermal Cells…….. 101

Figure 53 Plot Profiles Illustrating Disrupted Cell Surface Translocation in *fibronectin* (*fn1a/1b*) Morphant Mesodermal Cells…….. 101

Figure 54 Confocal Micrograph of *fibronectin* (*fn1a/1b*) Morpholino-Injected *vangl2* Mutant Embryo Ectodermal Cell…… 105

Figure 55 Membrane Protrusions in *fibronectin* (*fn1a/1b*) Morpholino-Injected *vangl2* Mutant Embryos…… 106

Figure 56 Polarized Membrane Protrusions in *fibronectin* (*fn1a/1b*) Morpholino-Injected *vangl2* Mutant Embryos……. 108

List of Tables

Table 1 Membrane Protrusion Classifications……. 15

Table of Abbreviations

dlx3	Distal-less Homeobox 3 Gene, Forebrain Marker
ECM	Extracellular Matrix
fn	Fibronectin
FRAP	Fluorescence Recovery After Photobleaching
hgg1	Cathepsin Gene, Neural Crest Marker
JNK	c-Jun N-Terminal Kinase
LWR	Length-Width Ratio
memGFP	Membrane-Targeted Green Fluorescent Protein
memRFP	Membrane-Targeted Red Fluorescent Protein
MLA	Mediolateral Alignment
MO	Morpholino
PCP	Planar Cell Polarity
shh	Sonic Hedgehog Gene, Notochord Marker
t	Time
Vangl2	Vang-like2
WT	Wild Type

CHAPTER ONE. Introduction

Planar cell polarity (PCP) occurs as animal cells organize into sheets and exhibit a coordinated behavior (Goodrich and Strutt, 2011). Primarily seen in epithelial tissues, PCP encompasses a variety of cellular processes ranging from polarized formation of actin-rich hairs to proper cellular elongation and mediolateral alignment. PCP was first discovered when Peter Lawrence noticed insect hair-forming cells progressively orient, aligning with one another and the anteroposterior axis (Lawrence, 1966). Lawrence noticed the resulting hairs also align, referring to them as "polarity indicators" (Lawrence, 1966). As time went on, Lawrence's work translated to fly ommatidia comprising the compound eye. Today, we know of a multitude of organisms and morphogenetic processes requiring PCP, including gastrulation movements and neural tube closure (Goodrich and Strutt, 2011; Gray et al., 2011; Jessen and Solnica-Krezel, 2005).

As *Danio rerio* (zebrafish) embryos undergo gastrulation, mesendodermal and ectodermal germ layers naturally exhibit PCP. Convergence and extension movements begin around mid-gastrulation (80% epiboly) and continue through the end of gastrulation, tailbud stage (Figure 1)(Jessen and Solnica-Krezel, 2005). During a process known as collective migration, mesodermal and ectodermal progenitor cells migrate in synchronized sheets toward the dorsal body axis, which forms the anterior head and dorsal notochord of the zebrafish embryo (Jessen and Solnica-Krezel, 2005). As progenitor cells arrive at the dorsal body axis, the notochord narrows and elongates.

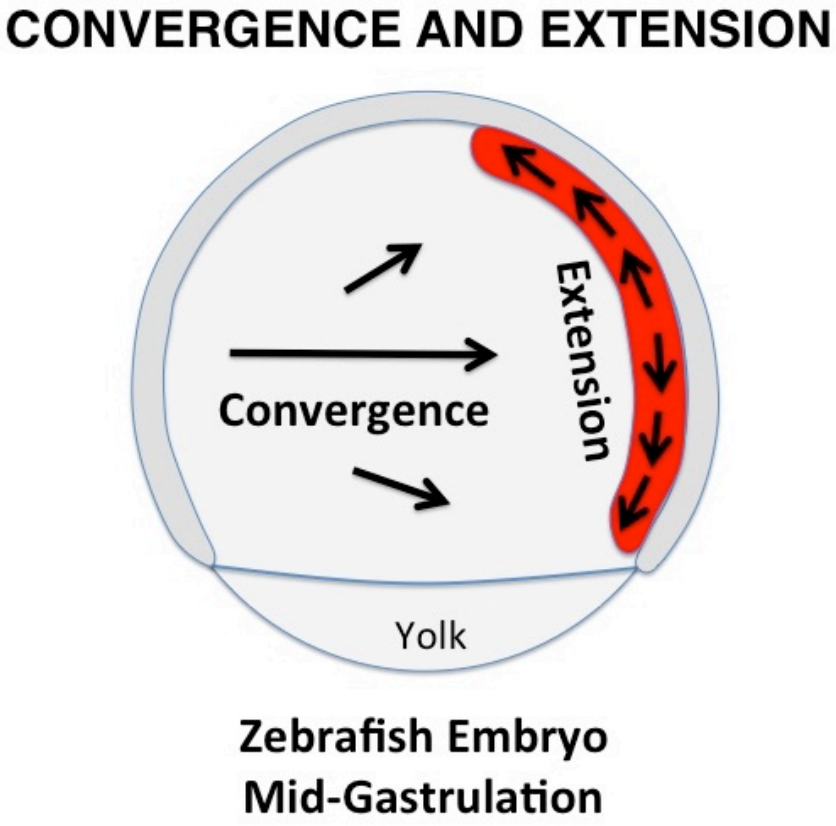

Figure 1 Convergence and Extension Movements: Cells undergoing PCP migrate dorsally toward the embryonic notochord (red) during convergence. The dorsoventral body axis elongates as extension occurs.

These progenitor cells require effective PCP for successful collective migration and, in turn, embryonic dorsal body axis convergence and extension. Defective PCP results in neural tube defects in vertebrates, including an embryonic lethal convergence and extension phenotype in zebrafish.

1.1 Cell Movements of the Zebrafish Gastrula

During zebrafish embryogenesis, gastrula cells undergo four types of cell movements: epiboly, internalization, and convergence and extension (Solnica-Krezel and Sepich, 2012)(Figure 2). These movements are critical to morphogenesis and tissue patterning. The blastoderm thins and spreads to cover the yolk during epiboly, beginning around 4 hours post-fertilization (hpf) (Kimmel et al., 1995). Once the embryo reaches approximately 50% epiboly, gastrulation commences. The onset of gastrulation coincides with the onset of internalization (Warga and Kimmel, 1990). During internalization the blastoderm transitions from a single layer of cells into two distinct layers, the epiblast and hypoblast (Trinkhaus, 1984). As epiboly progresses, convergence and extension processes begin. Convergence and extension movements promote the narrowing and elongation of the dorsoventral body axis (Wallingford et al., 2002). Cell movements of the zebrafish gastrula, including epiboly, internalization, convergence and extension, are essential for establishing germ layers and developing major body axes.

Epiboly

Zebrafish blastulae have three distinct layers prior to epiboly, the enveloping layer (EVL), blastoderm, and yolk syncytial layer (YSL) (Lepage and Bruce, 2010). Radial intercalation is the process whereby blastoderm cells in one tissue layer move to a more

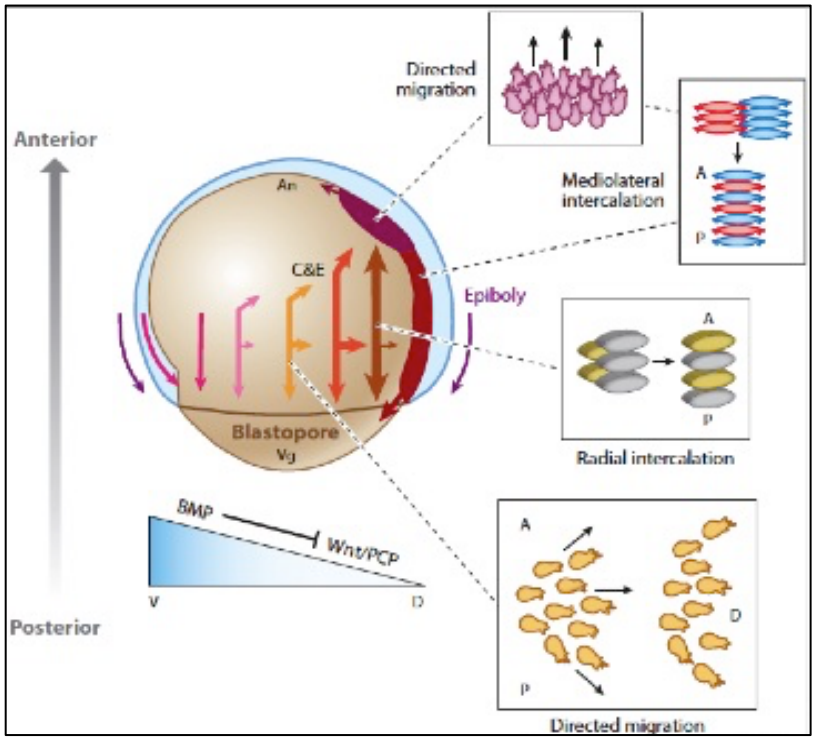

Figure 2 Cell Movements during Zebrafish Gastrulation: Diagram of cellular movements in zebrafish gastrulae. Embryonic cells radially intercalate to initiate epiboly. Via internalization cells fold under the posterior margin to develop the epiblast and hypoblast layers. Cells engage in directed migration and mediolateral intercalation to promote convergence and extension.

Solnica-Krezel and Sepich, 2012

superficial layer (Warga and Kimmel, 1990). Radial intercalation is required to initiate epiboly and, therefore, tissue spreading and yolk plug closure (Keller et al., 1989). Once the embryo reaches 50% epiboly, these movements briefly pause as gastrulation starts and cells begin to converge dorsally (Solnica-Krezel and Driever, 1994; Warga and Kimmel, 1990).

Internalization

During epiboly cells at the blastoderm margin migrate deeper into the blastoderm to form an inner layer, the hypoblast (Kane and Adams, 2002). In essence, the migrating tissue folds underneath itself to produce the germ ring, an area of germ cell progenitor tissue piling. The remaining outer layer becomes the epiblast. Cells from the hypoblast are mesendodermal progenitor cells, while epiblast cells differentiate into the ectoderm (Warga and Nüsslein-Volhard, 1999). During internalization, cells function autonomously as individuals (Carmany-Rampey and Schier, 2001). Internalization continues for the duration of epiboly (Jessen and Solnica-Krezel, 2005). Researchers debate whether internalization occurs by involution (tissue folding) or ingression (directed cell movement from outer to inner tissue layers) or a combination of both (Jessen and Solnica-Krezel, 2005).

Convergence and Extension

As the zebrafish blastula becomes a gastrula (6 hpf), radial intercalation gives way to mediolateral intercalation, supporting convergence and extension cell movements (Keller et al., 1989; Kimmel et al., 1995). During convergence and extension, the embryonic dorsoventral body axis narrows and lengthens. Convergent extension in the

African clawed frog (*Xenopus laevis*) consists of simultaneous, dependent movements (Keller et al., 2000). Unlike convergent extension seen in the frog convergence and extension are two independent cell movements in the zebrafish gastrula.

Laterally situated cells from the epiblast and hypoblast migrate dorsally, driving convergence and extension movements (Jessen et al., 2002; Topczewski et al., 2001). In the early gastrula, mesendoderm extension engages as hypoblast cells migrate toward the animal pole, and epiblast cells migrate toward the vegetal pole (Sepich et al., 2005). After extension movements are underway but prior to mid-gastrulation, convergence movements initiate when the mesendodermal cells migrate dorsally toward the embryonic midline (Sepich et al., 2005).

By the end of gastrulation, migrating cells become tightly packed as their trajectory slows and these cells transition from a round, amoeboid shape to a mediolaterally elongated ovoid shape (Jessen and Solnica-Krezel, 2005). These organizational and morphological changes occur in a polarized fashion and require functional PCP signaling. Loss of a core PCP protein function leads to failed convergence and extension, resulting in a shortened and broadened body axis. Cell-cell and cell-matrix interactions are required for effective convergence and extension (Coyle et al., 2008; Dohn et al., 2013). Convergence and extension movements persist after gastrulation into the developing embryo's segmentation period (Jessen and Solnica-Krezel, 2005).

1.2 Planar Cell Polarity Pathway

The *Drosophila melanogaste*r (fruit fly) PCP pathway is composed of six core genes, *van gogh* (*stbm*), *prickle* (*pk*), *dishevelled* (*dsh*), *frizzled* (*fz*), *flamingo*

(*fmi*/*starrynight*/*stan*), and *diego* (*dgo*) (Goodrich and Strutt, 2011). These genes are considered "core" to the pathway due to their known activities and their close affiliation with the adherens junction region of cells (Goodrich and Strutt, 2011). The vertebrate PCP pathway initiates when a Wnt ligand binds with a seven-pass transmembrane receptor, Frizzled (Goodrich and Strutt, 2011)(Figure 3). Glypican4 is a heparan sulfate proteoglycan acting as a Wnt co-receptor for the PCP pathway (Yang and Mlodzik, 2015). Dishevelled is a cytoplasmic protein functioning as a signal transducer by way of its three protein-protein interaction domains, DEP, DIX, and PDZ (Boutros and Mlodzik, 1999; Theisen et al., 1994; Wallingford and Habas, 2005). A four-pass transmembrane scaffolding protein, Vangl2, interacts with the cytoplasmic protein Prickle to, perhaps, regulate actin rearrangement (Carreira-Barbosa et al., 2003; Jenny, 2003; Montcouquiol, 2006; Veeman et al., 2003)(Figure 3). Prickle has many protein-protein interaction domains, and while loss of Prickle disrupts PCP and convergence and extension its signaling mechanism is unknown (Veeman et al., 2003). Vangl2 and Frizzled bind with Dishevelled to initiate actin cytoskeletal remodeling via doswnstream effectors, including RhoA, Rac, Cdc42, and c-Jun N-terminal kinase (JNK) (Boutros and Mlodzik, 1999; Hall, 2005; Ridley, 2006; Yang and Mlodzik, 2015).

Members of the Rho family of small GTPases, Rac, Rho, and Cdc42 are active when bound to guanosine triphosphate (GTP) and inactive when bound to guanosine diphosphate (GDP) (Hall, 2005; Ridley, 2001; Settleman, 2001). Guanine nucleotide exchange factors (GEF) and GTPase-activating proteins (GAP) modulate Rho GTPase activity, but the specific GEFs and GAPs present during zebrafish gastrulation are

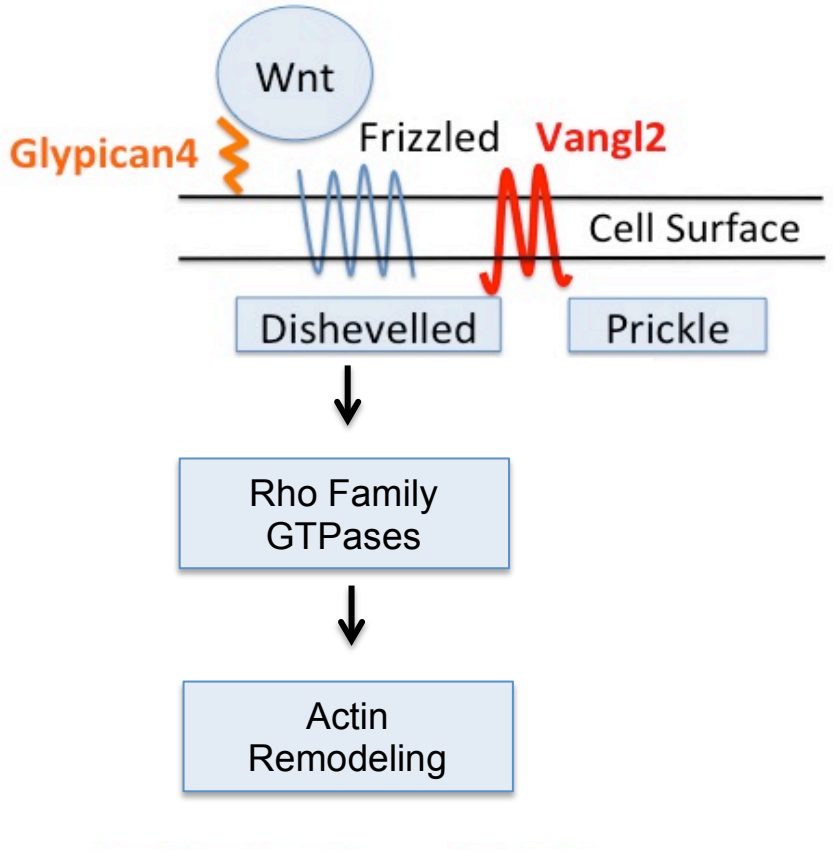

Figure 3 Vertebrate Planar Cell Polarity Pathway: A Wnt/Frizzled complex with co-receptor Glypican4 triggers the PCP cascade. The cytoplasmic protein Dishevelled signals to Rho GTPases, functioning as downstream effectors of actin remodeling. The four-pass transmembrane protein Vangl2 binds with Prickle but their functions are unclear.

unreported (Hall, 2005; Ridley, 2001; Settleman, 2001). RhoA regulates the assembly of actin-myosin filaments to generate contractile force (Schlessinger et al., 2009). Rac and Cdc42 support actin polymerization to promote membrane protrusion formation and cell polarity (Schlessinger et al., 2009). Rac and Cdc42 initaite the JNK pathway, but its function in the PCP context is unknown (Schlessinger et al., 2009).

Defective PCP in the fly results in disrupted actin-rich wing hair organization, as the hairs are no longer polarized with a common distal orientation (Gubb and García-Bellido, 1982). In the fly wing, PCP core proteins asymmetrically localize on the apical surface of wing epithelial cells. Cytoplasmic proteins, Diego and Dishevelled, and the seven-pass transmembrane protein, Frizzled, are distally located (Goodrich and Strutt, 2011). The cytoplasmic protein, Prickle, and the four-pass transmembrane protein, Van Gogh, are on the proximal side of the cell (Goodrich and Strutt, 2011). Flamingo, a seven-pass transmembrane atypical cadherin, is distributed symmetrically at both the proximal and distal sides of the cell (Goodrich and Strutt, 2011).

PCP protein distribution is difficult to assess in the zebrafish gastrula. The use of fluorescent fusion proteins has allowed some protein localization studies, but because PCP protein overexpression is a concern low doses of injected synthetic RNA are required (Roszko et al., 2015). In non-migrating neuroectodermal and axial mesodermal cells, Prickle and Vangl2 are concentrated at the anterior membrane, while Dishevelled has a posterior membrane bias (Ciruna et al., 2006; Roszko et al., 2015; Yin et al., 2008). Asymmetric localization of PCP core proteins remains unconfirmed in migrating zebrafish gastrula cells.

Additional studies characterizing PCP in the fly provide evidence for non-autonomous protein function for several PCP proteins (Gubb and García-Bellido, 1982; Taylor et al., 1998; Vinson and Adler, 1987). Loss of *frizzled* in cell groups causes adjacent cells to orient their hairs toward mutant cells, while loss of *van gogh* causes neighboring cells to orient their hairs in the opposite direction (Goodrich and Strutt, 2011). These studies illustrate the non-autonomous characteristics of *frizzled* and *van gogh* as their defective polarity is propagated to neighboring wild-type cells. Frizzled and Van Gogh are versatile and are capable of behaving non-autonomously and autonomously, while Dishevelled and Prickle only function autonomously (Adler et al., 2000; Boutros and Mlodzik, 1999; Jessen et al., 2002; Strutt and Strutt, 2002; Taylor et al., 1998; Theisen et al., 1994; Veeman et al., 2003; Wallingford and Habas, 2005).

The core vertebrate PCP protein Vang-like 2 (Vangl2) was genetically linked with vertebrate gastrulation movements when it was discovered as the defective gene in *trilobite* mutant zebrafish (Jessen et al., 2002; Solnica-Krezel et al., 1996). The *trilobite* gene was discovered as part of a large-scale mutagenesis screen and noted for its gastrulation phenotype (Solnica-Krezel et al., 1996). When labeled with a somite marker and viewed dorsally, *trilobite* mutant embryos resemble the trilobite fossil (Solnica-Krezel et al., 1996). The *trilobite* mutant will be referred to as the *vangl2* mutant going forward. Vangl2 and its known binding partner, Prickle, form a functional complex capable of modulating Frizzled/Dishevelled activity in the fly wing and potentially during gastrulation (Bastock et al., 2003; Carreira-Barbosa et al., 2003; Dohn et al., 2013; Jenny, 2003). Vangl2 is involved with the cell membrane recruitment of Prickle, which, in turn,

plays a role in the localization and clustering of Vangl2 at the cell membrane (Carreira-Barbosa et al., 2003; Jenny, 2003). Loss of Vangl2 or other core PCP proteins causes ineffective convergence and extension movements during gastrulation (Goodrich and Strutt, 2011; Jenny, 2003; Jessen et al., 2002; Solnica-Krezel et al., 1996).

When PCP fails in zebrafish gastrulae, mesendodermal and ectodermal progenitor cells from the epiblast and hypoblast no longer arrive effectively at the dorsal body axis. Instead, these progenitor cells follow an ineffectual, indirect trajectory resulting in the PCP convergence and extension phenotype (Jessen et al., 2002)(Figure 4). *vangl2* mutant embryos are characterized by a distinct phenotype, consisting of a shortened and broadened body axis (Figure 4). The resulting phenotype in *vangl2* mutant embryos occurs as mesendodermal and ectodermal germ cells fail to polarize and migrate effectively toward the developing dorsal body axis during gastrulation convergence and extension cell movements.

Another protein closely affiliated with the PCP pathway, Glypican4 (*gpc4*; *kny*; *knypek*, Polish for "shorty") is thought to function as a Frizzled co-receptor for the Wnt ligand or ligands responsible for PCP cascade initiation (Ohkawara, 2003). Loss of Glypican4 results in a whole embryo convergence and extension defect similar to that of *vangl2* mutant embryos (Topczewski et al., 2001)(Figure4). At the molecular level, the Glypican4/Wnt/Frizzled/Dishevelled side of the pathway is thought to work in opposition to the Vangl2/Prickle side of the pathway. Some of the key differences found between the Glypican4/Wnt/Frizzled/Dishevelled and Vangl2/Prickle sides of the pathway include: fibronectin protein levels and fibrillogenesis, cell-cell adhesion, and proteolytic activity

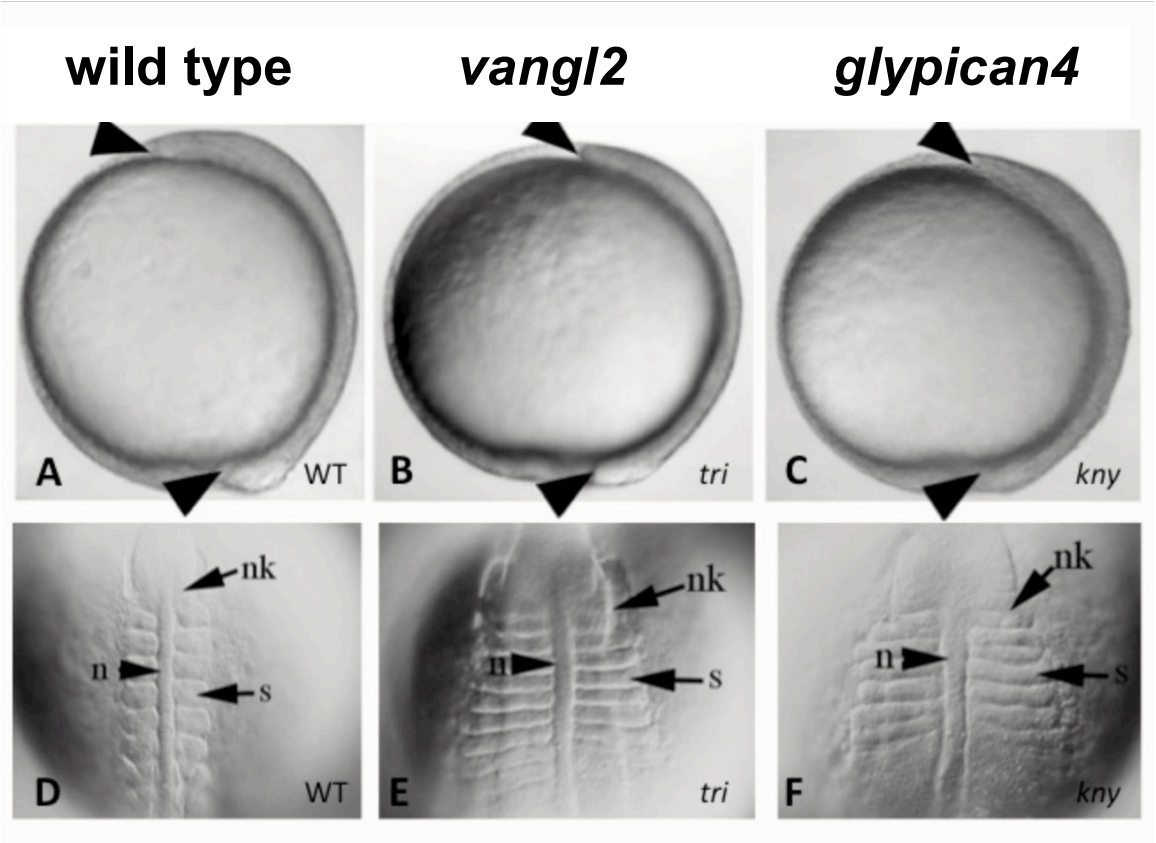

Figure 4 Planar Cell Polarity Mutant Phenotypes: Differential interference contrast (DIC) micrograph images. Wild-type tailbud stage embryo; lateral (A), dorsal (D). *vangl2* mutant tailbud stage embryo; lateral (B), dorsal (E). *glypican4* mutant tailbud stage embryo; lateral (C), dorsal (F).

nk = neural keel; n = notochord; s = somite
Image Credit (D,E,F): Marlow et al., 1998

(Dohn et al., 2013; Williams et al., 2012a). For instance, *glypican4* mutant embryos have increased fibronectin fibrillogenesis and cadherin-mediated cell adhesion, while *vangl2* mutant embryos have decreased total fibronectin protein levels and increased matrix metalloproteinase activity (Dohn et al., 2013; Williams et al., 2012a).

Although *glypican4* and *vangl2* mutant embryos have similar convergence and extension phenotypes, a combinatorial loss of Glypican4 and Vangl2 results in a phenotype more severe than loss of the proteins as individuals (Marlow et al., 1998). These findings indicate distinct roles for Glypican4 and Vangl2 in PCP-dependent convergence and extension. Similarly Glypican4 can potentiate Wnt11 signaling, as *glypican4*/*wnt11* double mutants also have an enhanced phenotype compared to individual mutants, suggesting distinct roles for Glypican4 and Wnt11 in gastrulation PCP signaling (Topczewski et al., 2001).

1.3 Why is planar cell polarity important?

PCP has a wide variety of applications, a few of which I will highlight here. Dysfunctional PCP during embryonic neurulation can result in neural tube defects, including craniorachischisis, spina bifida, and exencephaly (Wu et al., 2011). When neural tube closure is unsuccessful *in utero*, the central nervous system is detrimentally exposed to amniotic fluid. Additional to neural tube defects, PCP is often misappropriated by tumor cells. Some scientists report a tumor-suppressing role for PCP, as PCP promotes cell-cell communication and homeostasis (Lee and Vasioukhin, 2008; Olson and Gibo, 1998; Ying et al., 2007, 2008; Yu et al., 2008). Others claim deregulated

PCP aids tumorigenesis by promoting angiogenesis, tumor cell invasion, and metastasis (Cirone et al., 2008; Wei et al., 2008). In the mouse, researchers established defective cochlear outgrowth, cellular patterning, and hair cell orientation associated with PCP-driven ciliopathy (May-Simera, 2016). Other works implicates loss of PCP in neurological disorders, including myoclonic epilepsy, Parkinson's disease, and Alzheimer's disease, as neuronal polarity relies on effective PCP signaling (May-Simera and Chunqiao, 2013). Because of PCP's broad role during embryonic morphogenesis and processes such as cell migratory behaviors, many of its functions and mechanisms remain unclear.

1.4 Membrane Protrusions

As cells migrate, they produce a variety of plasma membrane protrusions, including blebs, lamellipodia, lamellae, ruffles, invadopodia, and filopodia (Table 1). Classifying membrane protrusions can be complicated as different types may superficially look similar and many hybrid protrusions have been documented. For the purpose of my dissertation work, lamellae and lamellipodia are categorized as "large protrusions" (Table 1). Lamellipodia and filopodia are the most prevalent types of membrane protrusions in zebrafish gastrulae (Figure 5). Progenitor germ cells of the early to middle gastrulation stages primarily produce blebs as they participate in disorganized, amoeboid-like migration (Diz-Muñoz et al., 2016; Paluch and Raz, 2013). By late gastrulation blebs are predominantly seen in cells undergoing mitosis and apoptosis and, therefore, play a minor role in late gastrulation cell movements. Cells form membrane protrusions to improve migratory efficacy, communicate with neighboring cells, and sense the extracellular environment.

Table 1 Membrane Protrusion Classifications: Table describing a variety of actin-rich membrane protrusions, their structures, and their primary functions.

Protrusion	Structure	Primary Function
Filopodium	Finger-like, actin-rich	Sensory/Migratory
Lamellipodium	Flat, branched actin network composition	Migratory
Lamella	Flat, unbranched actin network composition	Migratory
Lamellifilopodium	Combination	Sensory/Migratory
Bleb	Round, initially actin-free	Mitosis/Apoptosis
Ruffles	Non-adhesive, actin-rich, extend vertically	Internalization
Invadopodium	Actin-rich, protease-rich	Invasive Migration

Lamellipodia are flat, actin-rich projections responsible for generating traction (Figure 5). Forming beneath lamellipodia, lamellae are also flat projections. Lamellipodia are comprised of two distinct branched networks of actin filaments, while lamellae are composed of unbranched, loose actin filaments (Iwasa and Mullins, 2007; Ponti, 2004; Svitkina and Borisy, 1999) (Figure 5). Lamellae are slower moving and longer lasting than lamellipodia. Most polarized migrating cells undergo mesenchymal migration, meaning lamellipodia and filopodia form at the cell's leading and trailing edges as the cell adheres to the extracellular matrix to generate traction.

Highly dynamic finger-like structures, filopodia primarily act as the cell's sensory organs (Figure 5). Similar to large protrusions, filopodia are actin-rich and serve to assist cell motility. Often, filopodia are extensions of large protrusions. As cells migrate filopodia explore the environment, interact with the extracellular matrix and adjacent cells, and assist in establishing cell directionality, adhesion, and traction. Since the discovery of filopodia in 1970, their role has grown to include many functions, including tumor cell metastasis, wound healing, neuronal path development, immune cell function, morphogenesis, gastrulation, and cell invasion (Abercrombie et al., 1970; Jacinto and Wolpert, 2001; Rørth, 2003).

Large membrane protrusions may be considered "productive." A protrusion receives a "productive" classification if it results in cell body translocation in the direction of the protrusion. In other words, a productive protrusion develops and extends outward from the cell body and pulls the cell body forward. Productive protrusions drive the

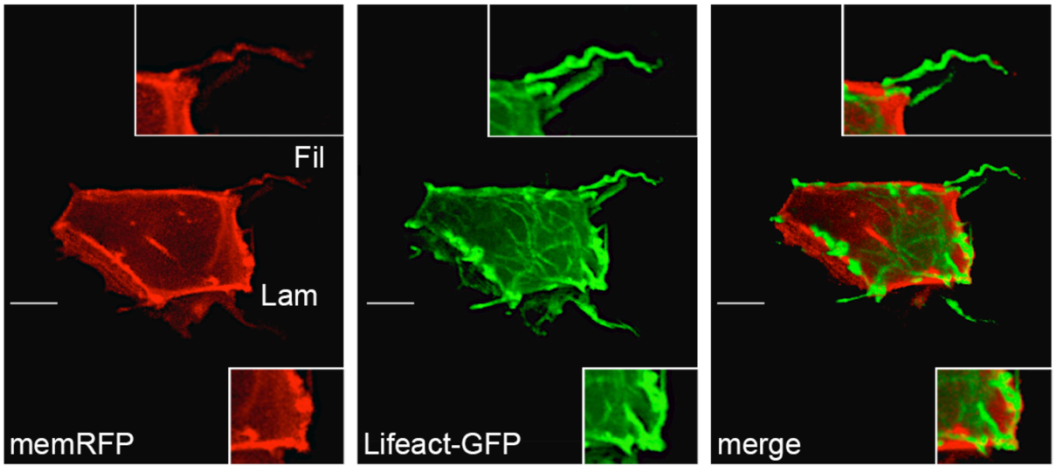

Figure 5 Filopodia and Large Membrane Protrusions: Wild-type zebrafish gastrula ectodermal cell at tailbud stage with filopodia and lamellipodia-like large membrane protrusions. Inset boxes are enlarged examples of filopodia and a lamellipodium. Scale bar = 5 µm.
Membrane-targeted red fluorescent protein (memRFP); Actin-targeted green fluorescent protein (Lifeact-GFP, Riedl et al., 2008); Filopodium (Fil); Lamellipodium (Lam)

mesenchymal mode of migration so they are especially significant to the migrating cells of the zebrafish gastrula.

1.5 Fibronectin Extracellular Matrix

The most prevalent extracellular matrix protein in the zebrafish gastrula, fibronectin is a large glycoprotein capable of interacting with both cell-surface and ECM protein binding partners. Most vertebrates have two types of fibronectin, plasma fibronectin for wound healing and cellular fibronectin. Fibroblasts, chondrocytes, endothelial cells, synovial cells, and myocytes produce cellular fibronectin (Mao and Schwarzbauer, 2005). Cellular fibronectin participates in cell adhesion, migration, spreading, and proliferation, as well as, extracellular matrix deposition. Fibronectin is initially secreted as a dimer with the subunits joined by a disulfide bond, and as fibronectin levels increase the once punctate proteins bind homophilically to generate fibronectin fibrils in a process known as fibrillogenesis.

Migrating gastrula cells undergoing collective and directed migration interact with fibronectin fibrils via cell-surface receptors known as integrins (Banères et al., 1998). In the frog integrin recognition of fibronectin is essential for convergent extension and polarized membrane protrusion formation (Davidson et al., 2006). Inhibition of fibronectin or fibronectin-integrin interactions disrupts radial intercalation required for epiboly movements (Marsden and DeSimone, 2001). Additionally, fibronectin-integrin interactions work to suppress non-polarized membrane protrusion formation in frog explants (Davidson et al., 2006).

Fibronectin assembly and deposition is not well understood, but studies suggest fibronectin extracellular matrix assembly requires cellular interactions (Curnis et al., 2006; Xu et al., 2010; Zamir et al., 1999). Zebrafish gastrulae have two distinct layers of fibronectin (Latimer and Jessen, 2010). The first fibronectin layer is located between the ectoderm and mesoderm, while the second layer is between the mesoderm and endoderm.

Work in the frog first suggested a link between PCP protein function and fibronectin extracellular matrix deposition and assembly. Inhibiting PCP protein expression in the frog alters radially polarized fibronectin fibril assembly, polarized motility, and intercalation (Goto et al., 2005). Later, it was shown that *vangl2* mutant zebrafish have decreased levels of fibronectin, while *glypican4* mutant zebrafish have increased fibrillogenesis (Figures 6, 7)(Dohn et al., 2013; Williams et al., 2012b). In wild-type zebrafish gastrulae, fibronectin deficiency results in a mild convergence and extension phenotype (Figure 8)(Latimer and Jessen, 2010). Migrating lateral ectodermal cells in zebrafish gastrulae interact with laminin in addition to fibronectin; however, loss of laminin does not result in a convergence and extension phenotype (Parsons et al., 2002).

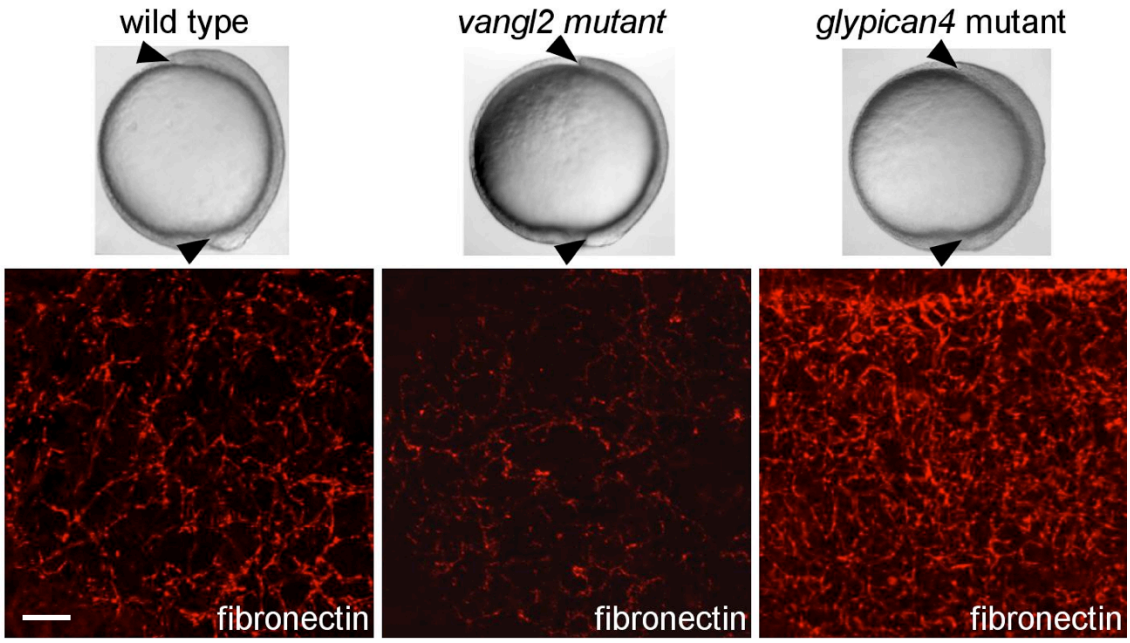

Figure 6 Fibronectin in PCP Mutants: Differential interference contrast (DIC) images of tailbud stage embryos; lateral (top). Confocal micrographs of tailbud stage zebrafish embryos with fibronectin immunostaining (red). *vangl2* mutant zebrafish have decreased fibronectin levels at tailbud stage, while *glypican4* mutant embryos have increased fibronectin fibrillogenesis. Scale bar = 20 μm.

Figure Credit: Dohn et al., 2013

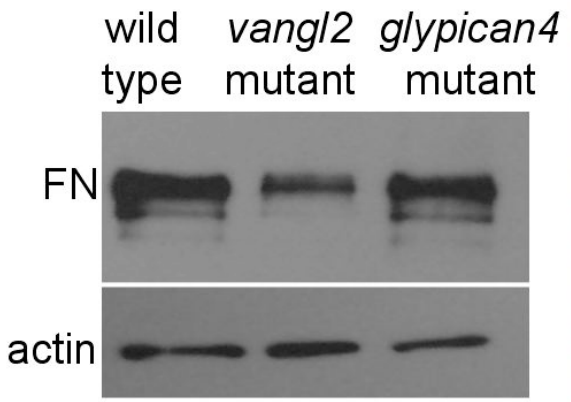

Figure 7 Fibronectin Protein in PCP Mutants: Western blot with fibronectin antibody. *vangl2* mutant embryos have decreased fibronectin protein. *glypican4* mutant embryos have no significant change in total fibronectin levels.

Figure Credit: Dohn et al., 2013

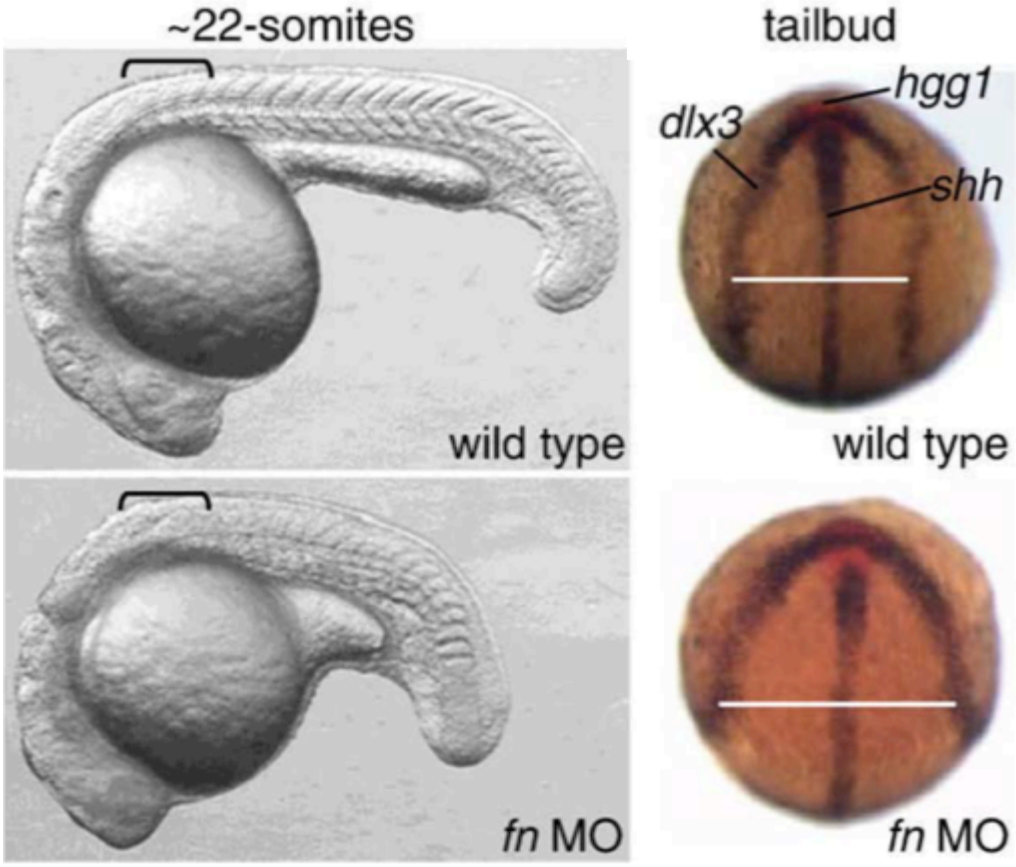

Figure 8 Loss of Fibronectin in Wild-Type Zebrafish Embryos: Lateral aspect of 22-somite stage zebrafish embryos illustrating extension defect in wild-type embryos injected with *fibronectin* (*fn1a/1b*) morpholinos (A). Whole-mount *in situ* hybridization of tailbud stage zebrafish embryos. Dorsal aspect of embryos with broadened body axis illustrating convergence defect (B).

f*ibronectin* morpholino (*fn* MO), prechordal plate (*hgg1*), notochord (*shh*), neural plate (*dlx3*)

Figure Credit: Latimer and Jessen, 2010

1.6 Dissertation Goal

With previously reported background information in mind, my dissertation research aimed to characterize PCP-dependent regulation of membrane-protrusive activity underlying convergence and extension movements and to identify a role for the fibronectin ECM. To achieve this goal, I identified aspects of membrane-protrusive activity regulated by PCP proteins and the fibronectin ECM during gastrulation. I hypothesized Vangl2 works to suppress non-polarized membrane protrusion formation. My hypothesis is based on decreased fibronectin expression and the resulting loss of cell-matrix interactions found in *vangl2* mutant embryos. Previous work in the frog showing cell-matrix interactions are required for polarized membrane protrusion formation supports my hypothesis (Davidson et al., 2006).

CHAPTER TWO. The Planar Cell Polarity Proteins, Vangl2 and Glypican4, Differentially Regulate Membrane Protrusion Formation

2.1 Introduction

During zebrafish gastrulation, polarized wild-type progenitor cells of the ectoderm and mesendoderm undergo collective and directed migration toward the developing dorsal body axis (Solnica-Krezel and Sepich, 2012). When PCP fails, convergence and extension movements also fail, leaving the dorsal body axis short and broad (Myers et al., 2002; Wallingford et al., 2002). While the PCP cause and effect is apparent, the mechanism of these failures is not. Previous works indicated a loss of PCP results in meandering cells and abnormal membrane-protrusive activity (Jessen et al., 2002).

vangl2 mutant embryos produce less total fibronectin protein than wild-type embryos (Dohn et al., 2013). Due to their decreased fibronectin ECM substrate, cell-matrix interactions are limited. However, *glypican4* mutant embryos have enhanced fibrillogenesis but not total fibronectin protein (Dohn et al., 2013). Work in the frog purports cell-matrix, specifically integrin-fibronectin, interactions are required for proper convergent extension and polarized membrane protrusion formation (Davidson et al., 2006). The same researchers suggest cell-matrix interactions function, in part, to suppress random membrane protrusions (Davidson et al., 2006). These data indicate increased membrane protrusion activity in *vangl2* mutant embryos.

Additional to a potential for cell-matrix interactions, *vangl2* mutant embryos have increased cell surface matrix metalloproteinase proteolytic activity (Coyle et al., 2008; Williams et al., 2012a). Proteases are known to localize in the membrane protrusions of migrating cells where they function to modify the ECM and promote efficient migration (He and Wirtz, 2014).

glypican4 mutant embryos have no significant change in protease activity (Dohn et al., 2013). However, cadherin levels and, in turn, cell-cell adhesion are increased in *glypican4* mutants (Dohn et al., 2013). Some studies theorize cadherin-integrin crosstalk suppresses membrane protrusion formation by inhibiting Rac, a known activator of actin cytoskeletal rearrangement and protrusion formation (Martinez-Rico et al., 2010). This notion is supported by reports claiming Rac weakens cadherin-dependent adhesions and initiates membrane protrusions in E-cadherin-producing cells (Chu et al., 2004; Martinez-Rico et al., 2010).

To date, researchers have not characterized membrane protrusions in PCP mutant gastrulae. We hypothesized loss of the core PCP protein Vangl2 results in increased non-polarized membrane protrusions. Previous works indicating decreased cell-matrix interactions and increased proteolytic activity in *vangl2* mutant embryos support our hypothesis (Dohn et al., 2013; Williams et al., 2012a). Due to the cell adhesion properties of *glypican4* mutant embryos, we suspected *glypican4* mutants have no significant change in membrane protrusion numbers.

2.2 Results

vangl2 mutant ectodermal exhibit increased membrane-protrusive activity

We first aimed to quantify membrane protrusions to characterize membrane protrusion phenotypes in wild-type, *vangl2* mutant and *glypican4* mutant ectodermal cells. By fluorescently labeling ectodermal cell membranes and collecting time-lapse micrographs, we quantified filopodia and large protrusions in wild-type, *vangl2* mutant, and *glypican4* mutant zebrafish embryos *in vivo* (Figure 9). We generated mosaic fluorescent labeling by injecting single blastomeres at 8-cell stage with membrane-targeted green fluorescent protein (memGFP). Mosaic labeling allows confocal imaging of ectodermal cells without adjacent cell overlap. From the collected time-lapse images, we find wild-type ectodermal cells produce an average of 13.16 +/- 2.62 filopodia and 3.68 +/- 0.54 large membrane protrusions, while *vangl2* mutant ectodermal cells have an average of 24.84 +/- 5.55 filopodia and 5.77 +/- 0.94 large protrusions (Figures 10, 11). *glypican4* mutant and wild-type ectodermal cells have no significant difference in either filopodia or large membrane protrusions. *glypican4* mutant cells produce an average of 9.58 +/- 2.73 filopodia and 3.59 +/- 0.64 large protrusions (Figures 10, 11).

We conducted a limited membrane protrusion analysis to characterize membrane protrusion phenotypes in wild-type and Vangl2 knockdown ectodermal cells at mid-gastrulation (80% epiboly). Because the *vangl2* mutant convergence and extension defect is undetectable at this stage, we utilized a *vangl2* morpholino to create a loss of Vangl2 condition. First, we performed a membrane protrusion study in *vangl2* morphant

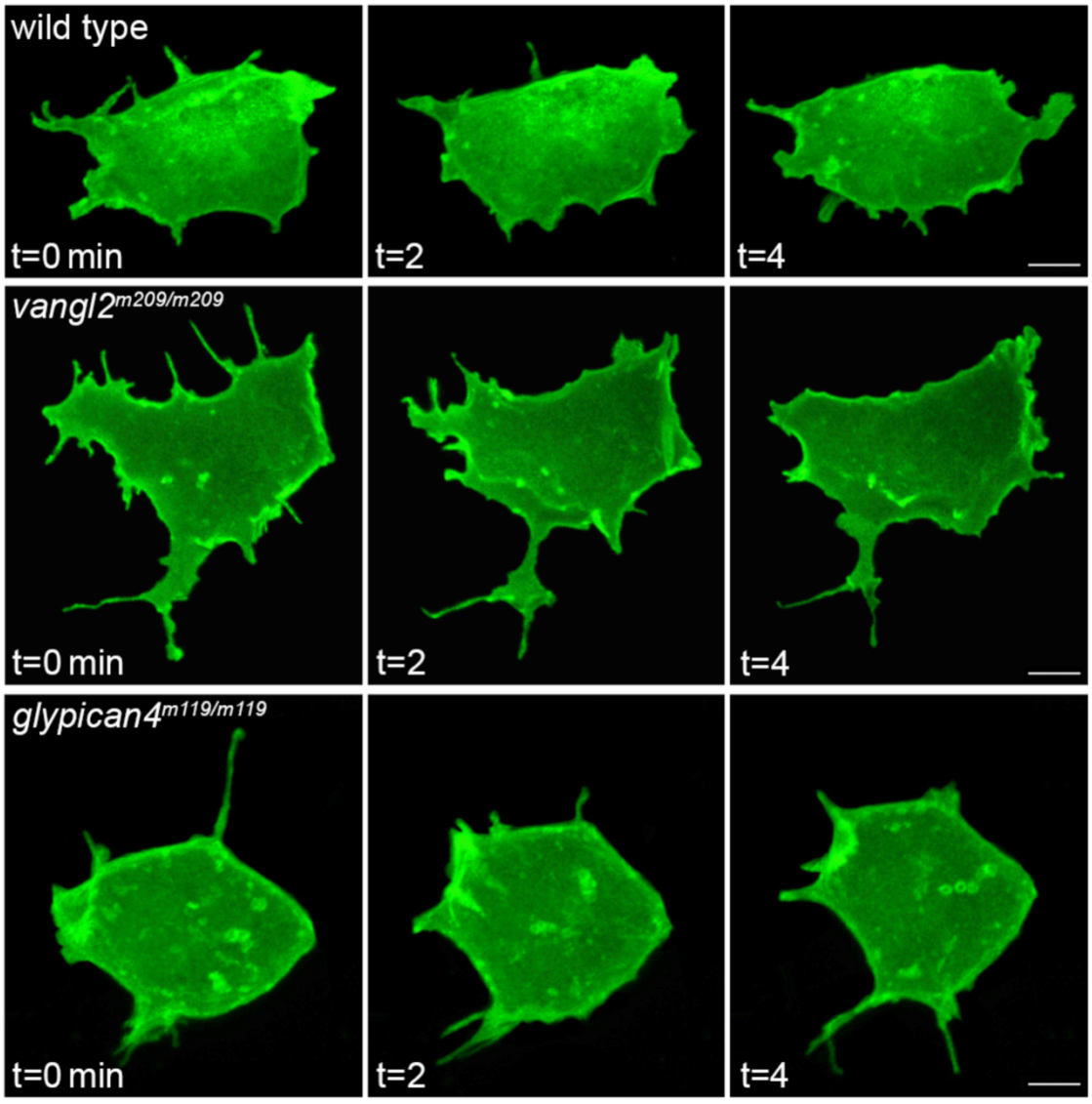

Figure 9 Wild-Type, *vangl2* Mutant, and *glypican4* Mutant Cell Micrographs: Representative wild-type, *vangl2* mutant, and *glypican4* mutant zebrafish ectodermal cells expressing mosaic memGFP *in vivo*. *vangl2* mutant cells produce surplus filopodia and large membrane protrusions. Confocal time-lapse micrographs collected with 2 min intervals for 20 minutes.

Scale Bar= 5μm

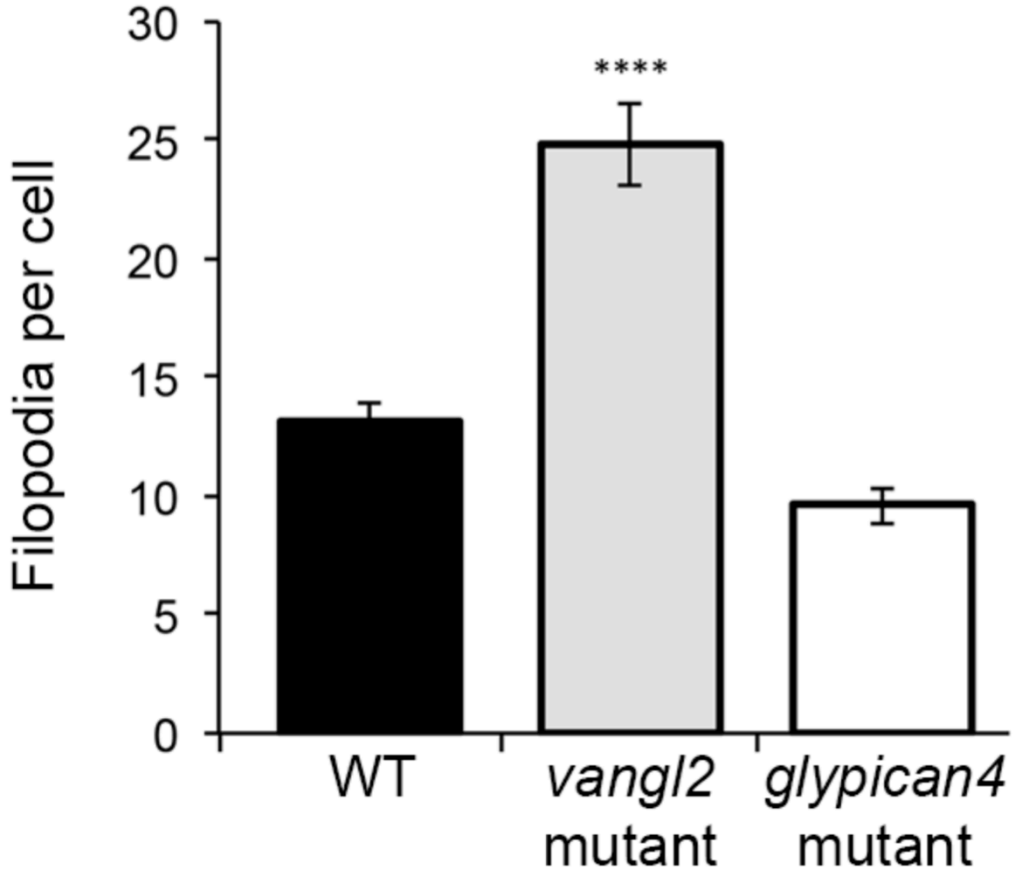

Figure 10 *vangl2* Mutant Ectodermal Cells Exhibit Increased Filopodia: Graph of average number of filopodia per ectodermal cell. Quantified from 10 micrographs over a 20 min time-lapse.

wild type (n=12 cells, 8 embryos), *vangl2*$^{m209/m209}$ (n=10 cells, 7 embryos), and *glypican4*$^{m119/m119}$ (n=12 cells, 5 embryos). All values are ± SD.
**P*<0.05, ***P*<0.01, ****P*<0.001, *****P*<0.0001. *P* values are versus wild type; one-way ANOVA significance test followed by Tukey HSD post-hoc tests

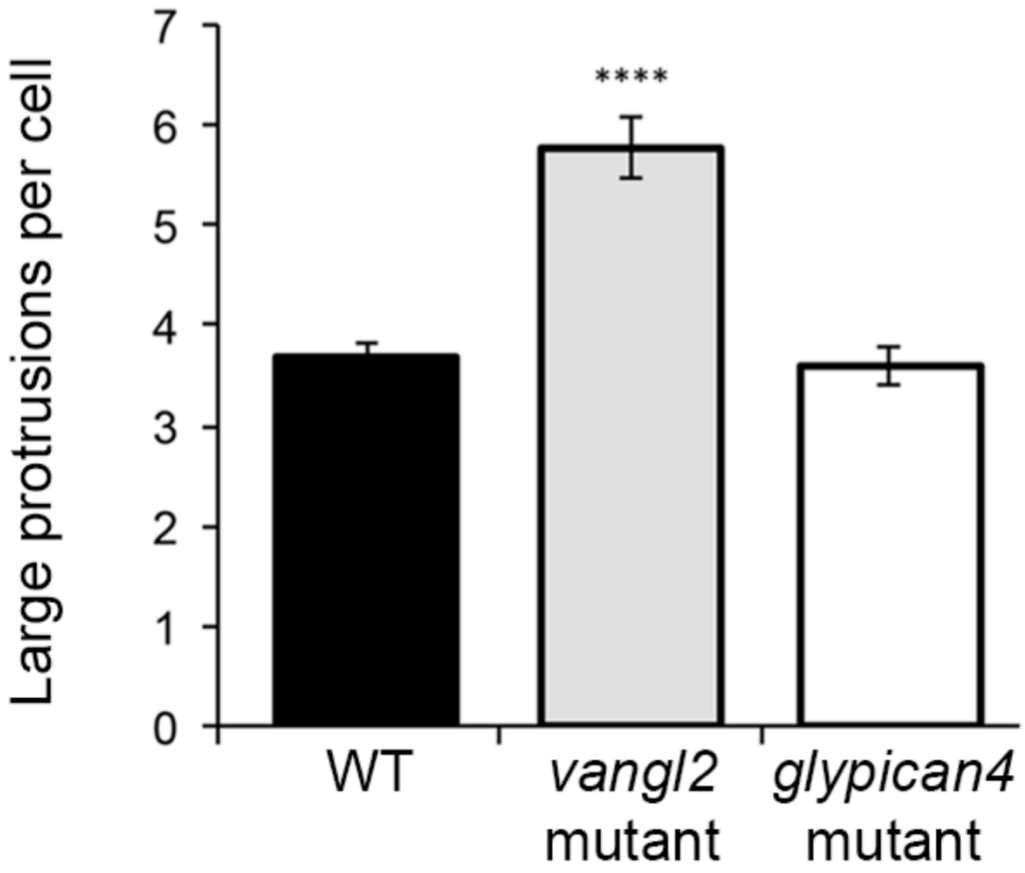

Figure 11 *vangl2* Mutant Ectodermal Cells Exhibit Increased Large Membrane Protrusions: Graph of large membrane protrusions per ectodermal cell. Quantified from 10 micrographs over 20 min time-lapse.

wild type (n=12 cells, 8 embryos), *vangl2*$^{m209/m209}$ (n=10 cells, 7 embryos), and *glypican4*$^{m119/m119}$ (n=12 cells, 5 embryos). All values are ± SD.
*P<0.05, **P<0.01, ***P<0.001, ****P<0.0001. P values are versus wild type; one-way ANOVA significance test followed by Tukey HSD post-hoc tests.

ectodermal cells at the end of gastrulation (tailbud) to confirm its phenotype relative to the *vangl2* mutant membrane protrusion phenotype (data not shown).

After injecting single-cell stage embryos with *vangl2* antisense oligonucleotide morpholino, we injected memGFP at 8-cell stage for mosaic expression (Figure 12A). Using confocal microscopy, treated embryos were imaged when they reached mid-gastrulation (80% epiboly) for 20 min at 2 min intervals. *vangl2* morphant ectodermal cells present an average of 19.96 +/- 5.55 filopodia and 5.55 +/- 0.99 large membrane protrusions at mid-gastrulation (Figures 12B, 12C). Wild-type ectodermal cells produce 18.27 +/- 4.07 filopodia and 4.20 +/- 0.66 large protrusions (Figures 12B, 12C). Because Vangl2 localizes to the cell surface around mid-gastrulation (80% epiboly) but PCP phenotypes are not visible until late gastrulation, we suspect Vangl2-dependent membrane-protrusive activity initiates at mid-gastrulation and becomes more severe by the end of gastrulation.

vangl2 and *glypican4* mutant ectodermal cells have a loss of large membrane protrusion polarity

Filopodia oriented within 45° of the path of migration are considered polarized for the purpose of this analysis. An examination of total polarized filopodia yielded no significant difference between either PCP mutant and wild-type ectodermal cells (Figure 14C). However looking more closely, we established a pattern of leading edge and trailing edge polarized membrane protrusions (Figure 13A, 13B). Wild-type ectodermal cells tend to produce a concentration of filopodia at the trailing edge (32.97% +/- 7.15%) of the cell,

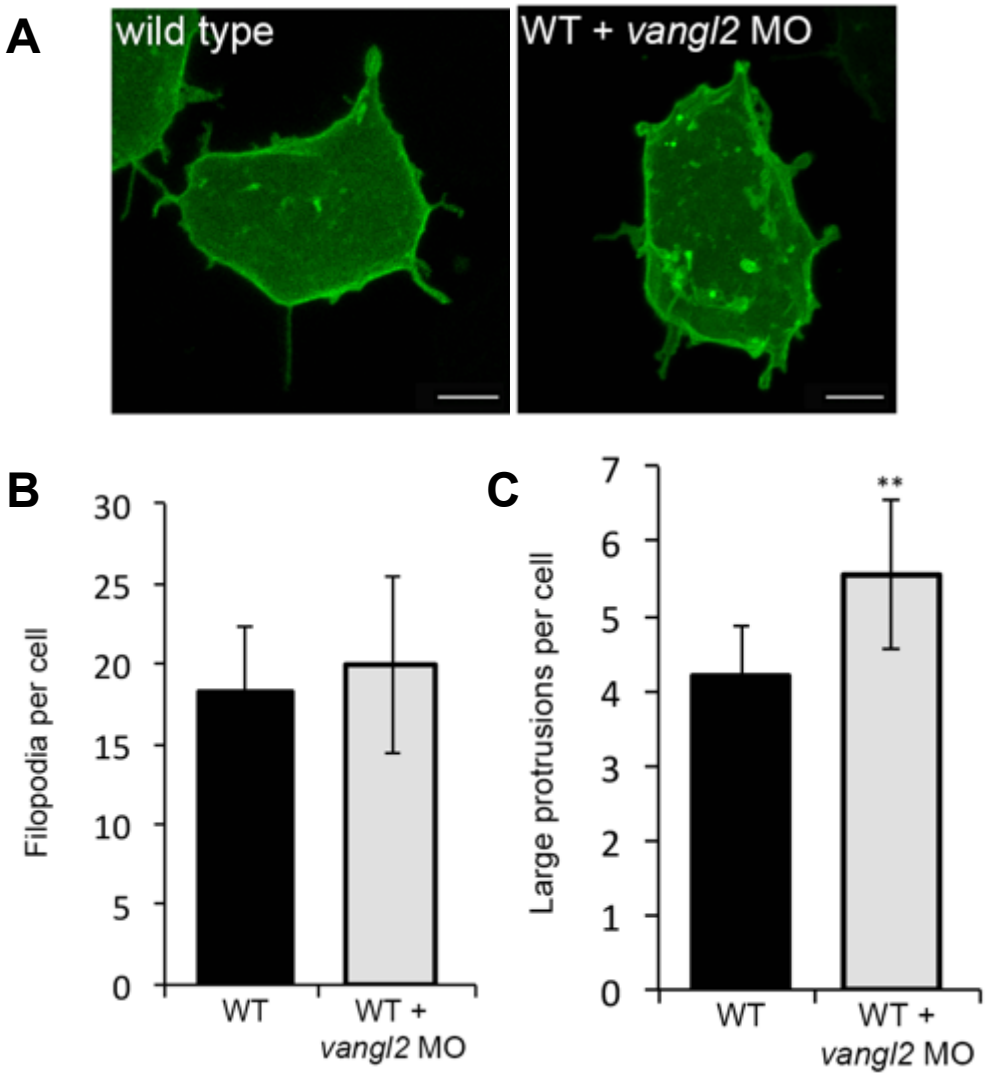

Figure 12 *vangl2* Morphant Ectodermal Cells Exhibit Mild Membrane Protrusion Defects at Mid-Gastrulation: Confocal micrographs of wild-type (WT) and *vangl2* morphant ectodermal cells at 80% epiboly expressing membrane-targeted green fluorescent protein (memGFP)(A). Scale bar = 5 μm. Graph of filopodia (B) and large membrane protrusions (C) per ectodermal cell in wild-type and *vangl2* morphant embryos at mid-gastrulation (80% epiboly).

wild type (n=9 cells, 7 embryos); *vangl2* morphant (MO) (n=10 cells, 6 embryos). All values are ± SD. $^{**}P<0.01$. *P* values are versus wild type; two-tailed unpaired *t*-test.

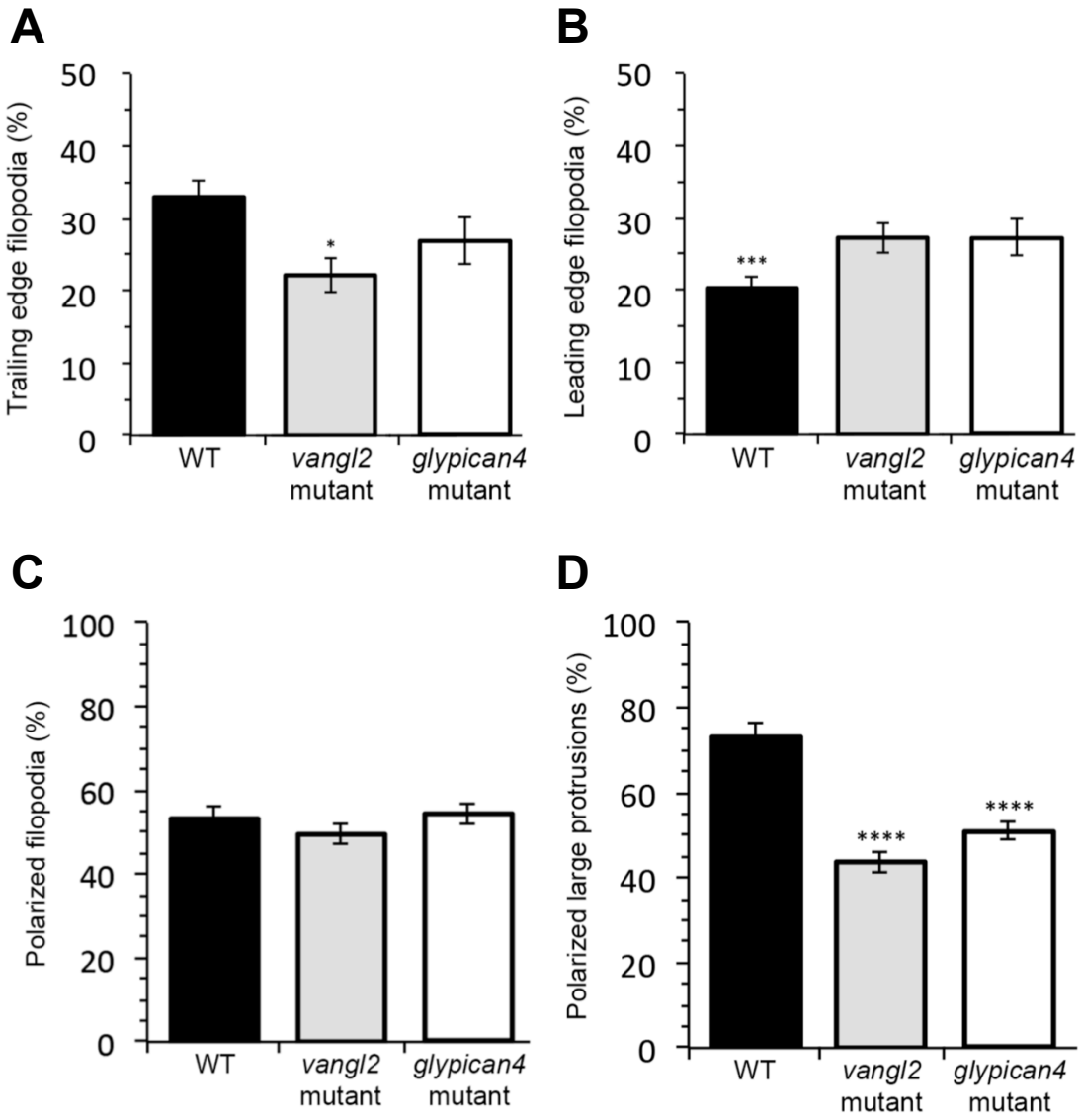

Figure 13 Planar Polarized Membrane Protrusions in Wild-Type versus PCP Mutant Cells: Graphs of polarized filopodia at the leading (A) and trailing (B) edges of ectodermal cells. Graph of total polarized filopodia (C) and large protrusions (D) in ectodermal cells.

wild type (n=12 cells, 8 embryos), *vangl2*$^{m209/m209}$ (n=10 cells, 7 embryos), and *glypican4*$^{m119/m119}$ (n=12 cells, 5 embryos). All values are ± SD.
$^{*}P<0.05$, $^{**}P<0.01$, $^{***}P<0.001$, $^{****}P<0.0001$. *P* values are versus wild type, except WT leading edge *P* value is versus WT trailing edge; one-way ANOVA significance test followed by Tukey HSD post-hoc tests.

while filopodia are concentrated at the leading edge of *vangl2* mutant cells (27.27% +/- 6.54%) (Figure 13A, 13B). *glypican4* cells have no membrane bias with an almost equal percentage of filopodia at the leading (27.26% +/- 8.33%) and trailing (27.01 +/- 10.89%) edges (Figure 13A, 13B). Because filopodia behave in a primarily sensory capacity, we suspected the *vangl2* mutant cells have concentrated filopodia at the leading edge in an effort to sense and correct cell trajectory (Jacinto and Wolpert, 2001). Previous research suggests wild-type cells predominantly produce membrane protrusions at the leading edge, but our work challenges these notions. We suspect wild-type cells produce more protrusions at the trailing edge to maintain mediolateral intercalation and cell trajectory for following cells.

In contrast, *vangl2* and *glypican4* mutant ectodermal cells have a significant reduction in the percentage of polarized large membrane protrusions when compared to wild-type ectodermal cells (Figures 13D, 14). In wild-type cells, an average of 73.10% +/- 11.28% of large protrusions are polarized relative to the path of migration (Figure 13D, 14). In *vangl2* mutant cells, only 43.76% +/- 8.24% of large protrusions are polarized, and 50.97% +/- 7.15% of large protrusions are polarized in *glypican4* mutant cells (Figure 13D, 14). Because large membrane protrusions are integral to force generation and, in turn, cell migration, the loss of large membrane protrusion polarity may explain the meandering trajectories observed in PCP mutant embryos.

Since Vangl2 localizes at the cell surface around mid-gastrulation but PCP phenotypes are not detectable until late gastrulation, we reviewed membrane polarization in *vangl2* morphant cells at mid-gastrulation to characterize large membrane protrusion

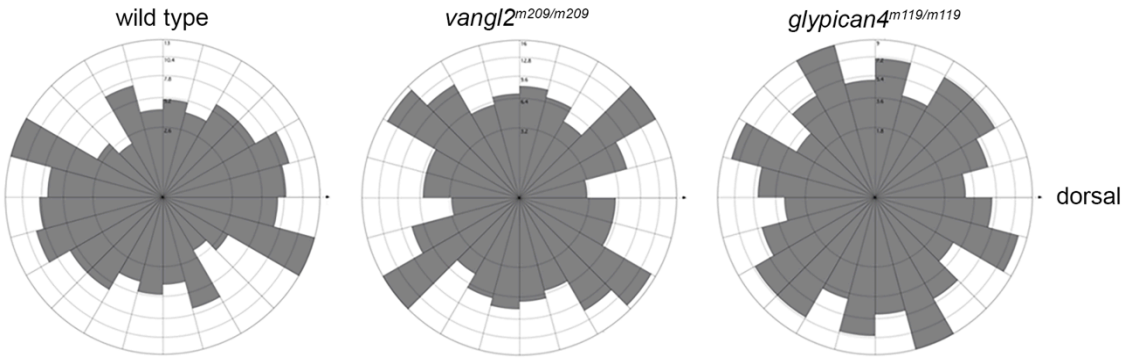

Figure 14 Large Membrane Protrusion Distributions in PCP Mutant Ectodermal Cells: Rose diagrams illustrating frequency and distribution of large membrane protrusions in wild-type, *vangl2* mutant, and *glypican4* mutant ectodermal cells to support large protrusion polarity assessment. Dorsal label indicates direction of migration path.

wild type (n=12 cells, 8 embryos), *vangl2*$^{m209/m209}$ (n=10 cells, 7 embryos), and *glypican4*$^{m119/m119}$ (n=12 cells, 5 embryos).

polarization. An analysis of polarized large membrane protrusions showed 51.88% +/- 7.45% of *vangl2* morphant large protrusions are polarized within 45° of the path of migration (Figure 15). Similarly, 51.16% +/- 10.67% of wild-type large membrane protrusions are polarized at this time (Figure 15). These results indicate large membrane protrusion polarization occurs after mid-gastrulation when PCP-dependent activities increase.

vangl2 mutant ectodermal cells have decreased directness

Next, we confirmed the meandering trajectories by manually tracking ectodermal cells, and calculating a directness value based on the cell's Euclidean distance versus its accumulated distance (Figure 16). Wild-type cells have a directness value of 0.96 +/- 0.03 (Figure 16B). A directness value of 1.00 represents a perfectly straight trajectory, but the directness value is not indicative of a cell's ability to travel along the path of migration. A cell may have a directness value of 1, but it may be traveling in the wrong direction. *vangl2* mutant cells exhibit a loss of directness with a value of 0.83 +/- 0.19. Surprisingly, *glypican4* mutant cells have no significant loss of directness 0.94 +/- 0.06 (Figure 16B).

vangl2 and *glypican4* mutant ectodermal cells produce increased productive large protrusions

Productive protrusions are a novel classification for the purpose of this membrane protrusion analysis. For a large plasma membrane protrusion to be classified as "productive," the cell body must translocate in the direction of the membrane protrusions. During zebrafish gastrulation wild-type ectodermal cells have an average of 1.58 +/- 0.79 productive protrusions (Figure 17). PCP mutants have an excess of

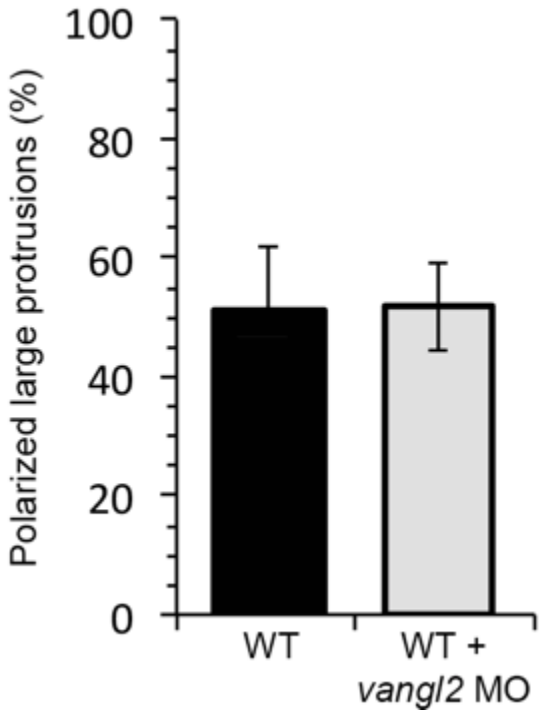

Figure 15 Large Membrane Protrusion Polarity is not Established at Mid-Gastrulation (80% Epiboly): Graph of polarized large membrane protrusions per ectodermal cell in wild-type and *vangl2* morphant embryos at mid-gastrulation (80% epiboly).

wild type (n=9 cells, 7 embryos); *vangl2* morphant (MO) (n=10 cells, 6 embryos). All values are ± SD. *P* values are versus wild type; two-tailed unpaired *t*-test.

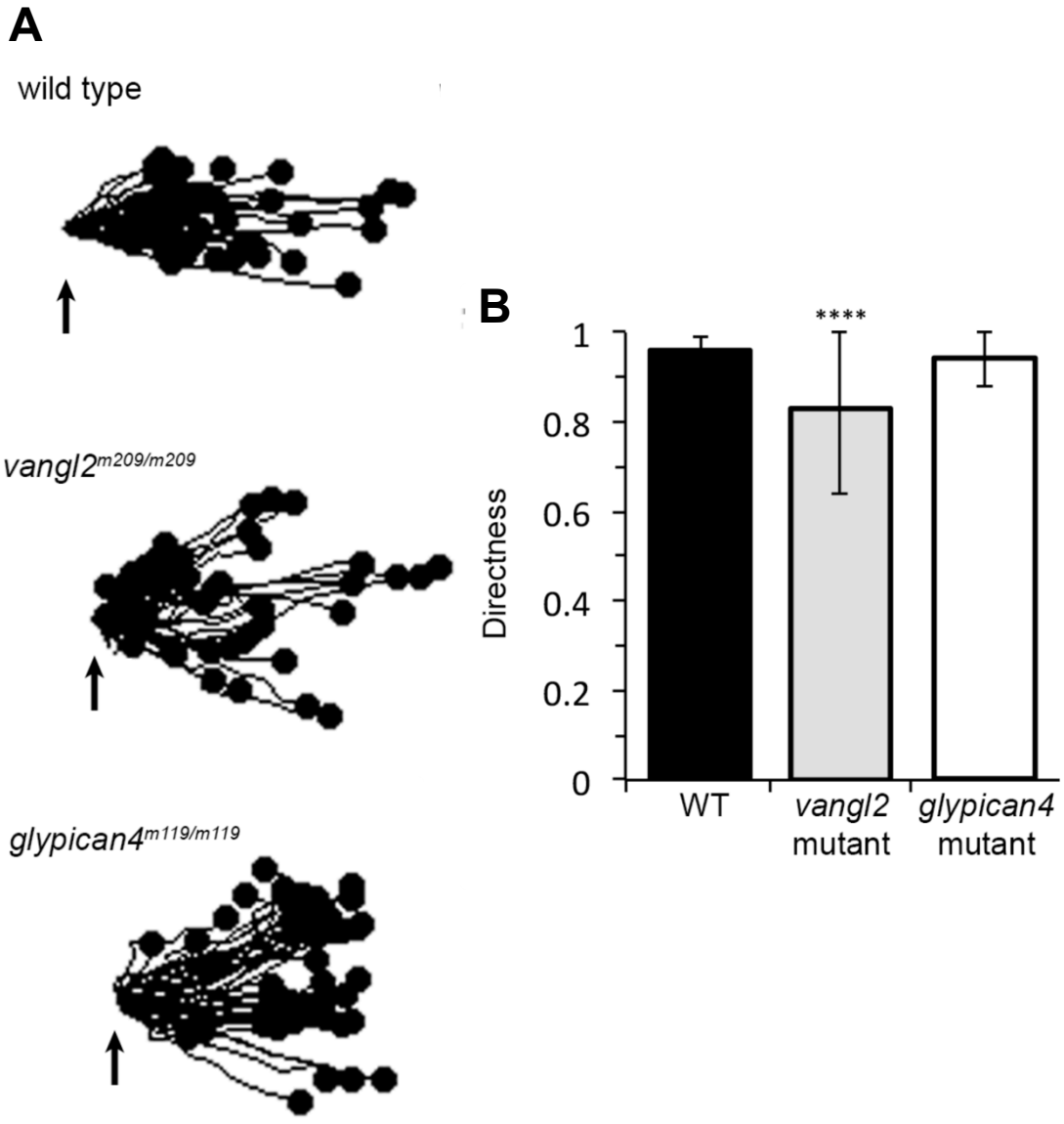

Figure 16 Trajectory Plots and Loss of Directness in PCP Mutant Ectodermal Cells: Wild-type, *vangl2* mutant, and *glypican4* mutant ectodermal cell trajectory plots (A). Arrows indicate origin. Graph of wild-type, *vangl2* mutant, and *glypican4* ectodermal directness values (B).

wild type (n=50 cells, 11 embryos), *vangl2*$^{m209/m209}$ (n=51 cells, 13 embryos), and *glypican4*$^{m119/m119}$ (n=50 cells, 8 embryos). All values are ± SD.
$P<0.05$, $^{**}P<0.01$, $^{***}P<0.001$, $^{****}P<0.0001$. *P* values are versus wild type; one-way ANOVA significance test followed by Tukey HSD post-hoc tests.

productive protrusions, which is especially relevant to the embryonic convergence and extension phenotype. *glypican4* mutants produce an average of 2.92 +/- 0.79 productive protrusions, and *vangl2* mutants produce an average of 2.50 +/- 0.71 productive protrusions (Figure 17). Conceptually, productive protrusions represent frequent directional changes and, therefore, contribute to the embryonic convergence and extension phenotype.

vangl2 and *glypican4* ectodermal cells exhibit planar cell polarity defects

Early work establishes cellular length-width ratios (LWR), mediolateral alignment (MLA), and velocity among mesodermal cells in *vangl2* mutant and wild-type gastrulae (Jessen et al., 2002). Mesodermal cells have a lower LWR and MLA in *vangl2* mutants compared to wild-type gastrulae. The LWR signifies cellular polarity as it indicates cell body elongation. To confirm the rounder cellular phenotype in *glypican4* and *vangl2* mutant ectodermal cells, we measured the length and width of cell bodies to generate LWRs in our mutant cell populations. Wild-type ectodermal cells in the zebrafish gastrula have an average LWR of 2.04 +/- 0.58 (Figure 18). PCP mutant cells have decreased LWRs, representative of their loss of polarity. Of the ectodermal gastrulae cells examined, *vangl2* mutant cells have an average LWR of 1.46 +/- 0.35, while *glypican4* mutant cells have an average LWR of 1.54 +/- 0.34 (Figure 18). Similarly, a lower MLA correlates to a loss of mediolateral intercalation and organized planar trajectory. To quantify MLA, we measured the angle of the cell body relative to the path of migration. 92.00% of wild-type ectodermal cells are oriented within 20° of the path of migration (Figure 18). In contrast only 20.00% of *vangl2* and 32.65% of *glypican4* mutant ectodermal cells are oriented

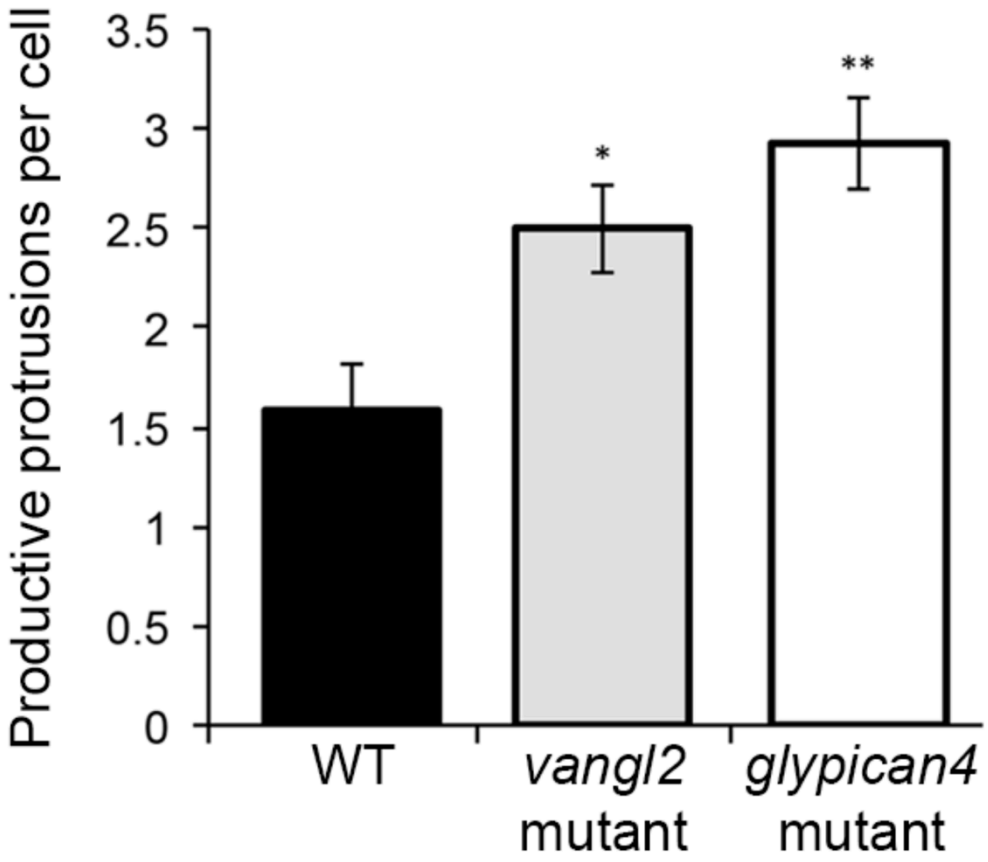

Figure 17 Large Membrane Protrusion Productivity Enhancement in PCP Mutant Ectodermal Cells: Graph of wild-type, *vangl2* mutant, and *glypican4* mutant ectodermal cell productive protrusions.

wild type (n=12 cells, 8 embryos), *vangl2*$^{m209/m209}$ (n=10 cells, 7 embryos), and *glypican4*$^{m119/m119}$ (n=12 cells, 5 embryos). All values are ± SD.
**P*<0.05, ***P*<0.01, ****P*<0.001, *****P*<0.0001
P values are versus wild type; one-way ANOVA significance test followed by Tukey HSD post-hoc tests.

	LWR	MLA (%)	velocity (μm/min)
wild type	2.04 +/- 0.58	92	1.08 +/- 0.49
vangl2$^{m209/m209}$	1.46 +/- 0.35**	20	0.98 +/- 0.54
glypican4$^{m119/m119}$	1.54 +/- 0.34****	33	1.18 +/- 0.28

Figure 18 PCP Mutant Ectodermal Cells Present Hallmarks of PCP: Table of length-width ratios (LWR), mediolateral alignment (MLA), and velocity for wild-type, *vangl2* mutant, and *glypican4* mutant ectodermal cells.

wild type (n=50 cells, 13 embryos); *vangl2*$^{m209/m209}$ (n=10 cells, 8 embryos); *glypican4*$^{m119/m119}$ (n=49 cells, 5 embryos). All values are ± SD.

$^{*}P<0.05$, $^{**}P<0.01$, $^{***}P<0.001$, $^{****}P<0.0001$
P values are versus wild type; one-way ANOVA significance test followed by Tukey HSD post-hoc tests.

properly. Between wild-type, *vangl2* mutant, and *glypican4* mutant ectodermal cells, cell velocity has no significant change (Figure 18).

2.3 Conclusion

In the early stages of zebrafish gastrulation, progenitor cells utilize an amoeboid mode of migration via the production of blebs and actin-rich filopodia and lamellipodia (Diz-Muñoz et al., 2016; Paluch and Raz, 2013). During this phase cells follow an indirect trajectory as they are loosely packed and radially intercalated to accommodate early epiboly and internalization (Marsden and DeSimone, 2001; Warga and Kimmel, 1990; Yin et al., 2008). As the PCP pathway becomes active during mid-gastrulation, migrating cells elongate and mediolaterally intercalate (Jessen and Solnica-Krezel, 2005). These organizational changes are integral to directed dorsal migration and convergence and extension movements. Cell trajectories straighten while they transition from an amoeboid to a mesenchymal mode of migration. As these PCP-mediated changes occur, cells generate increased numbers of lamelliopodia and filopodia and fewer blebs.

When compared to late gastrulae stage wild-type embryos, *vangl2* mutant embryos have an increase in filopodia and lamellipodia-like large membrane protrusions, while the percentage of polarized large membrane protrusions lowers significantly. *vangl2* mutant ectodermal cells may have increased non-polarized membrane protrusions because of their diminished ability to form cell-matrix interactions (Latimer and Jessen, 2010). *glypican4* ectodermal cells have no significant change in filopodia or large membrane protrusions relative to wild type. *glypican4* mutant embryos have total fibronectin protein levels consistent with those of wild-type embryos and, therefore, likely

have no defect in cell-matrix interactions (Latimer and Jessen, 2010). The number of productive protrusions increases in *vangl2* and *glypican4* mutant cells. The decrease in polarized large membrane protrusions and increase in productive protrusions corresponds with the loss of directness among the dorsally migrating cells and may be partially responsible for the *vangl2* mutant convergence and extension phenotype.

Interestingly, *glypican4* has no significant loss of directness. However, a review of the trajectory plots reveals a broad spread in cell paths. *glypican4* mutants may utilize productive protrusions to maintain their directness. Ectodermal cells in *glypican4* mutant embryos do not have an increase in the number of membrane protrusions. While *glypican4* mutant ectodermal cells do not have an increase in the number of membrane protrusions, they have a loss of polarized large membrane protrusions and an increase in productive protrusions. My analysis suggests *glypican4* ectodermal cells fail to form mediolaterally-oriented large membrane protrusions, which may, in part, drive their ineffective migration. The data presented here indicate Vangl2 and Glypican4 differentially regulate membrane-protrusive activity.

Since Vangl2 localizes at the cell surface at approximately mid-gastrulation (80% epiboly) but Vangl2-dependent phenotypes are not detectable until late gastrulation, we characterized membrane-protrusive activity in *vangl2* morphant embryos at mid-gastrulation. At this stage, *vangl2* morphant ectodermal cells produce increased large membrane protrusions but not filopodia. Neither wild-type or *vangl2* morphant ectodermal cells produce particularly polarized large membrane protrusions. We suspect

the membrane protrusion defects associated with Vangl2 activity begin to occur at mid-gastrulation and progress as gastrulation continues.

CHAPTER THREE. *vangl2* mRNA-Injected and *prickle1a* Morphant Ectodermal Cells Present Membrane Protrusion Defects

3.1 Introduction

A hallmark of PCP, core protein overexpression results in a convergence and extension phenotype more severe than that of the corresponding PCP null mutants (Yang and Mlodzik, 2015)(Figure 19A,B). A particular level of Vangl2 expression is required for effective PCP and, in turn, convergence and extension movements. However, published work has not addressed Vangl2 overexpression cellular phenotypes. In an effort to determine the effects of Vangl2 overexpression on cell membrane protrusion formation and polarization, we conducted an in depth membrane protrusion study using time-lapse microscopy.

In fly epithelial tissues, some core PCP proteins asymmetrically localize (Montcouquiol, 2006; Strutt et al., 2002) Vangl2 and Prickle1a localize at the proximal side of the cell, while Frizzled, Diego, and Dishevelled localize distally (Goodrich and Strutt, 2011). Early work in fly revealed the cytoplasmic protein Prickle physically binds to Van Gogh and modulates its function (Bastock et al., 2003; Jenny, 2003). Since then, our lab established a corresponding relationship between Vangl2 and Prickle1a in zebrafish (Dohn et al., 2013). Wild-type embryos injected with *prickle1a* morpholino exhibit a convergence and extension defect slightly less severe than *vangl2* mutant embryos (Carreira-Barbosa et al., 2003; Veeman et al., 2003)(Figure 19C). Additional work from our lab concluded loss of Prickle results in decreased fibronectin protein levels similar to those of *vangl2* mutants (Dohn et al., 2013). To date, published reports do not

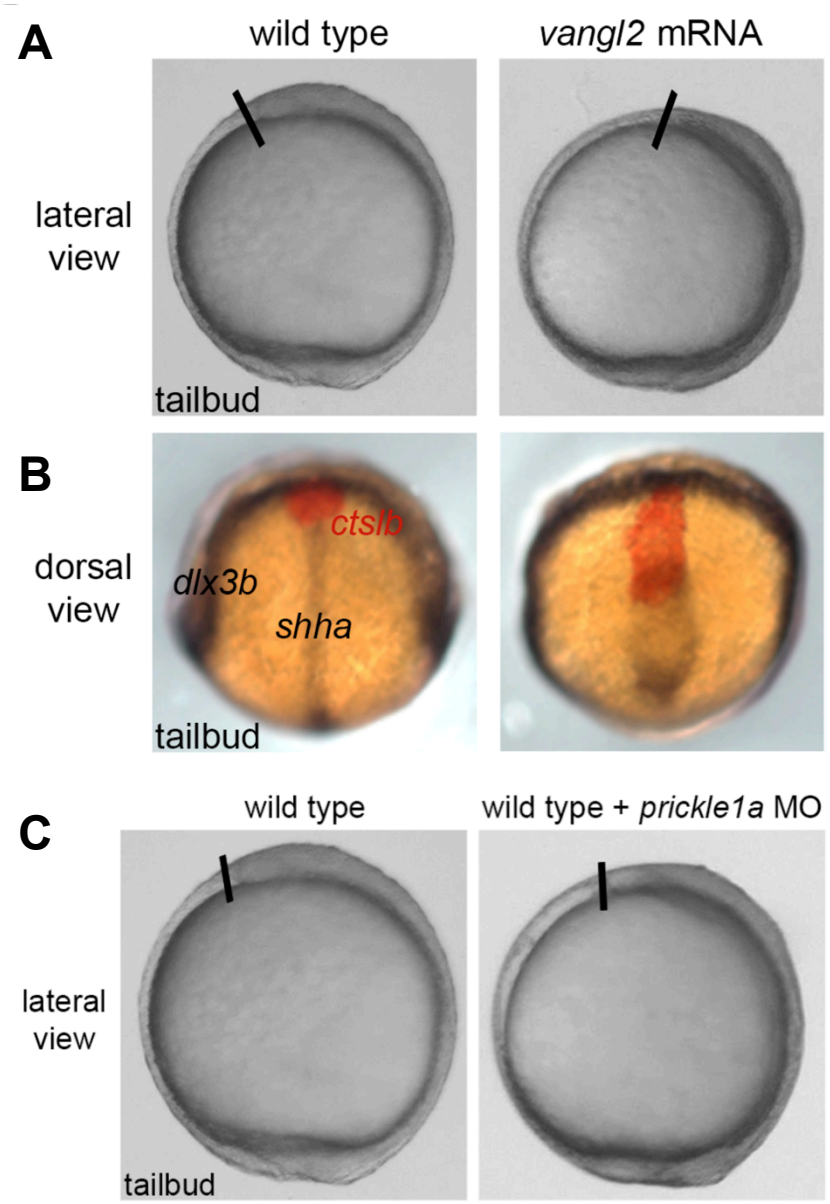

Figure 19 Convergence and Extension Phenotypes in *prickle1a* Morphant Embryos and Embryos with Vangl2 Overexpression: Differential interference contrast (DIC) images of wild-type embryo versus wild-type embryo injected with synthetic *vangl2* mRNA, lateral view (A). Whole-mount *in situ* hybridization of wild-type embryo versus wild-type embryo injected with *vangl2* mRNA, dorsal view (B). DIC images of wild-type versus *prickle1a* morphant embryos, lateral view (C).

cover the effects of Prickle1a on PCP, directed migration, or membrane protrusion formation and polarization.

Because Vangl2 overexpression mimics the *vangl2* mutant convergence and extension phenotype, we hypothesized Vangl2 overexpression results in excessive non-polarized membrane protrusions, loss of directness, and decreased mediolateral alignment and length-width ratios. Because they are binding partners and co-localize at the plasma membrane in the fly, we hypothesized Prickle1a regulates membrane-protrusive activity similar to Vangl2.

3.2 Results

Vangl2 mRNA-injected wild-type and *prickle1a* morphant ectodermal cells produce excess non-polarized membrane protrusions

To test our hypothesis that Vangl2 overexpression and loss of Prickle1a results in a membrane protrusion defect similar to that of *vangl2* mutant embryos, we performed a membrane protrusion analysis, quantifying membrane protrusions. The functionality of the *vangl*2 mRNA for Vangl2 overexpression studies was confirmed with western blot and immunohistochemistry (Figure 20). Our data from a time-lapse confocal microscopy study indicates Vangl2 overexpression in wild-type embryos increases the number of membrane protrusions in migrating ectodermal cells (Figure 21A). Cells with Vangl2 overexpression produce an average of 27.63 +/- 4.38 filopodia and 6.44 +/- 0.55 large protrusions, even more than *vangl2* mutant ectodermal cells (Figures 21B, 21C). *prickle1a* morphant embryos underwent the same preparations and procedures indicated

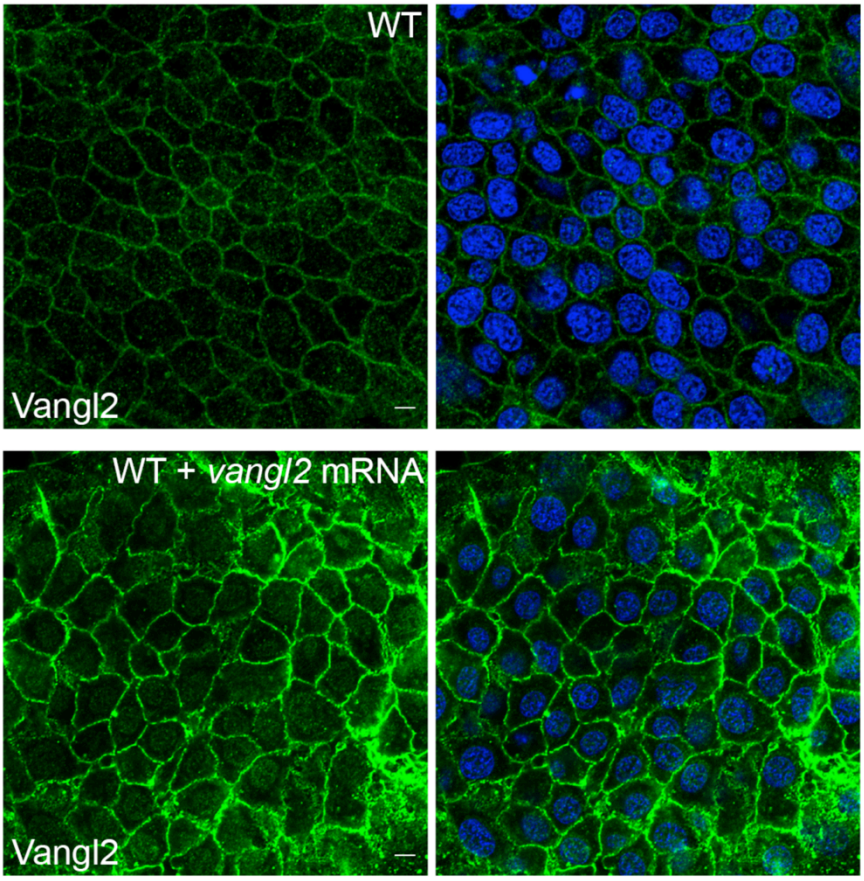

Figure 20 *vangl2* mRNA Validation: Non-injected wild-type embryos versus wild-type (WT) embryos injected with *vangl2* mRNA. Confocal micrographs of embryos treated with Vangl2 polyclonal antibody (green) and DAPI (blue). Scale bar = 5 μm.

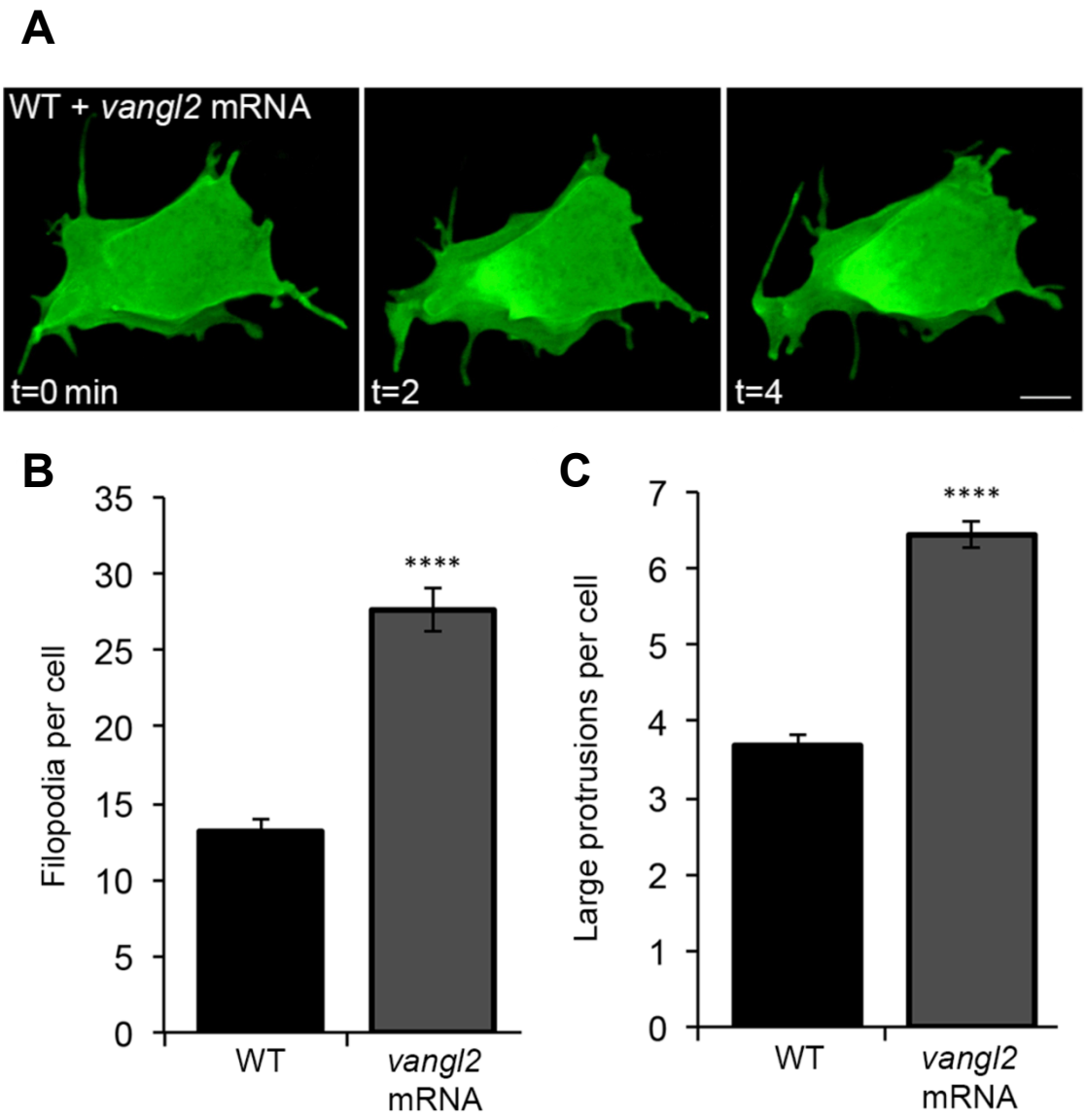

Figure 21 Vangl2 Overexpression Causes Increased Membrane-Protrusive Activity: Time-lapse Confocal micrographs of ectodermal cells from embryos injected with *vangl2* mRNA at 1-cell stage and membrane green fluorescent protein (memGFP) at 8-cell stage (A). Time-lapse duration of 20 min with 2 min intervals. Scale bar = 5 µm. Graph depicting average number of filopodia (B) and large membrane protrusions (C) per ectodermal cell.

wild type (n=11 cells, 8 embryos); *vangl2*-injected wild-type embryos (n=10 cells, 7 embryos). All values are ± SD. ****P<0.0001; P values are versus wild type; two-tailed unpaired t-test.

with all previous membrane protrusion studies in this work (Figure 22A). As hypothesized, *prickle1a* morphant ectodermal cells produce more plasma membrane protrusions with an average of 22.07 +/- 3.94 filopodia and 5.34 +/- 0.49 large membrane protrusions (Figures 22B, 22C).

We measured filopodia polarity against the path of migration to determine the effects of Vangl2 overexpression and loss of Prickle1a on polarized protrusive activity. *vangl2* mutant ectodermal cells have no significant loss of polarized filopodia when compared to wild type, but cells from wild-type embryos injected with *vangl2* mRNA or *prickle1a* morpholino have less polarized filopodia than wild type (52.23% +/- 9.95%). 40.74% +/- 4.28% of filopodia from cells with Vangl2 overexpression and 40.42% +/- 2.52% of filopodia in *prickle1a* morphant cells are polarized (Figures 23A, 24A). We found no significant difference between the percentage of polarized filopodia at the leading edge and trailing edge in either Vangl2 overexpression cells or *prickle1a* morphant cells. In wild-type cells, the trailing edge has a subtle increase in polarized filopodia, and *vangl2* mutant cells have slightly more polarized filopodia at the leading edge. Because filopodia behave primarily in a sensory capacity, we suspect their fluctuations may be indicative of changes to the fibronectin extracellular matrix.

An analysis of large protrusion polarity revealed a significant drop in large membrane protrusion polarity in ectodermal cells with Vangl2 overexpression and Prickle1a knockdown. In cells treated with *vangl2* mRNA, only 49.64% +/- 17.45% of large membrane protrusions are polarized relative to the path of migration (Figures 23B, 23C). Of the total number of large protrusions from *prickle1a* morphant cells, 47.91% +/-

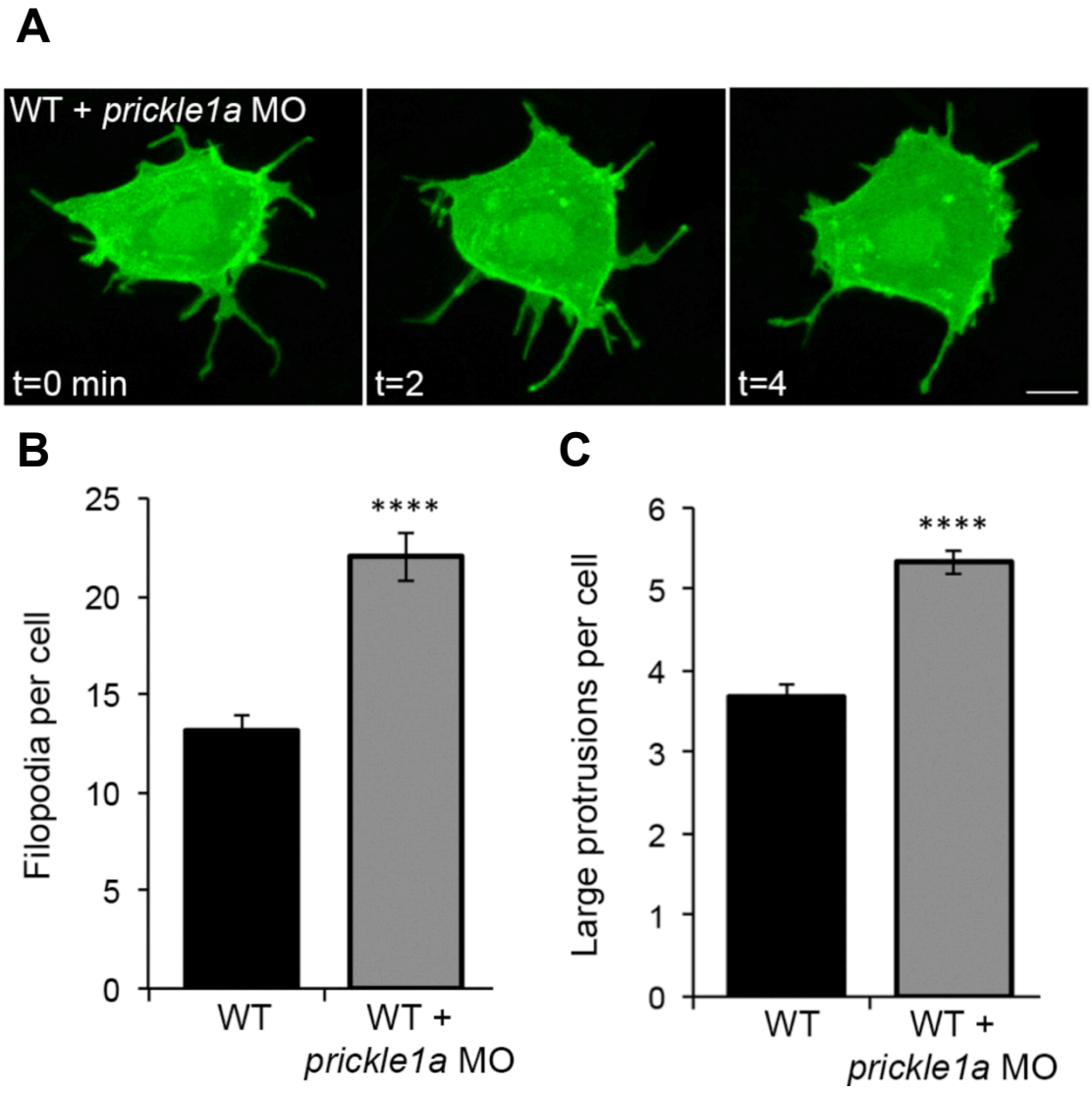

Figure 22 Loss of Prickle1a Causes Increased Membrane-Protrusive Activity: Confocal micrographs of ectodermal cells from *prickle1a* morphant embryos with mosaic membrane green fluorescent protein (memGFP) at expression (A). Time-lapse duration of 20 min with 2 min intervals. Scale bar = 5 μm. Graph depicting average number of filopodia (B) and large membrane protrusions (C) per ectodermal cell. Wild type (n=11 cells, 8 embryos); *prickle1a* morphant embryos (n=10 cells, 8 embryos). All values are ± SD. ****$P<0.0001$; P values are versus wild type; two-tailed unpaired t-test.

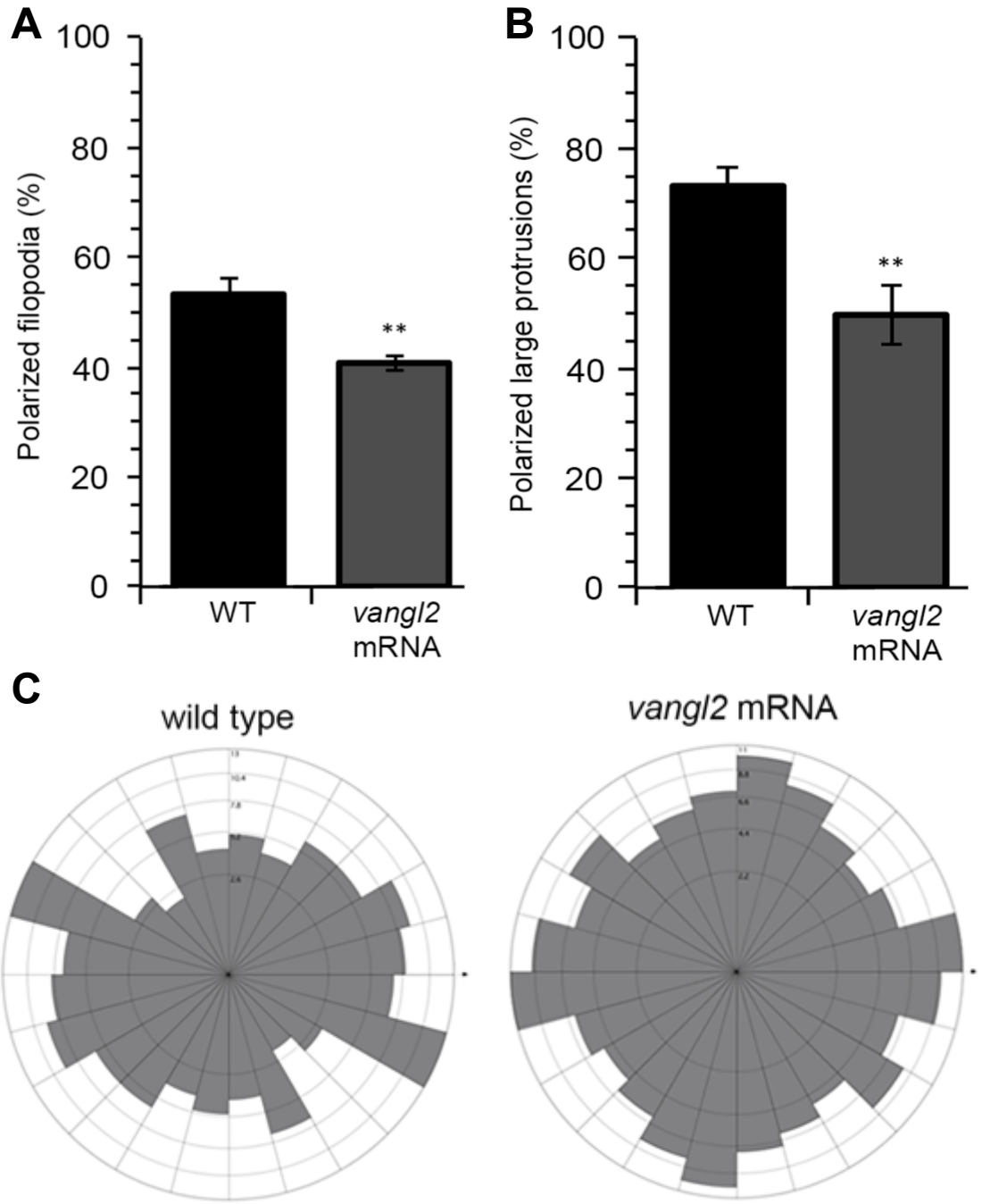

Figure 23 Decreased Polarized Membrane Protrusions in *vangl2*-Injected Embryos: Graph of polarized filopodia (A) and large protrusions (B) in wild-type and *vangl2*-injected embryos. Rose diagrams depicting frequency and distribution of large protrusions (C). Wild type (n=11 cells, 8 embryos); *vangl2*-injected embryos (n=10 cells, 8 embryos). All values are ± SD. $^{**}P<0.01$; *P* values are versus wild type; two-tailed unpaired *t*-test.

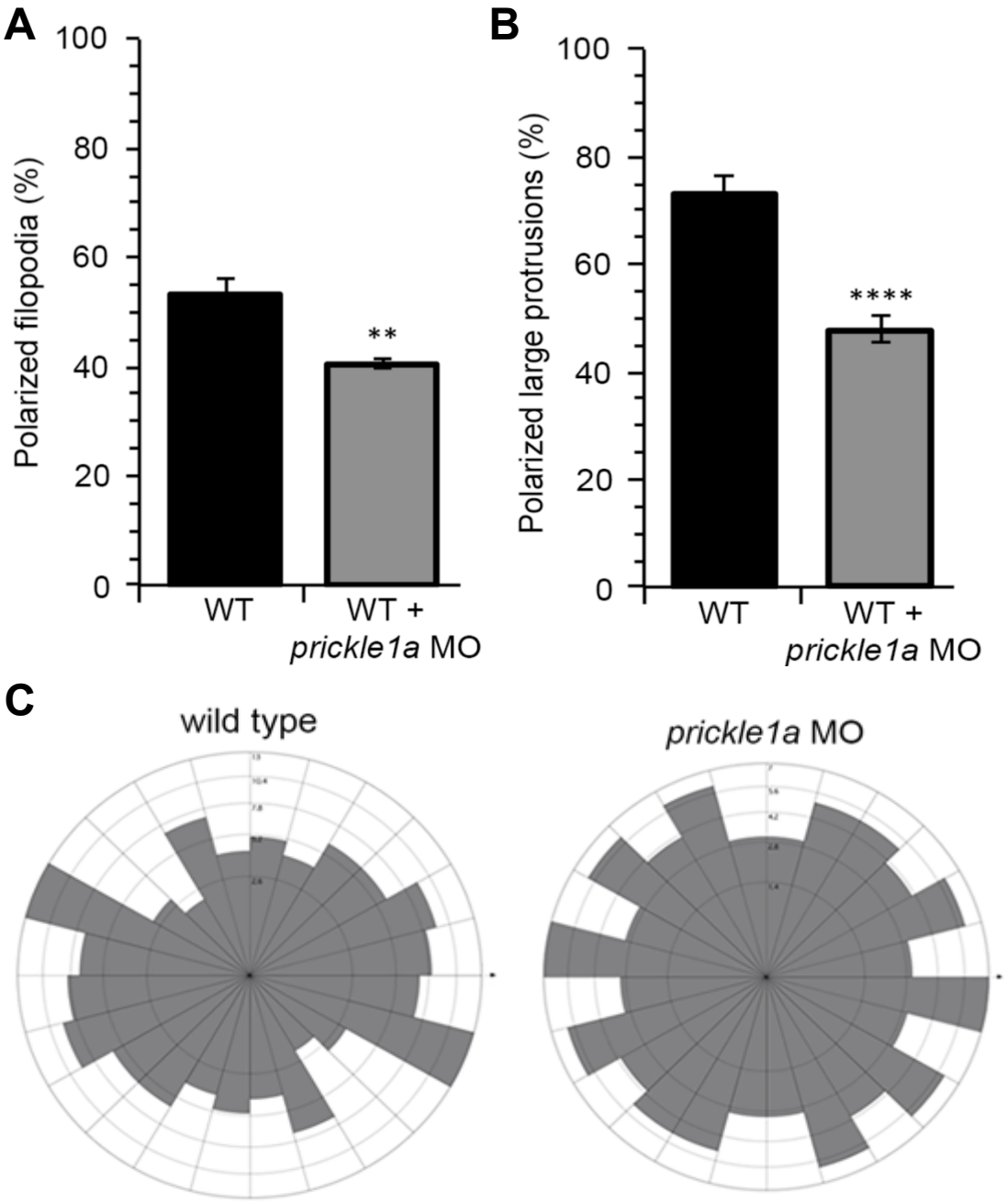

Figure 24 Decreased Polarized Membrane Protrusions in *prickle1a* Morphant Embryos: Graph of polarized filopodia (A) and large protrusions (B) in wild-type and *prickle1a* morphant embryos. Rose diagrams depicting frequency and distribution of large protrusions (C). wild type (n=11 cells, 8 embryos); *prickle1a* morphant embryos (n=10 cells, 8 embryos). All values are ± SD. $^{**}P<0.01$, $^{****}P<0.0001$; *P* values are versus wild type; two-tailed unpaired *t*-test.

7.45% are polarized (Figures 24B, 24C). The percentages of polarized large membrane protrusions from both of these studies are in line with the percentage of polarized large protrusions in *vangl2* mutant cells. Because the cell has four distinct sides and approximately half of the large protrusions are polarized at the leading edge and trailing edge, we can assume the distribution of large membrane protrusions is randomized in all directions in *vangl2* mutants, *prickle1a* morphants, and wild-type embryos with Vangl2 overexpression (Figures 23C, 24C). Randomized large membrane protrusions may contribute to loss of directness among these groups.

vangl2 mRNA-injected and *prickle1a* morphant ectodermal cells exhibit PCP defects

We performed manual tracking to establish if loss of Prickle1a and gain of Vangl2 results in loss of cell trajectory directness similar to the loss of directness observed in *vangl2* mutant ectodermal cells. In Vangl2 gain of function and Prickle1a loss of function studies, ectodermal cells exhibit loss of directionality when tracked through a time-lapse set of micrographs (Figures 25, 26). *prickle1a* morphant cells have an average directness value of 0.83 +/- 0.25, while *vangl2* mutant cells have a directness value of 0.83 +/- 0.19 (Figures 26). With a directness value of 0.69 +/- 0.26, ectodermal cells treated with *vangl2* mRNA for overexpression have the most dramatic loss of directness (Figures 25). Notably, Vangl2 overexpression results in an embryonic phenotype more severe than *vangl2* mutants. The severity of the phenotype corresponds with the migrating cells' loss of directness during convergence and extension movements.

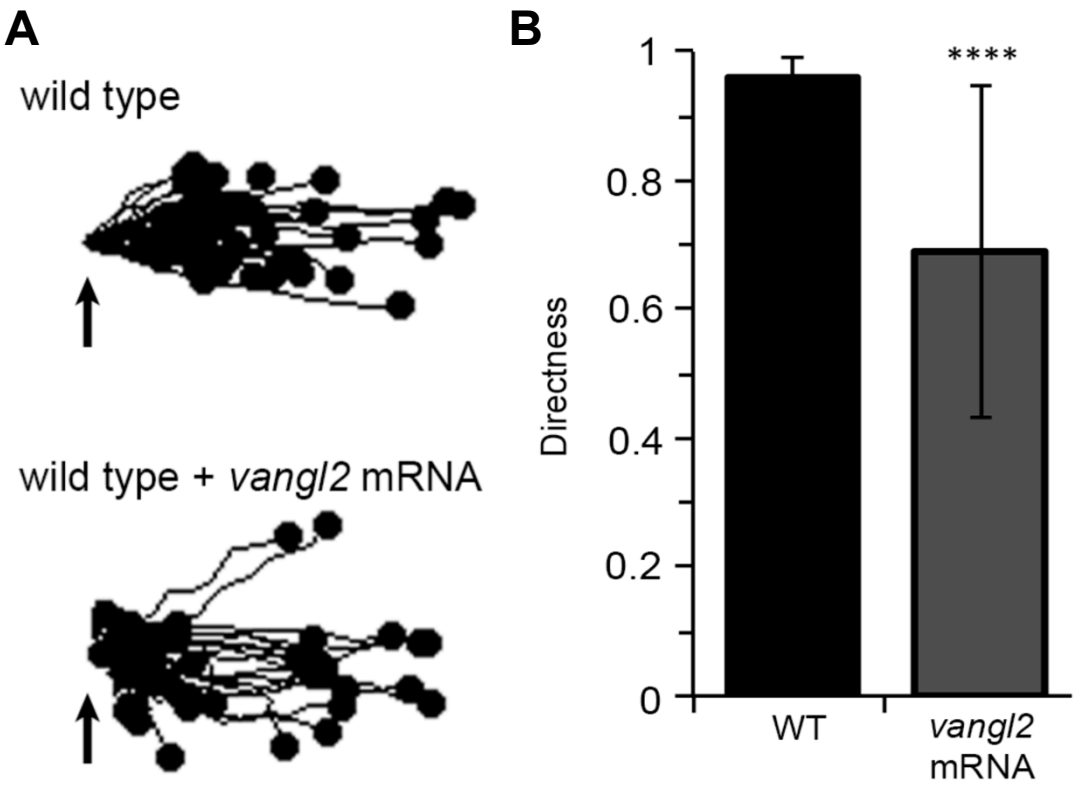

C

	LWR	MLA (%)	velocity (μm/min)
wild type	2.04 +/- 0.58	92	1.08 +/- 0.49
wild type + *vangl2* mRNA	1.56 +/- 0.43****	54	0.8 +/- 0.43

Figure 25 Defective Cell Migration and PCP in *vangl2*-Injected Embryos: Trajectory plots for wild-type (WT) and *vangl2*-injected embryos (A). Arrow marks origin. Graph of directness values for wild-type and *vangl2*-injected embryos (B). Table with length-width ratios (LWR), mediolateral alignment (MLA), and velocity for WT versus *vangl2*-injected embryos (C).
WT (n=50 cells, 11 embryos); *vangl2*-injected (n=43 cells, 9 embryos). All values are ± SD. ****$P<0.0001$; P values are versus wild type; two-tailed unpaired t-test.

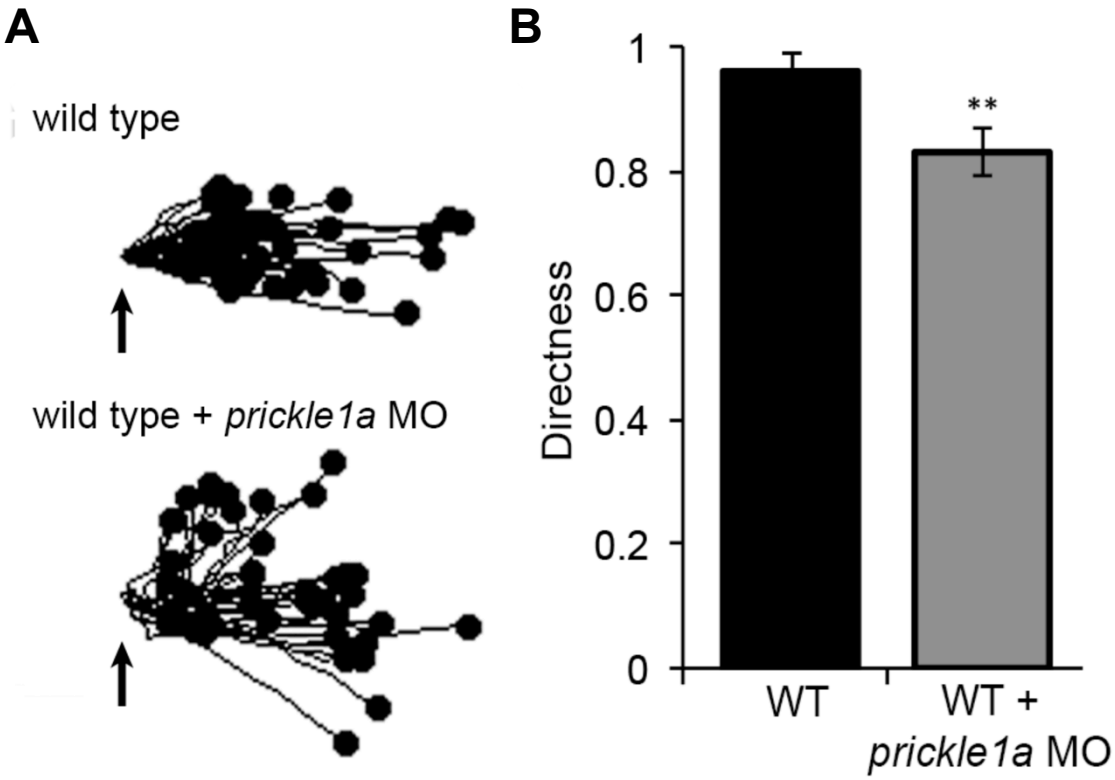

C

	LWR	MLA (%)	velocity (μm/min)
wild type	2.04 +/- 0.58	92	1.08 +/- 0.49
wild type + *prickle1a* MO	1.56 +/- 0.39****	56	0.99 +/- 0.34

Figure 26 Defective Cell Migration and PCP in *prickle1a* Morphant Embryos: Trajectory plots for wild-type (WT) and *prickle1a* morphant embryos (A). Arrow marks origin. Graph of directness values for wild-type and *prickle1a* morphant embryos (B). Table with length-width ratios (LWR), mediolateral alignment (MLA), and velocity for WT versus *prickle1a* morphant embryos (C).
WT (n=50 cells, 11 embryos); *prickle1a* morphants (n=45 cells, 9 embryos). All values are ± SD. $^{**}P<0.01$, $^{****}P<0.0001$; *P* values are versus wild type; two-tailed unpaired *t*-test.

We collected length-width ratios (LWR) and mediolateral alignment (MLA) to confirm cell polarity defects in treated embryos. As previously noted, wild-type ectodermal cells have a LWR of 2.04 +/- 0.58, indicating wild-type cells are twice as long as they are wide. Additionally with a MLA of 92.00%, a high percentage of these wild-type cells are oriented within 45° of the migratory path. *vangl2* mutant cells have a loss of LWR with a value of 1.46 +/- 0.35 and a MLA of 20.00%. We hypothesized treating cells with *vangl2* mRNA or *prickle1a* morpholino would result in values similar to those of *vangl2* mutant cells. Ectodermal cells with Vangl2 overexpression have an LWR of 1.56 +/ 0.43, and *prickle1a* morphant cells have an LWR of 1.56 +/- 0.39 (Figures 25C, 26C). However, the MLAs of cells under the two conditions are not as severe as the MLA of *vangl2* mutant cells. Cells with Vangl2 overexpression have a mean MLA of 54.00% and cells with *prickle1a* morpholino have a mean MLA of 55.56% (Figures 25C, 26C).

3.3 Conclusion

A hallmark of core PCP proteins, overexpression results in convergence and extension defects in line with the corresponding loss of protein (Yang and Mlodzik, 2015). The convergence and extension phenotype of *vangl2*-injected wild-type embryos is more severe than the phenotype of *vangl2* mutants. However, work characterizing the cellular effects of Vangl2 overexpression has not been reported. We hypothesized overexpression of Vangl2 results in cell polarity and membrane protrusion defects similar to those of *vangl2* mutants. Further, Prickle and Vangl2 have many similarities, which supports our hypothesis that loss of Prickle1a results in cell polarity and membrane protrusion phenotypes similar to those of *vangl2* mutants. Published reports on the core

PCP protein Prickle indicate Prickle not only localizes asymmetrically with Vangl2 on the proximal side of the cell, but also forms a functional complex with Vangl2 (Bastock et al., 2003; Jenny, 2003). Prickle1a knockdown cells have decreased cell surface localization of Vangl2, which may contribute to the similarities between *vangl2* mutant and *prickle1a* morphant embryos as well as the *prickle1a* morphant convergence and extension phenotype (Dohn et al., 2013). At the molecular level, loss of Prickle1a causes diminished fibronectin comparable to *vangl2* mutant embryo fibronectin levels (Dohn et al., 2013).

We found that, similar to *vangl2* mutant embryos, *vangl2*-injected wild-type and *prickle1a* morphant embryos have excess membrane-protrusive activity and decreased membrane protrusion polarity compared to wild-type embryos. Ectodermal cells from *vangl2* mRNA-injected embryos exhibit the most extreme loss of directness, which may contribute to the severity of the embryonic convergence and extension defect. *prickle1a* morphant and *vangl2* mutant cells have similar directness values. An examination of cell polarity indicators, including LWR and MLA, indicates *prickle1a* morphant and *vangl2* mRNA-injected cells have a milder loss of MLA than *vangl2* mutant cells, while cells from *vangl2* mRNA-injected, *vangl2* mutant, and *prickle1a* morphant embryos have corresponding LWRs.

Together, these data confirm our hypothesis that ectodermal cells from *vangl2* mRNA-injected and *prickle1a* morphant embryos have membrane protrusion phenotypes similar to that of *vangl2* mutant embryos. I hypothesize the loss of directness and ineffectual migration trajectories among *vangl2* mRNA-injected cells may contribute, beyond their membrane protrusion defect, to the severity of their embryonic convergence

and extension defect. Additionally, the Vangl2 overexpression embryonic and membrane protrusion phenotypes indicates a particular level of Vangl2 protein is required at cell surface domains associated with its function, namely regulation of PCP and membrane-protrusive activity.

CHAPTER FOUR. Vangl2 Localizes in Erupting Large Membrane Protrusions

4.1 Introduction

Work in the fly established asymmetric localization of the core PCP proteins, Van Gogh, Prickle, Dishevelled, Diego, and Frizzled. Van Gogh and Prickle localize to the proximal side of the cell, while Frizzled, Dishevelled, and Diego localize to the distal side of the cell (Goodrich and Strutt, 2011). At mid-gastrulation stages, Vangl2 localizes at the plasma membrane as PCP-dependent activities, such as mediolateral intercalation, cell elongation, and directed dorsal migration, begin to occur (Sepich et al., 2005; Solnica-Krezel and Sepich, 2012).

In zebrafish, PCP protein localization is difficult to assess as traditional immunolabeling leads to membrane crowding from neighboring cells. Fluorescent fusion proteins have been used to circumvent this problem, but care must be taken to avoid PCP protein overexpression phenotypes (Jessen et al., 2002; Roszko et al., 2015). A previous study of highly polarized notochord cells reported GFP-VANGL2 is asymmetric with an anterior membrane bias (Roszko et al., 2015). However, the GFP-VANGL2 localization study was performed in non-migrating axial cells; therefore, we performed a similar study in migrating ectodermal cells in tailbud stage embryos. Tailbud stage marks the end of gastrulation as PCP is driving the directed migration required for convergence and extension movements during this stage. We hypothesized Vangl2 is enriched at the anterior membrane of migrating gastrula cells. To test this hypothesis, we performed a

GFP-VANGL2 localization analysis on the leading edge, trailing edge, anterior, and posterior cell membranes.

4.2 Results

Vangl2 does not asymmetrically localize in migrating gastrula cells

We injected 8-cell stage embryos with a mixture of human VANGL2 fused to green fluorescent protein (GFP-VANGL2) and membrane-targeted red fluorescent protein (memRFP)(Figure 27). After embryos reached tailbud stage, we collected time-lapse micrographs of the cells to analyze the average GFP-VANGL2 fluorescence intensities at the anterior, posterior, leading edge (dorsal), and trailing edge (ventral) membranes (Figures 28,30). Using the FIJI Plot Profile tool, we generated plot profiles across the anteroposterior and dorsoventral (leading edge/trailing edge) axes (Schindelin et al., 2012). From the memRFP and GFP-VANGL2 raw data, we calculated fluorescence intensity ratios for both anterior to posterior membrane apices and leading edge (dorsal) to trailing edge (ventral) membrane apices. A comparative analysis did not support Vangl2 asymmetry in migrating ectodermal cells at tailbud stage (Figures 29, 31).

Vangl2 is enriched in erupting large membrane protrusions

Despite a lack of evidence to support GFP-VANGL2 localization membrane bias, a close examination of the time-lapse micrographs indicated dynamic GFP-VANGL2 levels within large membrane protrusions. Early on, we hypothesized Vangl2 suppresses or limits membrane-protrusive activity to specific plasma membrane domains, supported by the aforementioned increase in large membrane protrusions and filopodia in *vangl2*

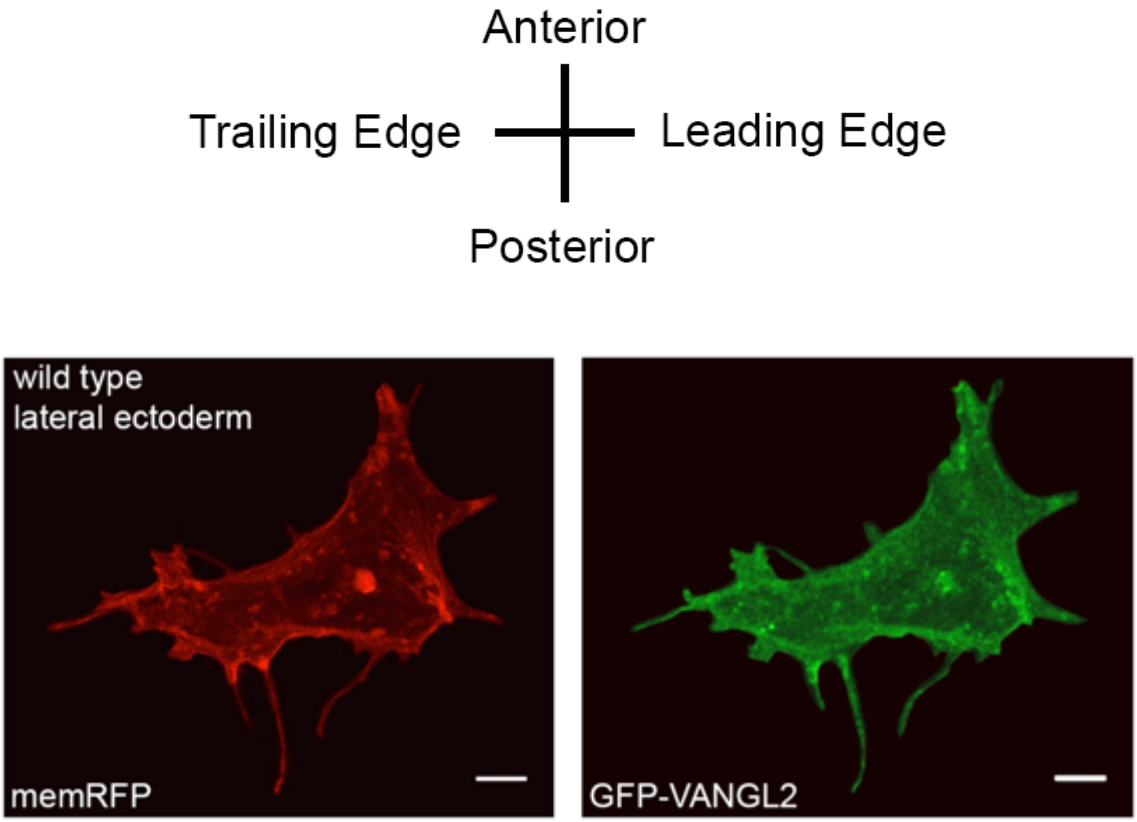

Figure 27 Confocal Micrographs of Wild-Type Ectodermal Cells: Micrographs of migrating lateral ectodermal cells from tailbud stage wild-type embryo injected with membrane-targeted red fluorescent protein (memRFP) and green fluorescent protein fused with VANGL2 (GFP-VANGL2). Scale bar = 5μm.

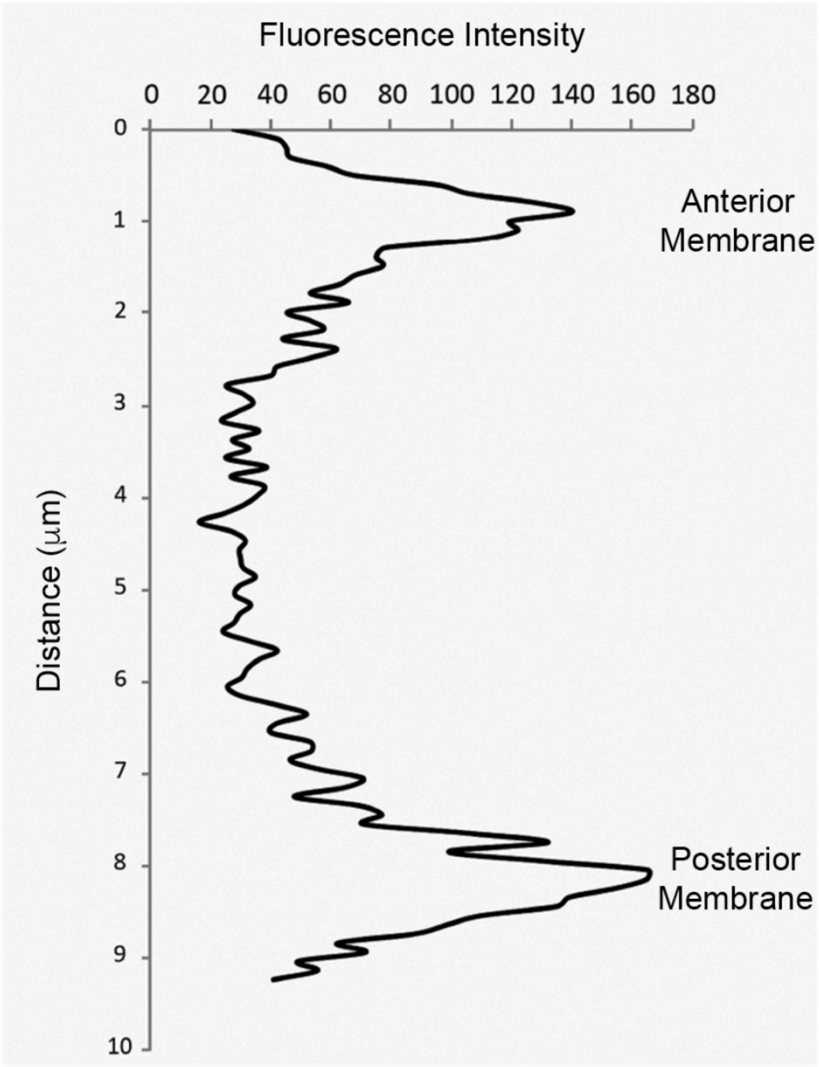

Figure 28 Anteroposterior Axis GFP-VANGL2 Fluorescence Intensity Plot Profile: GFP-VANGL2 fluorescence intensity across the anteroposterior axis of a tailbud stage migrating ectodermal cell. Anterior membrane peak and posterior membrane peak indicate cell surface localization of GFP-VANGL2.

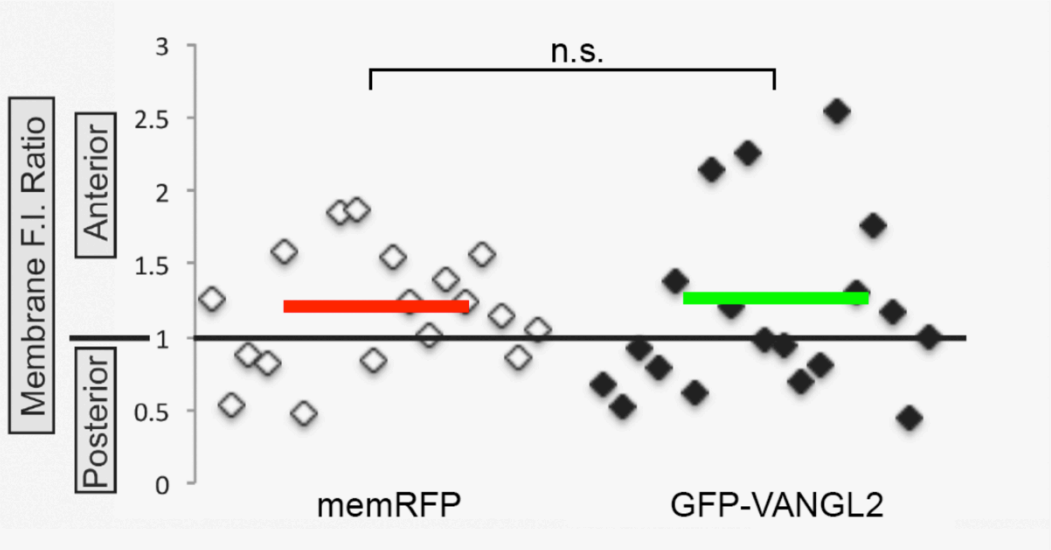

Figure 29 GFP-VANGL2 is not Enriched at Anterior or Posterior Membranes: Fluorescence intensity (F.I.) ratio plot of anterior to posterior apices. Red line indicates mean F.I. for membrane-targeted red fluorescent protein (memRFP). Green line indicates mean F.I. for GFP-VANGL2.
n=18 cells, 15 embryos. n.s. = not significant; two-tailed paired *t*-test.

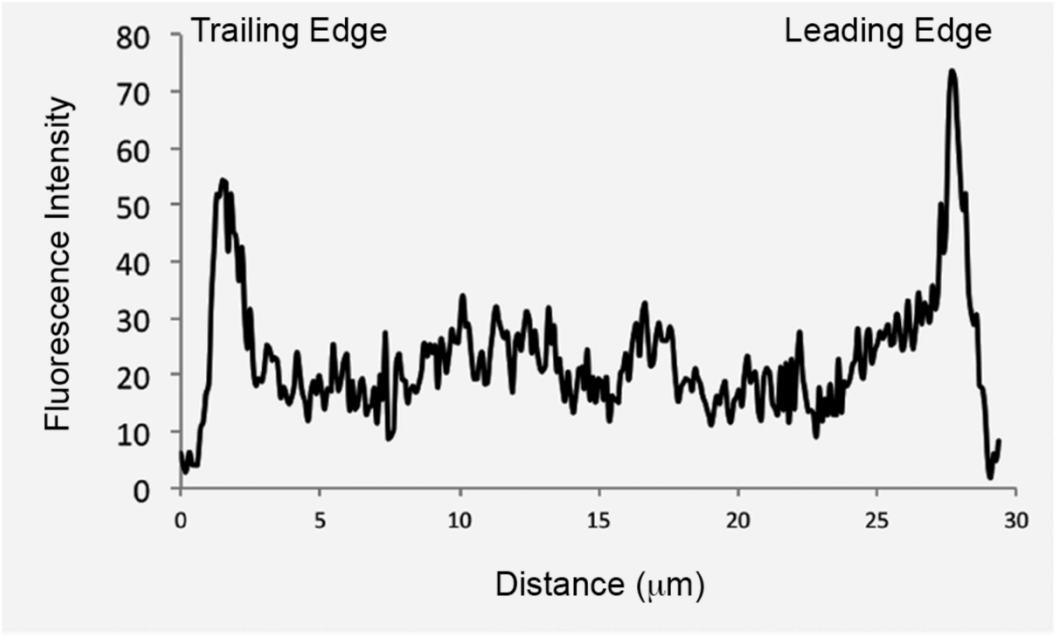

Figure 30 Dorsoventral Axis GFP-VANGL2 Fluorescence Intensity Plot Profile: GFP-VANGL2 fluorescence intensity across the dorsoventral axis of a tailbud stage migrating ectodermal cell. Trailing edge represents ventral membrane peak and leading edge represents dorsal membrane peak, indicating cell surface localization of GFP-VANGL2.

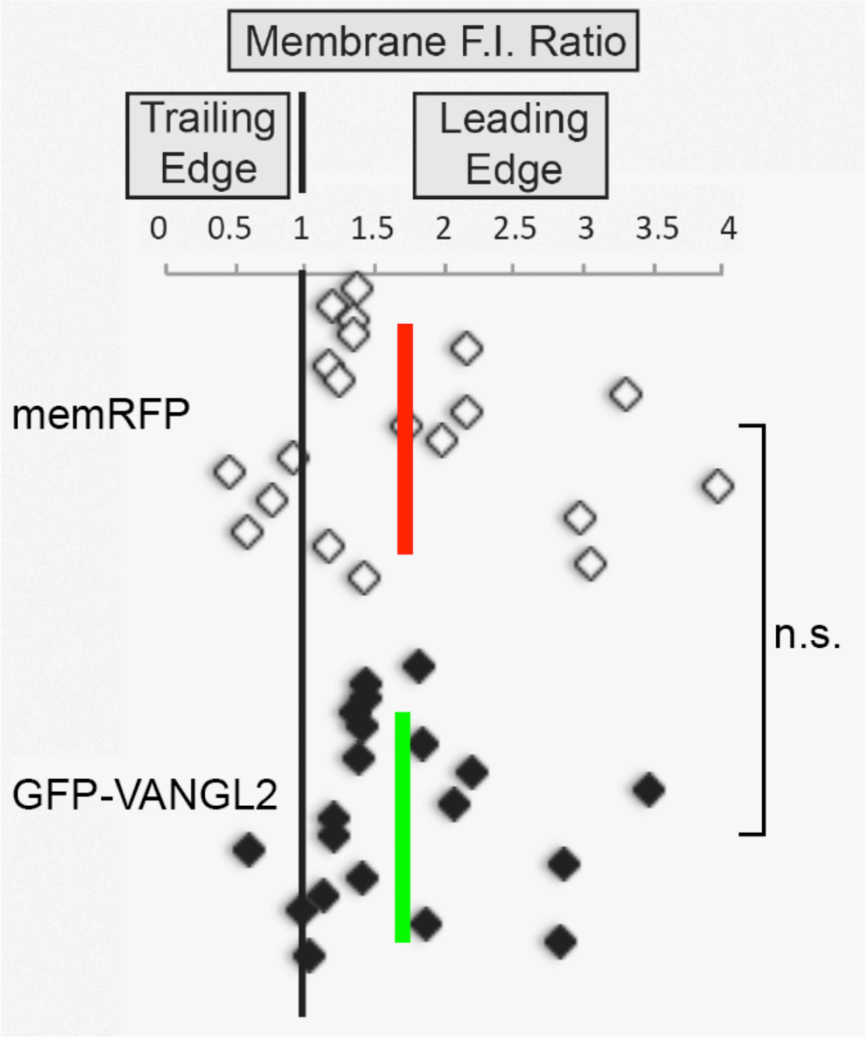

Figure 31 GFP-VANGL2 Symmetry at Dorsoventral Membranes: Fluorescence intensity (F.I.) ratio plot of trailing edge (ventral membrane) and leading edge (dorsal membrane) apices. Red line indicates mean F.I. for membrane-targeted red fluorescent protein (memRFP). Green line indicates mean F.I. for GFP-VANGL2.
n=20 cells, 15 embryos. n.s. = not significant; two-tailed paired *t*-test.

mutant ectodermal cells. We selected large membrane protrusions for this analysis because of their role in cell migratory processes.

Using the FIJI Plot Profile tool, we collected fluorescence intensities at large membrane protrusion domains during three subjectively named phases of protrusion development (Figures 32, 33)(Schindelin et al., 2012). The first collection occurred during the preparatory phase prior to protrusion eruption. Phase two, the eruption phase, coincides with actin remodeling and early large protrusion formation. During the eruption phase, the large protrusion becomes visible. The final phase, extension, occurs as the large membrane protrusion matures and fully extends. Typically, the large membrane protrusion begins to retract after maturation.

By calculating fluorescence intensity ratios between each phase (i.e. eruption phase: preparatory phase and extension phase: eruption phase), we tracked fluorescence intensity changes through the stages of large membrane protrusion development. Between the preparatory and eruption phases (ratio = eruption phase fluorescence intensity: preparatory phase fluorescence intensity), the GFP-VANGL2 ratio is 2.54 +/- 1.07, while the control memRFP ratio is 1.72 +/- 0.65 (Figure 34). As large membrane protrusion development progresses, the fluorescence intensity ratio between the eruption and extension phases (ratio = extension phase: eruption phase) drops to 0.48 +/- 0.22 for the GFP-VANGL2 channel and 0.55 +/- 0.32 for the memRFP control channel (Figure 35).

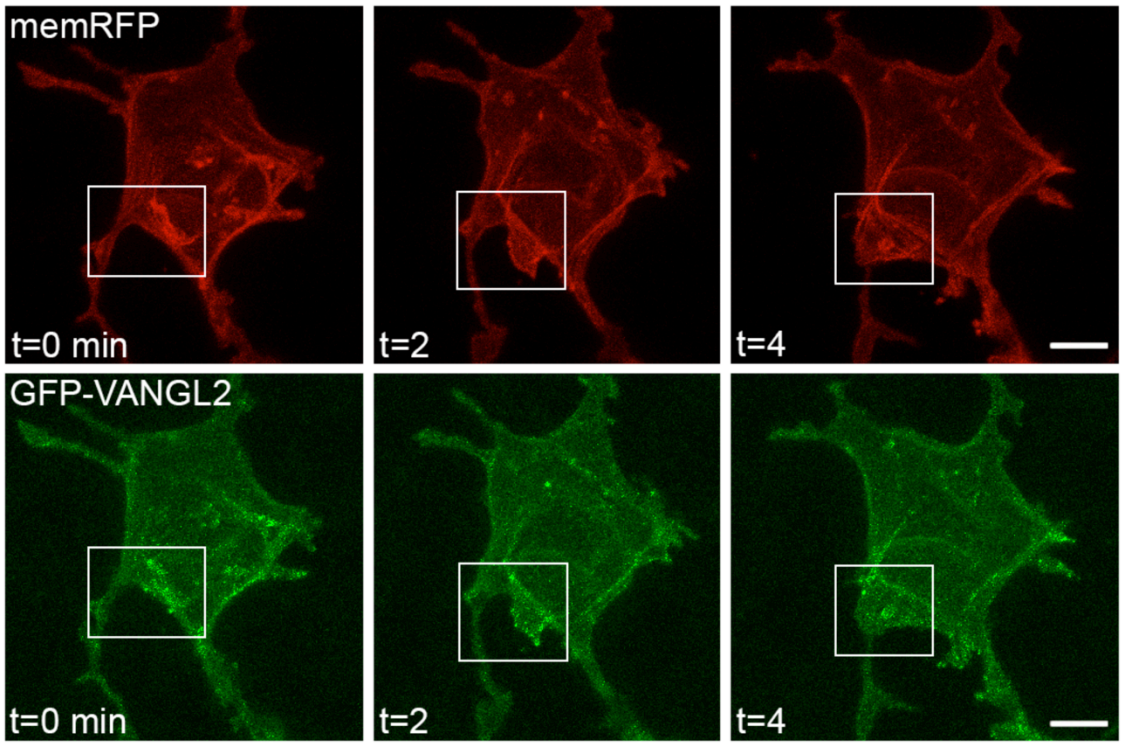

Figure 32 Time-Lapse Micrographs Illustrating Large Membrane Protrusion Phases: Large membrane protrusion phases (white boxes); preparatory phase (phase 1, time (t) = 0 min). Eruption phase (phase 2, t = 2). Extension phase (phase 3, t = 4). Membrane-targeted red fluorescent protein (memRFP) and GFP-VANGL2 fusion protein. Scale bar = 5μm.

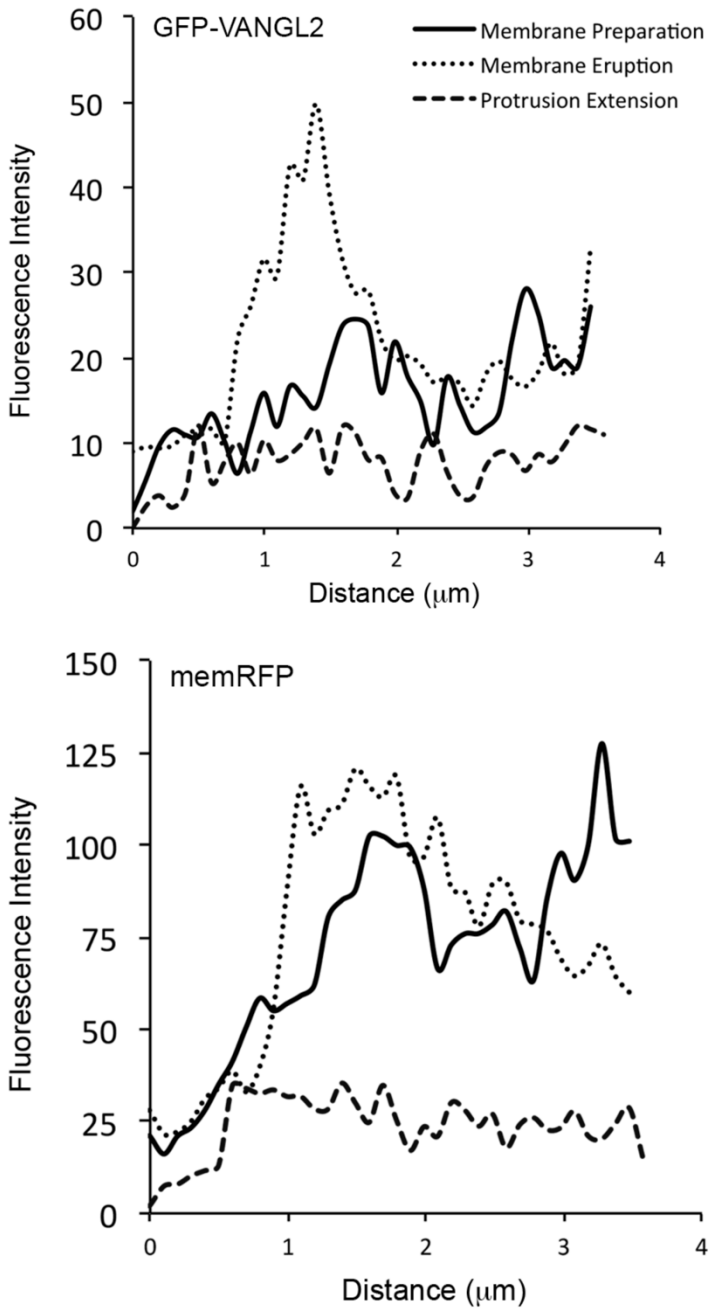

Figure 33 Plot Profile for Large Membrane Protrusion Development Phases: Representative fluorescence intensity (F.I.) plots profile for the three phases of large membrane protrusion development. Plot profile collected from protrusion tip (distance = 0 μm) inward. Membrane-targeted red fluorescent protein (memRFP) and VANGL2 fusion green fluorescent protein (GFP-VANGL2).

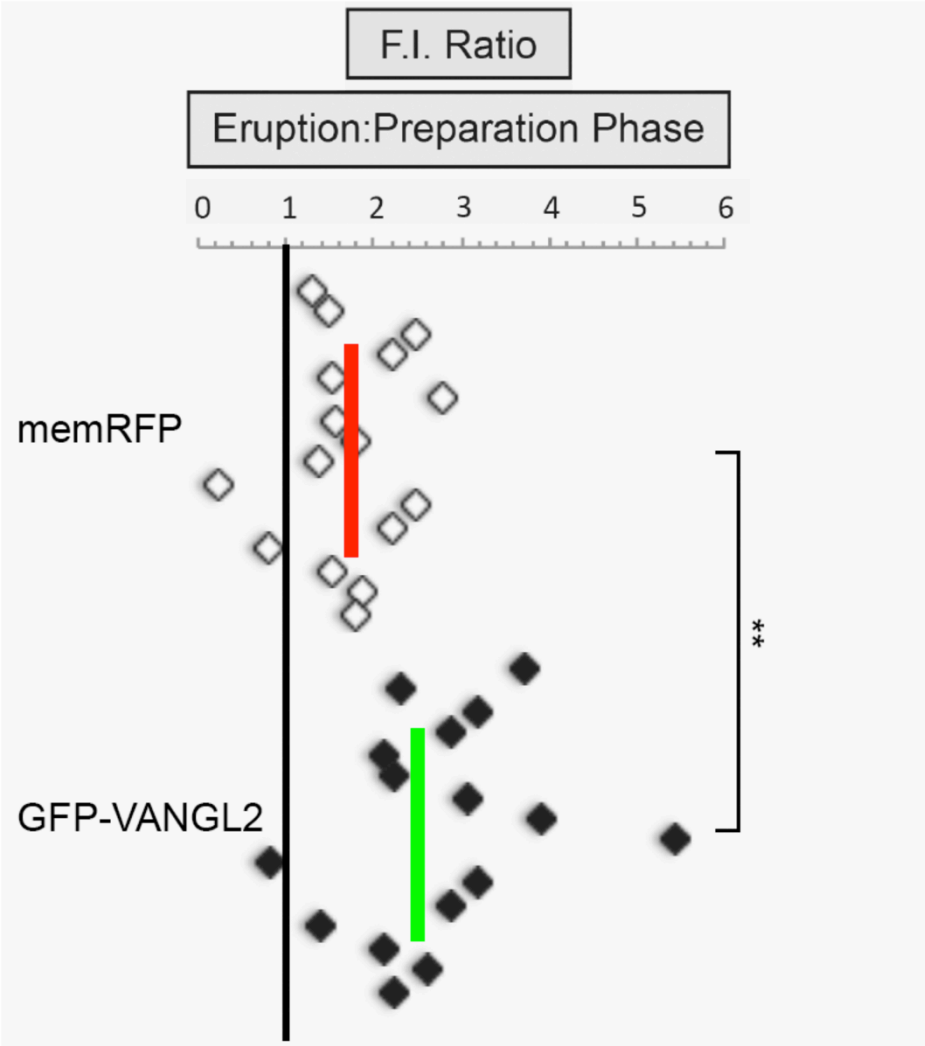

Figure 34 GFP-VANGL2 Enrichment in Eruption Phase Large Membrane Protrusions: Fluorescence intensity (F.I.) ratio plot of eruption phase (phase 2) to preparation phase (phase 1) apices. Red line represents mean F.I. for membrane-targeted red fluorescent protein (memRFP). Green line represents mean F.I. for green fluorescent protein-VANGL2 fusion protein (GFP-VANGL2). n =16 protrusions, 6 embryos. $^{**}P<0.01$; two-tailed paired *t*-test.

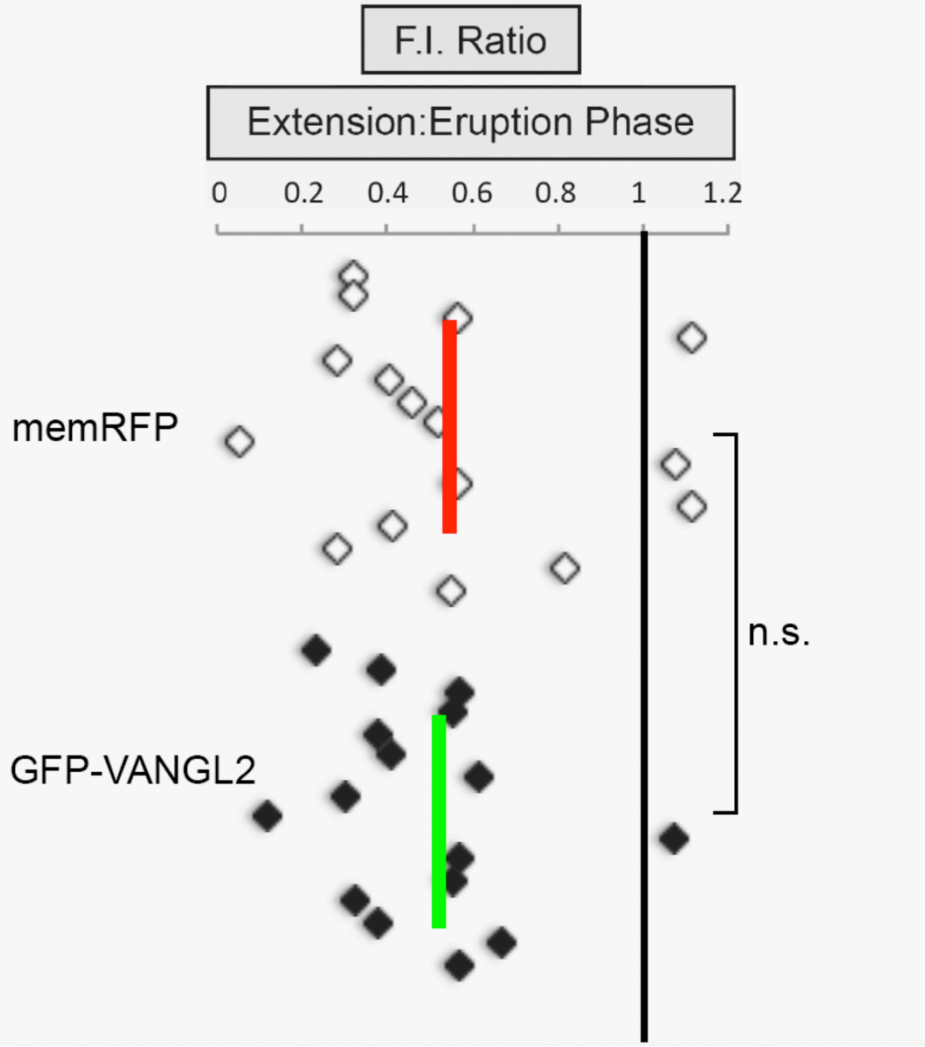

Figure 35 GFP-VANGL2 Localization Normalizes in Extension Phase Large Membrane Protrusions: Fluorescence intensity (F.I.) ratio plot of extension phase (phase 3) to eruption phase (phase 2) apices. Red line represents mean F.I. for membrane-targeted red fluorescent protein (memRFP). Green line represents mean F.I. for green fluorescent protein-VANGL2 fusion protein (GFP-VANGL2). n =16 protrusions, 6 embryos. n.s. = not significant; two-tailed paired *t*-test.

Using similar techniques, we analyzed GFP-VANGL2 localization in protrusive versus non-protrusive membrane domains. Peak eruption phase fluorescence intensities were compared to the fluorescence intensities of membrane domains lacking membrane protrusions. By comparing these values, we aimed to further support a concentration of GFP-VANGL2 in large membrane protrusions during the eruption phase of membrane protrusion development. The fluorescence intensity ratio for the memRFP control channel averages 1.02 +/- 0.40, indicating similar levels of memRFP in both non-protrusive domains and large membrane protrusions (Figure 36). The GFP-VANGL2 channel fluorescence intensity ratio averages 1.66 +/- 0.54, which illustrates a significant increase in GFP-VANGL2 in eruption phase large protrusions over non-protrusive domains (Figure 36). Our findings support the conclusion that GFP-VANGL2 accumulates in large membrane protrusions during the eruption phase.

A final look at GFP-VANGL2 localization includes an analysis of polarized versus non-polarized large membrane protrusions. Initially, we expected increased GFP-VANGL2 levels in non-polarized large membrane protrusions to support the notion Vangl2 works to suppress inappropriate membrane protrusions. However, the results indicated no significant difference in Vangl2 accumulation among polarized and non-polarized large membrane protrusions (Figure 37). The control memRFP fluorescence intensity ratio is 1.06 +/- 0.60 for polarized to non-polarized large membrane protrusions, and the corresponding Vangl2 fluorescence intensity ratio is 1.40 +/- 1.09 (Figure 37). We suspect Vangl2 localization is similar among polarized and non-polarized large membrane protrusions because it may function to trigger protrusion collapse.

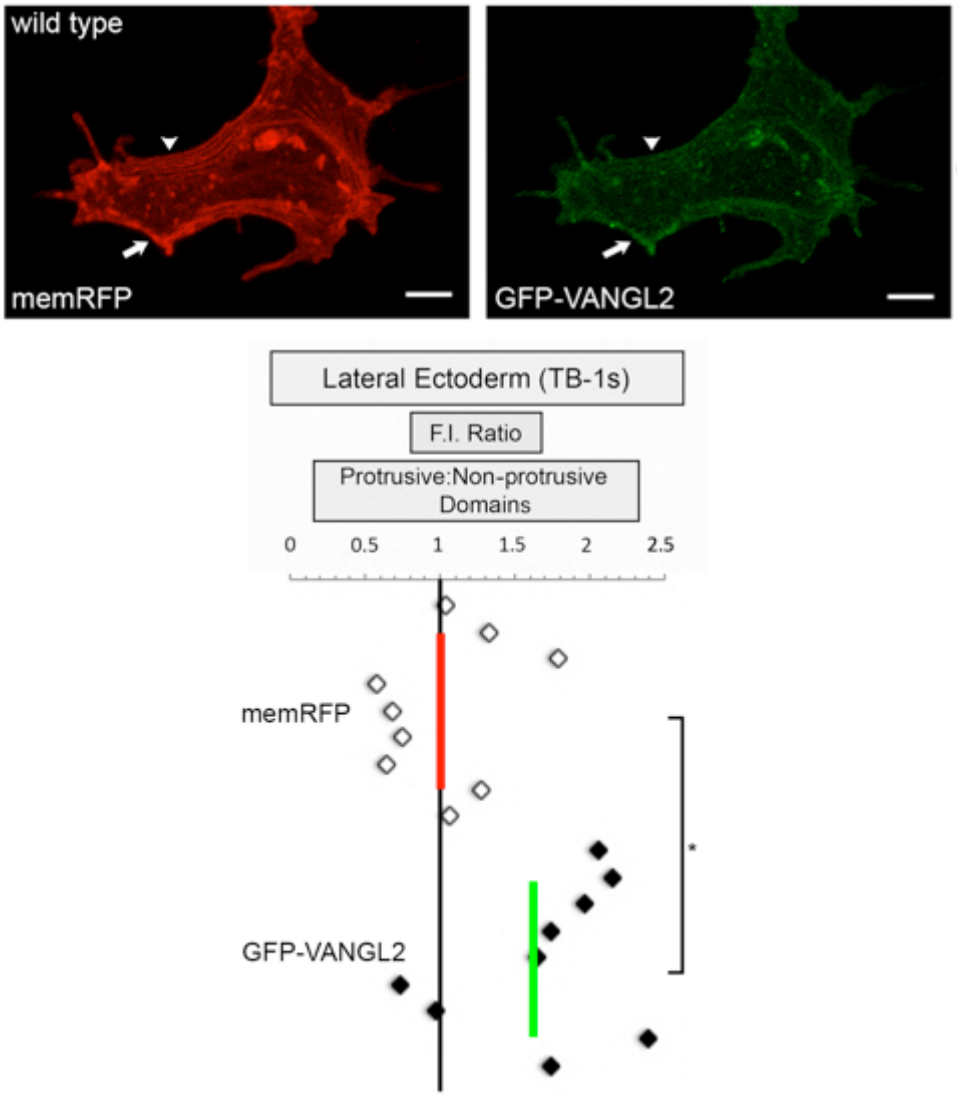

Figure 36 GFP-VANGL2 Enrichment in Protrusive Cellular Domains: Confocal micrographs of wild-type ectodermal cells from tailbud stage embryo injected with membrane-targeted red fluorescent protein (memRFP) and green fluorescent protein-VANGL2 fusion protein (GFP-VANGL2)(top). White arrowheads annotate non-protrusive domain; white arrows annotate large membrane protrusion. Dorsal midline at right. Scale = 5μm. Fluorescence intensity (F.I.) ratio plot of large protrusion extension phase apex to non-protrusive apex. Red line represents mean F.I. for memRFP. Green line represents mean F.I. for GFP-VANGL2. n = 9 protrusions, 6 embryos.*$P < 0.05$; two-tailed paired *t*-test.

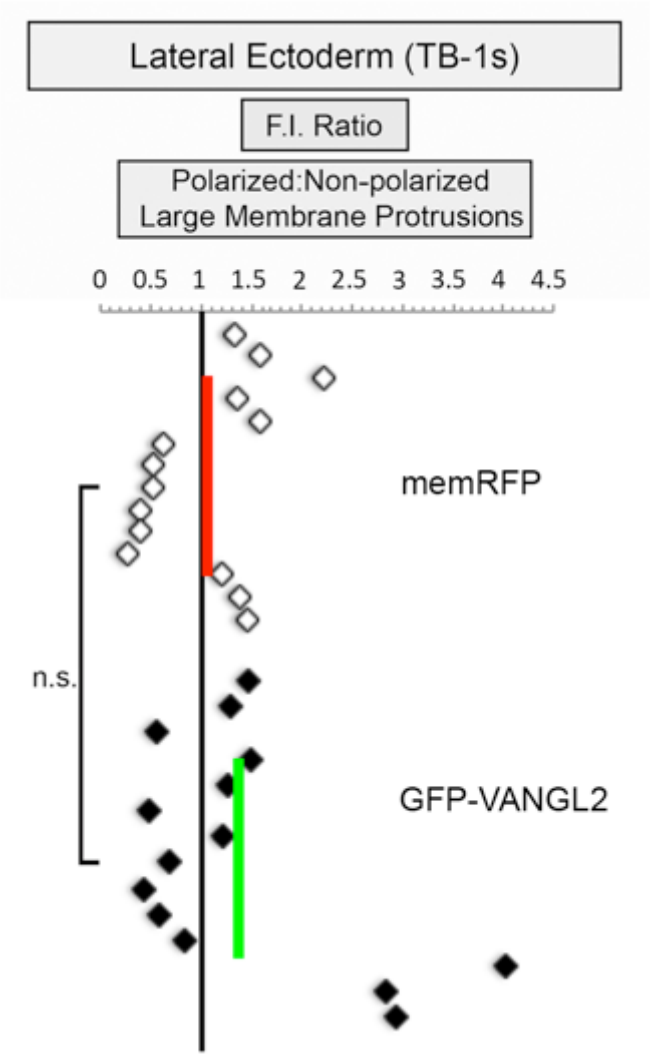

Figure 37 Polarized and Non-Polarized Large Protrusions Exhibit Symmetrical GFP-VANGL2 Distribution: Fluorescence intensity (F.I.) ratio plot of polarized large protrusion extension phase apex to non-polarized large protrusion extension phase apex. Red line represents mean F.I. for membrane-targeted red fluorescent protein (memRFP). Green line represents mean F.I. for green fluorescent protein-VANGL2 fusion protein GFP-VANGL2.
n=14 protrusions, 5 embryos. n.s. = not significant; two-tailed paired *t*-test.

Alternately, its localization could be a product of cytoskeletal protein mobility as the plasma membrane is restructuring. Lamellipodia eruption may trigger Vangl2 endocytosis, leading to Vangl2 accumulation within the large protrusion as its trafficked back in to the cytosol for recycling.

4.3 Conclusion

While Vangl2 has been shown to asymmetrically localize in fly epithelium and in non-migrating, highly polarized axial notochord cells, we were unable to establish GFP-VANGL2 asymmetry in migrating ectodermal cells of the zebrafish gastrula (Goodrich and Strutt, 2011; Roszko et al., 2015). We compared fluorescence intensities between the anterior to posterior membranes and leading edge (dorsal) to trailing edge (ventral) membranes. Vangl2 may not be asymmetric in these cells or it may localize transiently.

We performed an examination of GFP-VANGL2 within large membrane protrusions at three phases, preparatory (phase 1), eruption (phase 2), and extension (phase 3) phases. We found GFP-VANGL2 enrichment within large membrane protrusions by comparing the eruption phase apex to corresponding the fluorescence intensities of corresponding time points for the preparatory and extension phases. GFP-VANGL2 enrichment diminishes by the extension phase. Additionally, fluorescence intensity is enriched in the eruption phase relative to non-protrusive domains. However when we compared GFP-VANGL2 fluorescence intensities during the eruption phases of polarized and non-polarized large membrane protrusions, we found no significant difference.

Our data indicating GFP-VANGL2 enriches in erupting large membrane protrusions is reminiscent of the Vangl2 burst seen in migrating neuronal filopodia just prior to their collapse (Davey et al., 2016). These results indicate, rather than suppressing randomized large membrane protrusions, Vangl2 may work to restrict large membrane-protrusive activity or trigger large membrane protrusion collapse. The lack of asymmetry across anteroposterior and dorsoventral axes may be a result of cargo-sorting protein or Wnt signaling gradients across membrane domains (Gao et al., 2011; Merte et al., 2010).

CHAPTER FIVE. Loss of Fibronectin Disrupts Membrane Protrusion Formation and Polarization and *fibronectin* mRNA Injection Rescues *vangl2* Mutant Membrane Protrusion Phenotypes

5.1 Introduction

Providing a substrate for traction generation, the fibronectin extracellular matrix plays an important role in cell migration. The onset of fibronectin fibrillogenesis coincides with the onset of PCP at approximately mid-gastrulation (Latimer and Jessen, 2010; Roszko et al., 2015). By the end of gastrulation, layers of fibronectin form between the ectoderm and mesoderm and the mesendoderm and yolk (Figure 38). Our lab's previous work shows a decrease in total fibronectin protein in *vangl2* mutant and *prickle1a* morphant embryos (Dohn et al., 2013; Williams et al., 2012a). In contrast, we found *glypican4* mutant embryos have increased fibrillogenesis but no change in total fibronectin protein when compared to wild type (Dohn et al., 2013). Loss of fibronectin in wild-type embryos results in a mild convergence and extension defect (Latimer and Jessen, 2010)(Figure 39). Early work in the frog further implicates effective cell-matrix interactions are required for polarized membrane protrusion formation (Davidson et al., 2006).

Because *vangl2* mutants have a loss of total fibronectin protein, we hypothesized the number of membrane protrusions inversely correlates to the amount of fibronectin protein in zebrafish gastrulae (Dohn et al., 2013). Theoretically, a loss of fibronectin extracellular matrix leaves the cell lacking migratory substrate and, in turn, forming increased membrane protrusions as it struggles to sense and form stable interactions with

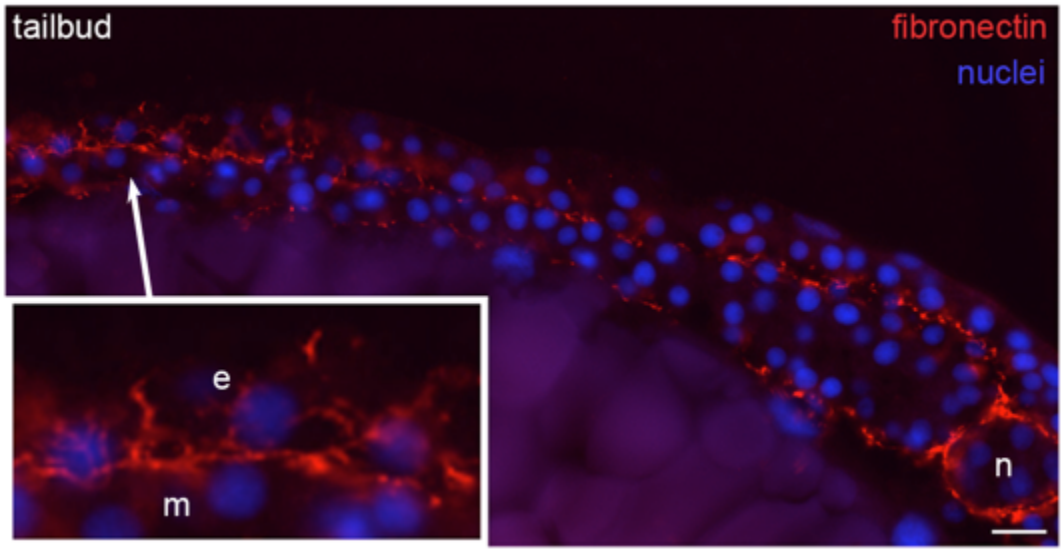

Figure 38 Fibronectin Extracellular Matrix in Tailbud Stage Wild-Type Embryo: Confocal micrograph of cryosection from tailbud stage wild-type embryo. White box enlargement of fibronectin extracellular matrix (red) layer between ectoderm (e) and mesoderm (m). Nuclei labeled with DAPI (blue). Scale bar = 20 μm.
notochord (n)

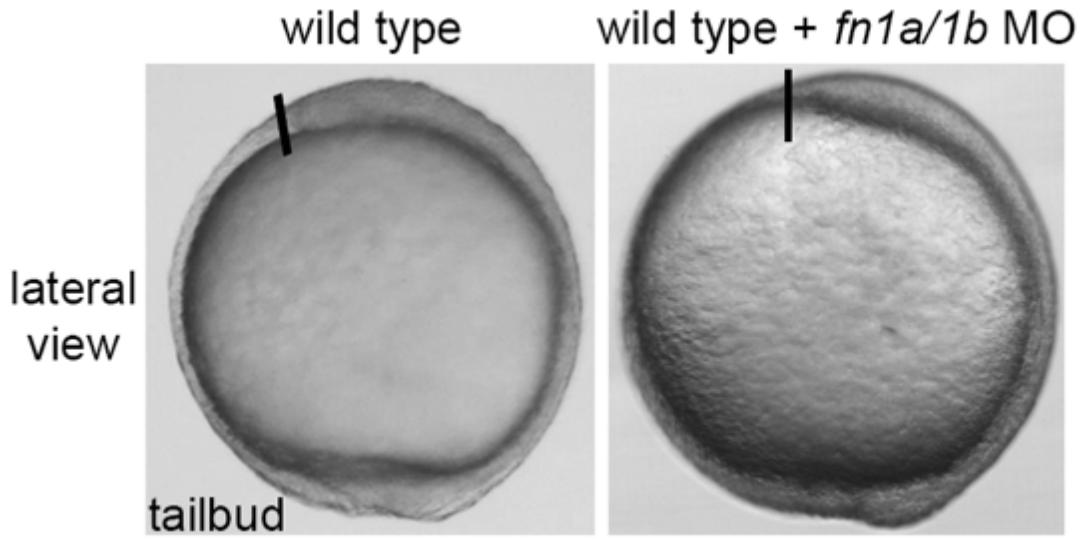

Figure 39 Tailbud Stage *fibronectin* (*fn1a/1b*) Morphant Embryo Convergence and Extension Phenotype: Brightfield micrograph of tailbud stage wild-type and *fibronectin* (*fn1a/1b*) morphant embryos, lateral view. Black lines indicate polsters.

its fibronectin extracellular matrix. Data from the frog reports fibronectin-cell interactions are required for proper membrane protrusion formation and polarization (Davidson et al., 2006). We suspected the loss of fibronectin in *vangl2* mutant embryos contributes to the observed membrane protrusion phenotype. We further expected a loss of directness, cell polarity, and mediolateral alignment.

5.2 Results

Loss of fibronectin results in increased non-polarized membrane-protrusive activity

To determine the role of fibronectin in the *vangl2* mutant membrane protrusion phenotypes, we performed a membrane protrusion analysis to quantify membrane protrusions. Using immunohistochemistry, we first verified functionality of the *fibronectin* (*fn1a/1b*) morpholinos (Figure 40). Wild-type zebrafish gastrulae were injected with *fibronectin 1a/1b* antisense oligonucleotide morpholinos to produce a loss of fibronectin condition. At the 8-cell stage, the *fibronectin* (*fn1a/1b*) morphant embryos were injected with membrane-targeted green fluorescent protein (memGFP)(Figure 41). We collected time-lapse confocal micrographs when the embryos reached tailbud stage. Ectodermal cells from *fibronectin* (*fn1a/1b*) morphant embryos produce an average of 25.42 +/- 5.42 filopodia and 5.94 +/- 0.64 large membrane protrusions (Figure 42). The quantities of membrane protrusions are in line with those of *vangl2* mutants and are significantly more than wild type, which produce an average of 13.16 +/- 2.62 filopodia and 3.68 +/- 0.54 large protrusions (Figure 41).

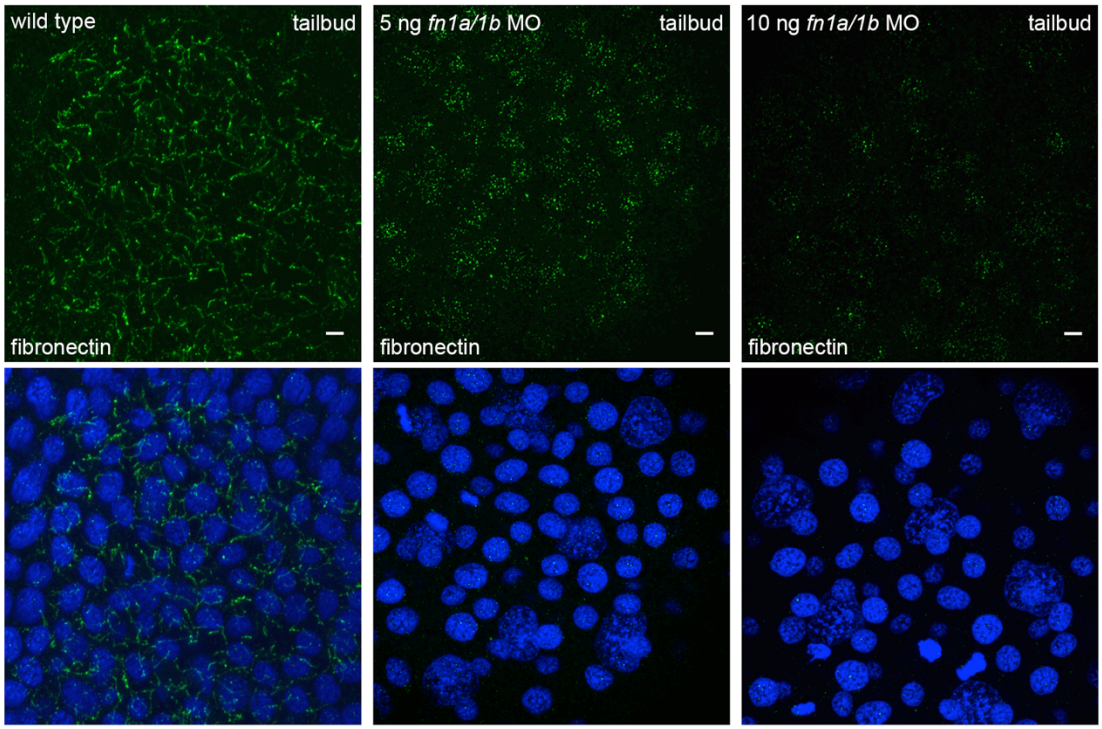

Figure 40 Confocal Micrographs of Wild-Type Embryos Injected with *fibronectin* (*fn1a/1b*) Morpholinos: Tailbud stage wild-type embryos versus wild-type embryos injected with 5ng and 10ng doses of *fibronectin* (*fn1a/1b)* morpholinos. Fibronectin immunohistochemistry (green). Nuclei labeled with DAPI (blue). Scale bar = 5 μm.

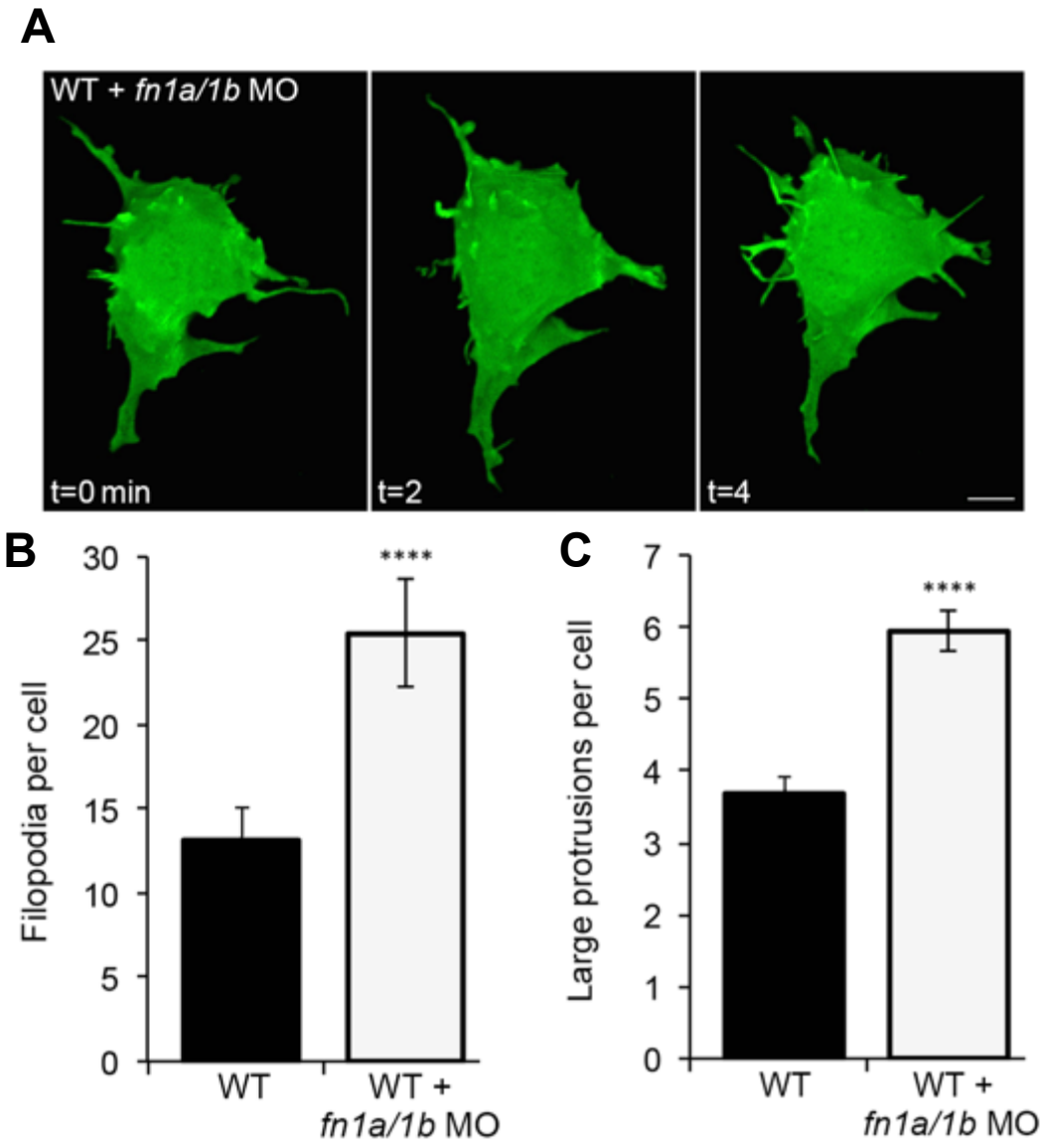

Figure 41 *fibronectin* (*fn1a/1b*) Morphant Embryos Produce Increased Membrane Protrusions: Confocal time-lapse micrographs of *fn1a/1b* morphant ectodermal cells expressing membrane-targeted green fluorescent protein (memGFP)(A). Scale bar = 5 μm. Average number of filopodia per ectodermal cell in wild-type (WT) versus *fn1a/1b* morphant embryos (B). Average number of large membrane protrusions per ectodermal cell in wild-type versus *fn1a/1b* morphant embryos (C). wild type (n=11 cells, 8 embryos); *fn1a/1b* morphant embryos (n=10 cells, 7 embryos). All values are ± SD. ****P<0.0001; P values are versus wild type;

Consistent with the results from *vangl2* mutants, loss of fibronectin in wild-type zebrafish gastrulae results in a loss of large membrane protrusion polarity. In ectodermal cells from *fibronectin* (*fn1a/1b*) morphant embryos, only 46.88% +/- 8.81% of large membrane protrusions are polarized along the path of migration (Figure 42B, 42C). *fibronectin* (*fn1a/1b*) morphant cells exhibit a significant loss in membrane protrusion polarity when compared to wild-type ectodermal cells with an average value of 73.10% +/- 11.28% (Figure 42B, 42C). *vangl2* mutant ectodermal cells have a polarized large membrane protrusion value of 43.76% +/- 8.24%. Similar to *vangl2* mutant ectodermal cells, *fibronectin* (*fn1a/1b*) morphant cells have no significant loss of filopodia polarity (Figure 42A).

Loss of fibronectin causes PCP defects in migrating gastrula cells

Using the confocal time-lapse micrographs, we performed manual cell tracking using FIJI software (Schindelin et al., 2012). These data were exported to Ibidi's Chemotaxis and Migration Tool to generate a directness value (Gerhard Trapp and Elias Horn, 2010). We predicted *fibronectin* (*fn1a/1b*) morphant cells lose directness similar to *vangl2* mutants, but we found only a mild loss of directness. Wild-type ectodermal cells have a directness value of 0.96 +/- 0.03, while *fibronectin (fn1a/1b)* morphant cells have a directness value of 0.91 +/- 0.10 (Figures 43A, 43B).

Length-width ratio (LWR) and mediolateral alighnment (MLA) represent the whole cell polarity. The average LWR is 1.62 +/- 0.37 for ectodermal cells in *fibronectin* (f*n1a/1b*) morphant embryos (Figure 43C). For reference, wild-type ectodermal cells have a LWR value of 2.04 +/- 0.58, and *vangl2* mutants have a LWR of 1.46 +/- 0.35 (Figure

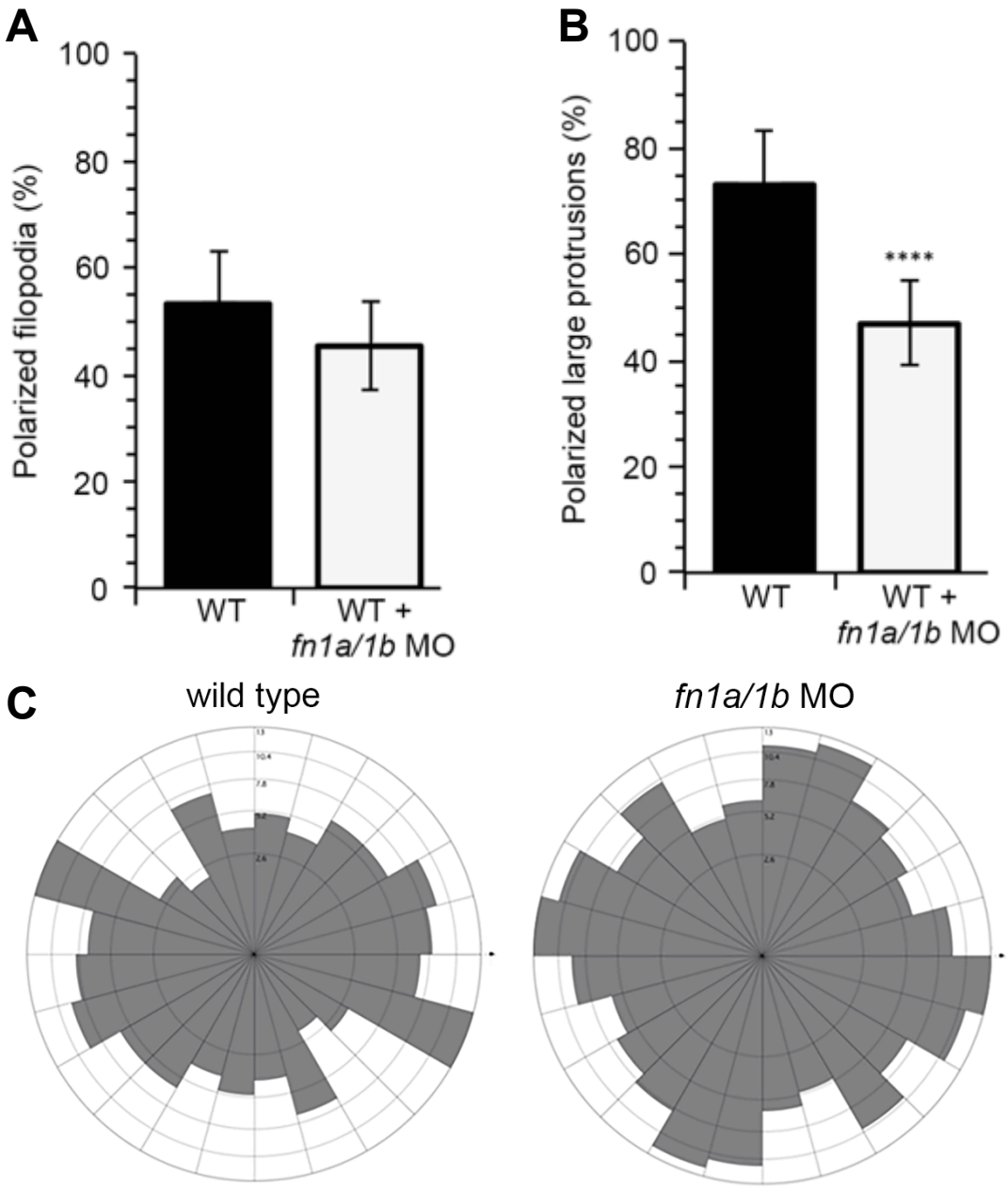

Figure 42 *fibronectin* (*fn1a/1b*) Morphant Embryos Exhibit Decreased Large Membrane Protrusion Polarity: Graphs of polarized filopodia (A) and large membrane protrusions (B) per ectodermal cell in wild-type (WT) versus *fn1a/1b* morphant embryos. Rose diagram of large membrane protrusion frequency and distribution (C). 0° is the horizontal axis (path of migration). Dorsal at right. wild type (n=11 cells, 8 embryos); *fn1a/1b* morphant embryos (n=10 cells, 7 embryos). All values are ± SD. ****P<0.0001; P values are versus wild type; two-tailed unpaired t-test.

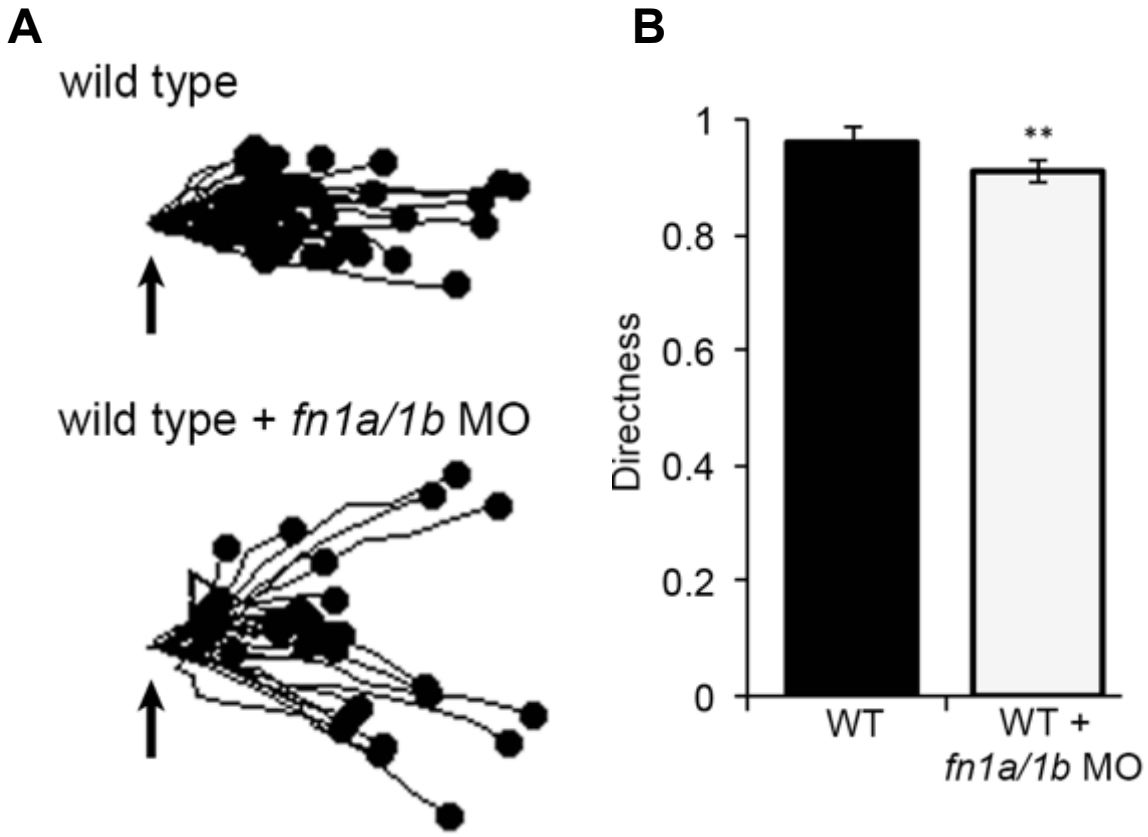

C

	LWR	MLA (%)	velocity (μm/min)
wild type	2.04 +/- 0.58	92	1.08 +/- 0.49
wild type + *fn1a/1b* MO	1.62 +/- 0.37****	73	1.38 +/- 0.64

Figure 43 *fibronectin* (*fn1a/1b*) Morphant Embryos Present PCP Defects: Trajectory plots (A) and directness graph (B) for wild-type versus *fn1a/1b* morphant ectodermal cells. Table with length-width ratios (LWR), mediolateral alignment (MLA), and velocity for wild-type and *fn1a/1b* morphant ectodermal cells (C).

Trajectory and directness: wild type (WT) n=50 cells, 13 embryos; *fn1a/1b* morphants n=32 cells, 10 embryos. LWR and MLA: WT n=50 cells, 13 embryos; *fn1a/1b* morpholino (MO)- injected wild type n=48 cells, 10 embryos. All values are ± SD. ** $P<0.01$, **** $P<0.0001$. *P* values are versus wild type; two-tailed unpaired *t*-

43C). The *fibronectin* morphant ectodermal cell LWR defect is not as severe as that of *vangl2* mutants. Likewise, 72.92% of *fibronectin* (*fn1a/1b*) morphant ectodermal cells are mediolaterally aligned to the path of migration (Figure 43C). Wild-type cells have an MLA value of 92.00%, and *vangl2* mutant cells have a value of 20.00%, meaning *fibronectin (fn1a/1b)* morphant cells are only somewhat affected (Figure 43C).

Fibronectin rescues membrane protrusion defects in *vangl2* mutants

To confirm the role of fibronectin in the *vangl2* mutant membrane protrusion phenotype, we injected *fibronectin* (*fn1a/1b*) synthetic mRNA into *vangl2* mutant embryos and performed a membrane protrusion analysis. Our lab previously cloned full-length cDNA encoding *fibronectin 1a/1b* into a pCS2+ vector. After preparing synthetic mRNA, we performed a fibronectin immunohistochemistry experiment to test its efficacy (Figure 44). Wild-type and *vangl2* mutant embryos were injected with *fibronectin* (*fn1a/1b*) mRNA at single cell stage. At tailbud stage, the treated embryos underwent the immunohistochemistry protocol using a fibronectin polyclonal antibody. *fibronectin* (*fn1a/1b*) mRNA-injected wild-type embryos produce increased amounts of fibronectin. However rather than restoring fibronectin to wild-type levels, *fibronectin* (*fn1a/1b*) mRNA-injected *vangl2* mutant embryos seemingly have increased fibronectin fibrillogenesis (Figure 44).

For continuity, we completed a series of time-lapse experiments and analyses similar to our previous membrane protrusion studies. At single cell stage, we injected *vangl2* mutants with *fibronectin* (*fn1a/1b*) mRNA, and when the embryos reached 8-cell stage, we injected membrane-targeted green fluorescent protein (memGFP) into a single

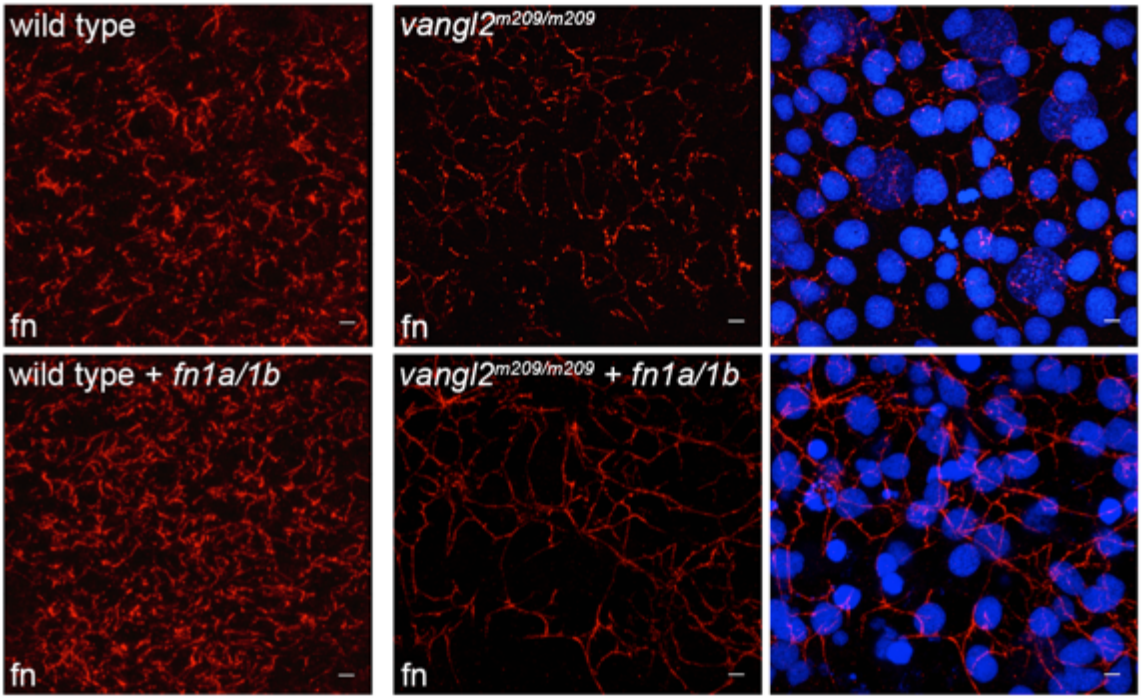

Figure 44 Confocal Micrographs of Fibronectin (fn) Expression in *fibronectin* (*fn1a/1b*) mRNA-Injected Wild-Type and *vangl2* Mutant Embryos: Micrographs of wild-type, *fn1a/1b* mRNA-injected wild-type, and *fn1a*/1b mRNA-injected *vangl2* mutant embryos with fibronectin immunohistochemistry (red). Nuclei labeled with DAPI (blue). Scale bar = 5 μm.

cell to achieve mosaic expression. We collected a series of time-lapse micrographs using a confocal microscope at the end of gastrulation. Each time-lapse is composed of 10 frames collected in 2 min intervals for a total duration of 20 min (Figure 45A). Untreated *vangl2* mutant embryos generate an average of 24.84 +/- 5.55 filopodia and 5.77 +/- 0.94 large membrane protrusions per cell (Figures 45B, 45C). *vangl2* mutant embryos injected with *fibronectin* (*fn1a/1b*) mRNA have a marked decrease in membrane protrusions with only 15.69 +/- 3.27 filopodia and 4.13 +/- 0.71 large protrusions per ectodermal cell (Figures 45B, 45C). The number of membrane protrusions in *vangl2* mutant embryos treated with *fibronectin* (*fn1a/1b*) mRNA are similar to those of non-injected wild-type embryos, which produce an average of 13.16 +/- 2.62 filopodia and 3.68 +/- 0.54 large protrusions per ectodermal cell (Figures 45B, 45C).

Next, we examined membrane protrusion polarity in migrating ectodermal cells. *vangl2* mutant ectodermal cells have no significant change in filopodia polarity when compared to wild-type cells, and *vangl2* mutant embryos injected with *fibronectin* (*fn1a/1b*) mRNA have no significant change in filopodia polarity (Figure 46A). Because filopodia fill a primarily sensory role, these results were consistent with our expectations. However, *vangl2* mutant embryos have a significant decrease in the percentage of polarized large protrusions with only 43.76% +/- 8.24% of large membrane protrusions polarized (Figures 46B, 46C). Wild-type ectodermal cells produce an average of 73.09% +/- 11.28% polarized large membrane protrusions, while *fibronectin* (*fn1a/1b*) mRNA-injected *vangl2* mutant embryos exhibit a mild rescue of large membrane protrusion

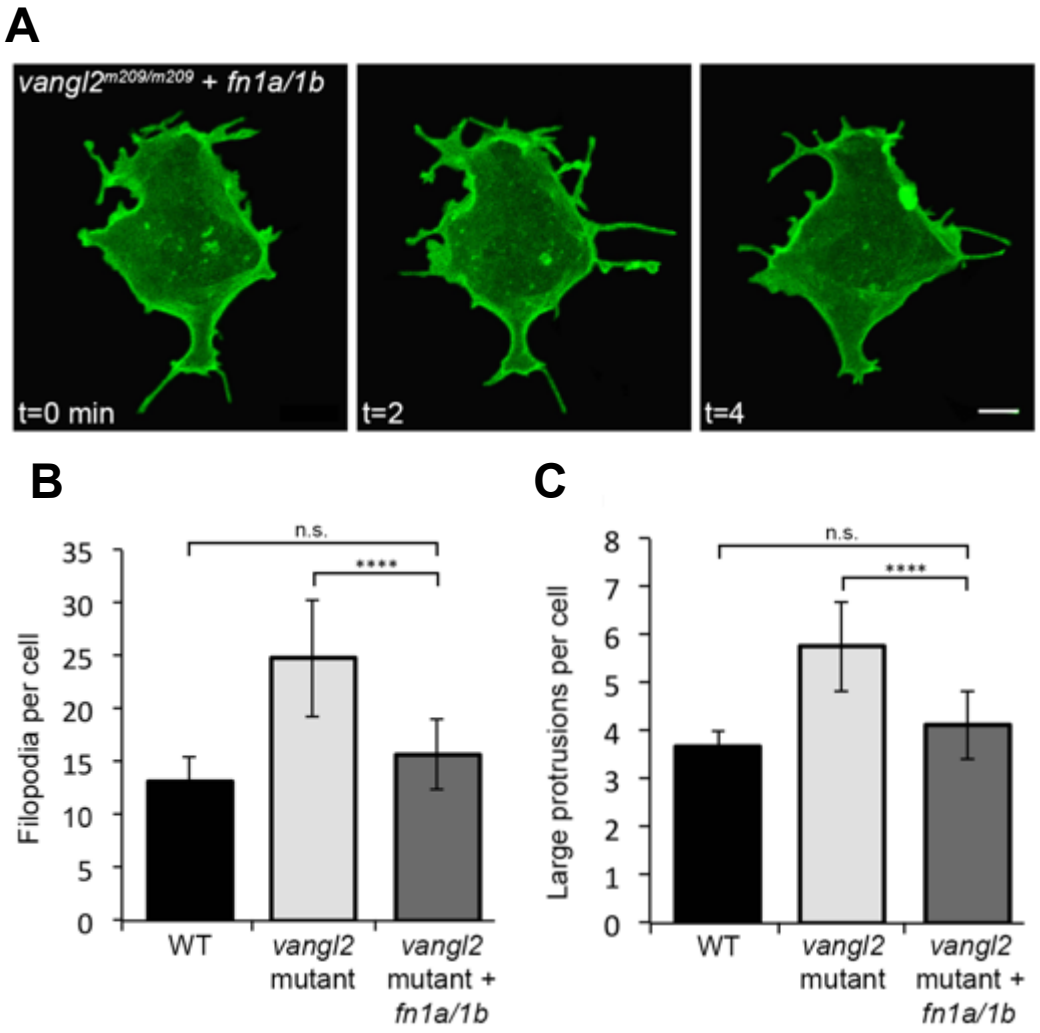

Figure 45 Fibronectin Rescues Membrane Protrusion Formation in *vangl2* Mutant Ectodermal Cells: Confocal micrographs of ectodermal cells from *fn1a/1b* mRNA-injected *vangl2* mutant embryos with mosaic expression of membrane-targeted green fluorescence protein (memGFP)(A). Scale bar = 5 µm. Graphs of filopodia (B) and large membrane protrusions (C) per ectodermal cell in wild-type (WT), *vangl2* mutant, and *fn1a/1b* mRNA-injected *vangl2* mutant embryos.

wild type (n=12 cells, 8 embryos), *vangl2*$^{m209/m209}$ (n=10 cells, 7 embryos), *fn1a/1b* mRNA-injected *vangl2*$^{m209/m209}$ mutants (n=10 cells, 7 embryos). All values are ± SD. ****P<0.0001, n.s. not significant; P values are versus wild type, except as indicated on the graphs; one-way ANOVA significance test followed by Tukey HSD post-hoc

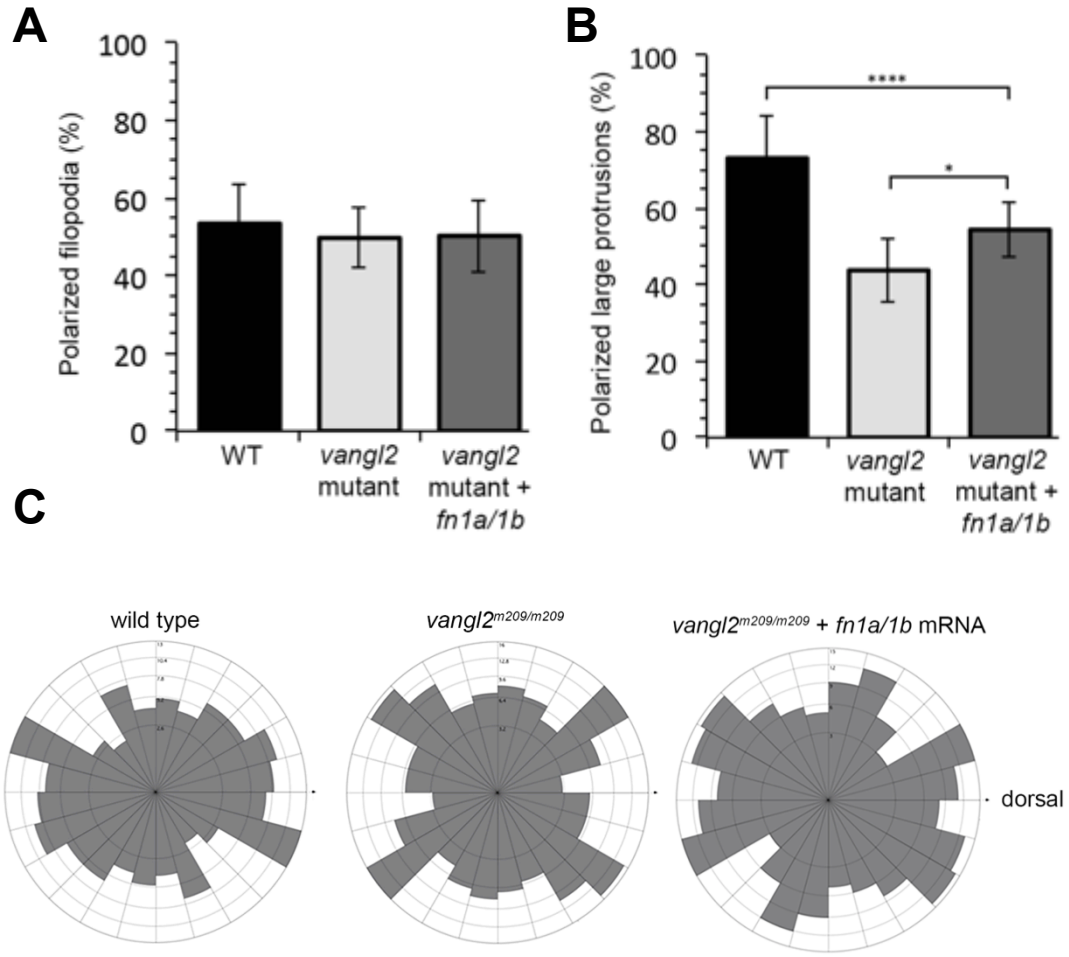

Figure 46 Fibronectin Rescues Large Membrane Protrusion Polarization in *vangl2* Mutant Ectodermal Cells: Graphs of polarized filopodia (A) and large membrane protrusions (B) per ectodermal cell in wild-type (WT), *vangl2* mutant, and *fn1a/1b* mRNA-injected *vangl2* mutant embryos. Rose diagrams depicting frequency and distribution of large membrane protrusions (C). 0° denotes the dorsoventral axis, perpendicular to the path of migration.

wild type (n=12 cells, 8 embryos), $vangl2^{m209/m209}$ (n=10 cells, 7 embryos), *fn1a/1b* mRNA-injected $vangl2^{m209/m209}$ mutants (n=10 cells, 7 embryos). All values are ± SD. **P*<0.05, *****P*<0.0001; *P* values are versus wild type, except as indicated on the graphs; one-way ANOVA significance test followed by Tukey HSD post-hoc tests.

polarity (54B, 54C). 54.37% +/- 7.11% of large protrusions are polarized in *vangl2* mutant embryos injected with *fibronectin* (*fn1a/1b*) mRNA (46B, 46C).

Fibronectin does not rescue PCP in *vangl2* mutant embryos

After completing the membrane protrusion analysis, we attempted to rescue the *vangl2* mutant embryonic convergence and extension phenotype. At single cell stage, we injected *fibronectin* (*fn1a/1b*) mRNA into *vangl2* mutants. Once embryos reached tailbud stage, we collected low magnification (10X) brightfield images of the injected embryos. We measured the angle from polster to tailbud to quantify the severity of the convergence and extension phenotype. We found *fibronectin* (*fn1a/1b*) mRNA does not rescue the convergence and extension phenotype in *vangl2* mutant embryos by the end of gastrulation (data not shown).

Fibronectin mRNA treatment rescues the *vangl2* mutant ectodermal cell directness value, indicative of a straighter trajectory. Wild-type embryos have an average directness value of 0.96 +/- 0.03, while *vangl2* mutant embryos have a reduced directness value of 0.83 +/- 0.19 (Figures 47A, 47B). *vangl2* mutant embryos injected with *fibronectin* (*fn1a/1b*) mRNA have an average directness value of 0.94 +/- 0.04 (Figures 47A, 47B).

While fibronectin restores ectodermal cell directness, it is unable to correct hallmarks of PCP, such as mediolateral alignment (MLA) and length-width ratio (LWR). Of the wild-type ectodermal cells examined, 92.00% were mediolaterally aligned with the path of migration (Figure 47C). Only 20.00% of ectodermal cells from *vangl2* mutants and 26.00% of cells from *vangl2* mutants injected with *fibronectin* (*fn1a/1b*) mRNA are

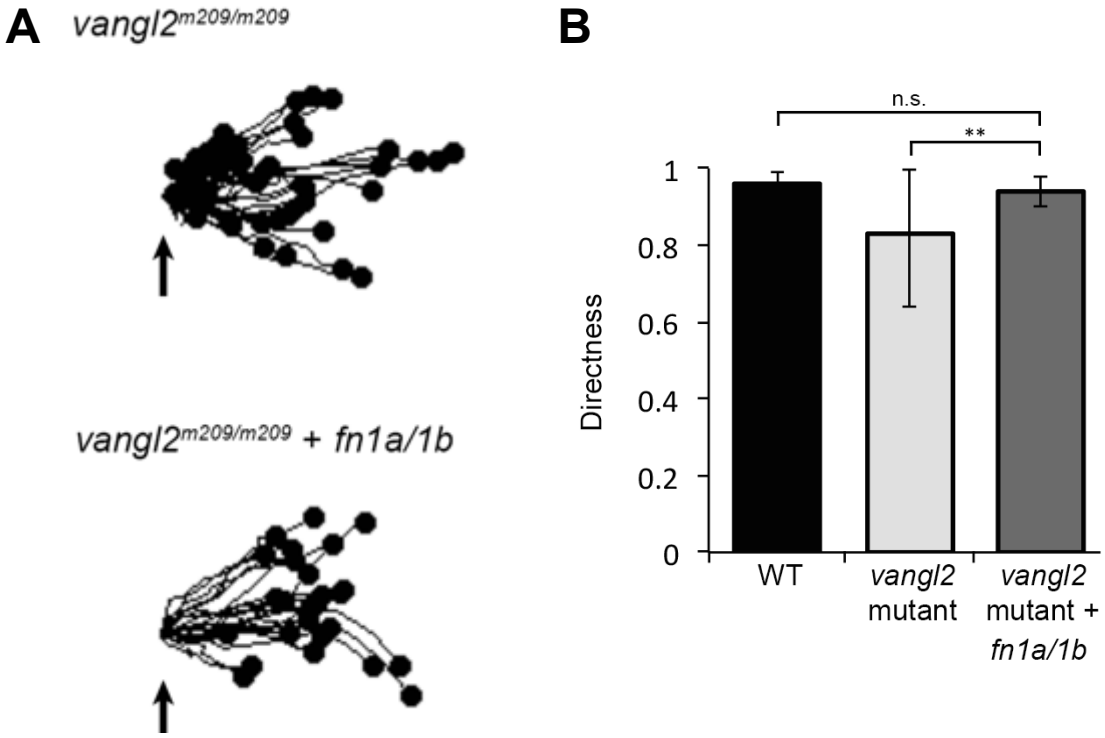

C

	LWR	MLA (%)
wild type	2.04 +/- 0.58	92
vangl2$^{m209/m209}$	1.46 +/- 0.35	20
vangl2$^{m209/m209}$ + *fn1a/1b*	1.51 +/- 0.29****	26

Figure 47 Fibronectin Fails to Rescue PCP Defects in *vangl2* Mutant Embryos: Trajectory plots (A) and directness graph (B) for wild-type, *vangl2* mutant, and *fn1a/1b* mRNA-injected *vangl2 mutant* ectodermal cells. Table of length-width ratios (LWR) and mediolateral alignment (MLA)(C). Trajectory and directness: wild type (WT) (n=50 cells, 13 embryos); *vangl2*$^{m209/m209}$ (n=51 cells, 13 embryos); *fn1a/1b*-injected *vangl2*$^{m209/m209}$ mutants (n=26 cells, 8 embryos). LWR and MLA: WT (n=50 cells, 13 embryos); *vangl2*$^{m209/m209}$ (n=51 cells, 13 embryos); *fn1a*/1b-injected *vangl2*$^{m209/m209}$ mutants (n=50 cells, 8 embryos). All values are ± SD. ***P*<0.01, n.s. = not significant. *P* values are versus wild type; one-way ANOVA with Tukey HSD post-hoc.

oriented within 20° of the path of migration (Figure 47C). Likewise, wild-type ectodermal cells have an average LWR of 2.04 +/- 0.58, while *vangl2* mutant cells treated with *fibronectin* (*fn1a/1b*) mRNA have an average LWR of 1.51 +/- 0.29 (Figure 47C). The LWR of *vangl2* mutant cells injected with *fibronectin* (*fn1a/1b*) mRNA is similar to that of *vangl2* mutant cells (1.46 +/- 0.35)(Figure 47C). These results indicate that, while fibronectin can rescue membrane protrusion defects in *vangl2* mutant embryos, it cannot rescue embryonic and cellular PCP phenotypes.

5.3 Conclusion

Loss of fibronectin results in increased numbers of filopodia and large membrane protrusions in ectodermal cells. The excess large membrane protrusions are not polarized along the path of migration. We predicted membrane-protrusive activity in *fibronectin* (*fn1a/1b*) morphant ectodermal cells to somewhat mimic that of ectodermal cells from *vangl2* mutant embryos, which have reduced fibronectin extracellular matrix (Dohn et al., 2013). The lack of fibronectin diminishes cell-matrix interactions, which are known to regulate polarized membrane-protrusive activity in the frog (Davidson et al., 2006). These results support our aforementioned central hypothesis that loss of cell-matrix interactions in *vangl2* mutant embryos contributes to increased membrane-protrusive activity and decreased large membrane protrusion polarity.

The results from the loss of fibronectin directionality, MLA, and LWR analyses indicate *fibronectin (fn1a/1b)* morphant cells have less severe cellular PCP defects than *vangl2* mutant cells. Previous work established *fibronectin* (*fn1a*/1b) morphant embryos have only a mild embryonic convergence and extension defect (Latimer and Jessen,

2010). Overall, these results suggest loss of fibronectin contributes to the convergence and extension phenotype and may be responsible for the membrane protrusion defect in *vangl2* mutant embryos. However, we suspect, while fibronectin is integral to proper membrane protrusion formation and large membrane protrusion polarity, other factors contribute to cell polarity and convergence and extension phenotypes in *vangl2* mutant embryos.

Fibronectin rescues membrane protrusion numbers and, to a lesser extent, large membrane protrusion polarity in *vangl2* mutant ectodermal cells. Migrating gastrula ectodermal cells likely require cell-matrix interactions to suppress excess membrane-protrusive activity as cells generate membrane protrusions to sense and form meaningful interactions with the extracellular matrix and adjacent cells. Work in the frog previously established cell-matrix interactions are required for polarized membrane protrusion formation (Davidson et al., 2006). Absence of the fibronectin extracellular matrix leaves the cell unsuccessfully searching for migratory substrate. Restoring the loss of fibronectin in *vangl2* mutant embryos may correct membrane protrusion numbers and partial large membrane protrusion polarity in migrating ectodermal cells during gastrulation (Latimer and Jessen, 2010).

Our data establish fibronectin is capable of rescuing membrane protrusion quantities, large membrane protrusion polarity, and trajectory directness in *vangl2* mutant ectodermal cells. However, fibronectin does not correct the embryonic convergence and extension defect, MLA, or LWR. These results indicate a significant role for fibronectin and, consequently, cell-matrix interactions in membrane protrusion

development and polarity, but overall failure of the PCP convergence and extension phenotype rescue indicates other mechanisms at work. Downstream PCP effectors, Rac and Rho, regulate actin cytoskeleton remodeling and are essential to convergence and extension movements. These processes may not rely on fibronectin or cell-matrix interactions and may explain the inability to rescue the embryonic convergence and extension phenotype in *vangl2* mutant embryos with fibronectin alone.

CHAPTER SIX. Vangl2 Cell Surface Localization Requires a Fibronectin Extracellular Matrix

6.1 Introduction

Vangl2 translocates from the endoplasmic reticulum to the cell surface via the Golgi apparatus at mid-gastrulation stages. Soon after cell surface localization of Vangl2 increases, the planar cell polarity (PCP) convergence and extension phenotype becomes visible during late gastrulation (Roszko et al., 2015; Sepich et al., 2005). As these Vangl2-dependent processes begin to occur, fibronectin extracellular matrix (ECM) assembly increases and transitions from a punctate to fibrillar structure (Latimer and Jessen, 2010). Because fibronectin fibrillogenesis occurs at approximately the same time as Vangl2 localizes at the cell surface, we hypothesized Vangl2 translocation to the cell surface requires an intact fibronectin ECM.

6.2 Results

In an effort to test our hypothesis, we performed a series of immunohistochemistry experiments. We injected wild-type embryos with *fibronectin* (*fn1a/1b*) morpholino at the single cell stage. After incubation, embryos were fixed with paraformaldehyde at two stages, 60% epiboly and tailbud stage. These embryos were treated with a Vangl2 polyclonal antibody. At 60% epiboly, Vangl2 is primarily cytoplasmic in non-injected wild-type control and *fibronectin* (*fn1a/1b*) morphant embryos (Figure 48, 49). By the end of gastrulation (tailbud stage), Vangl2 localizes primarily at the cell surface in non-injected wild-type control embryos (Figures 50, 51, 52, 53). However, Vangl2 fails to effectively localize at the cell surface in mesodermal and

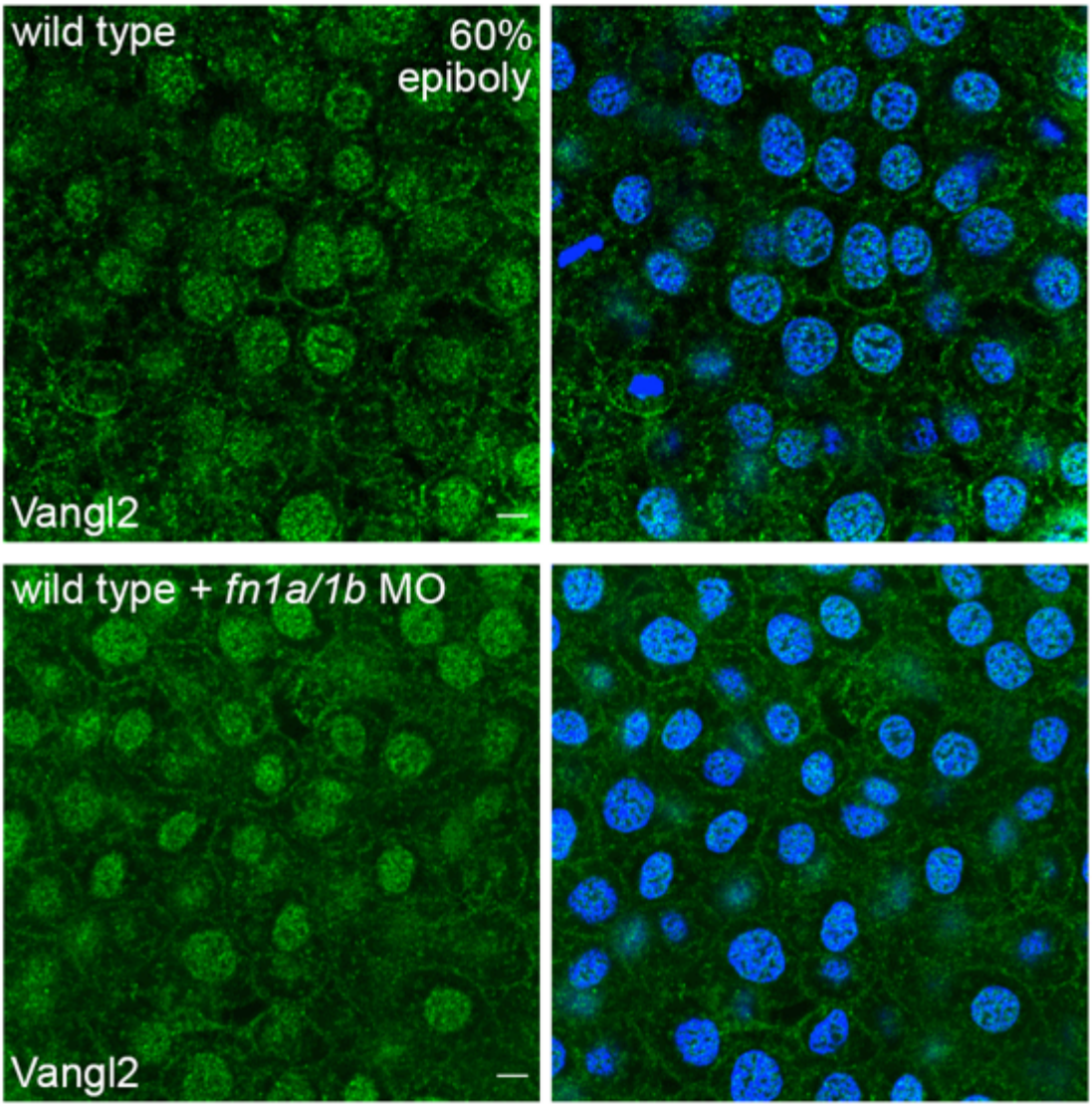

Figure 48 Confocal Micrographs of Cytoplasmic Vangl2 Localization during Early Gastrulation: Micrographs of wild-type versus *fn1a/1b* morphant ectodermal cells with Vangl2 immunohistochemistry (Green). Nuclei labeled with DAPI (blue). Scale bar = 5 μm.

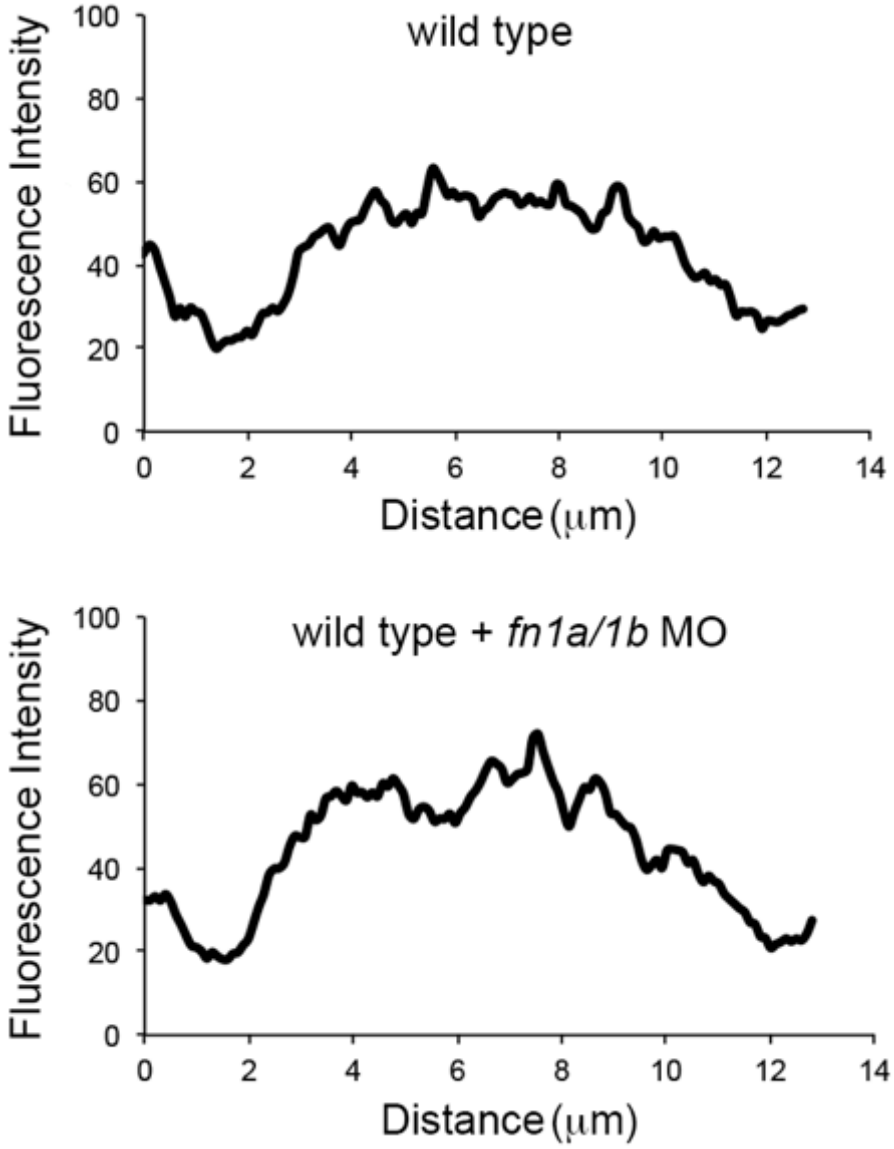

Figure 49 Plot Profiles of Cytoplasmic Vangl2 Localization during Early Gastrulation: Fluorescence intensity plot profiles of wild-type versus *fn1a/1b* morphant ectodermal cells. 0 μm distance value corresponds to anterior membrane, and 14 μm value corresponds to posterior membrane.

wild type (n = 30 cells, 10 embryos); *fibronectin* (*fn1a/1b*) morpholino (MO)-injected (n = 30 cells, 10 embryos).

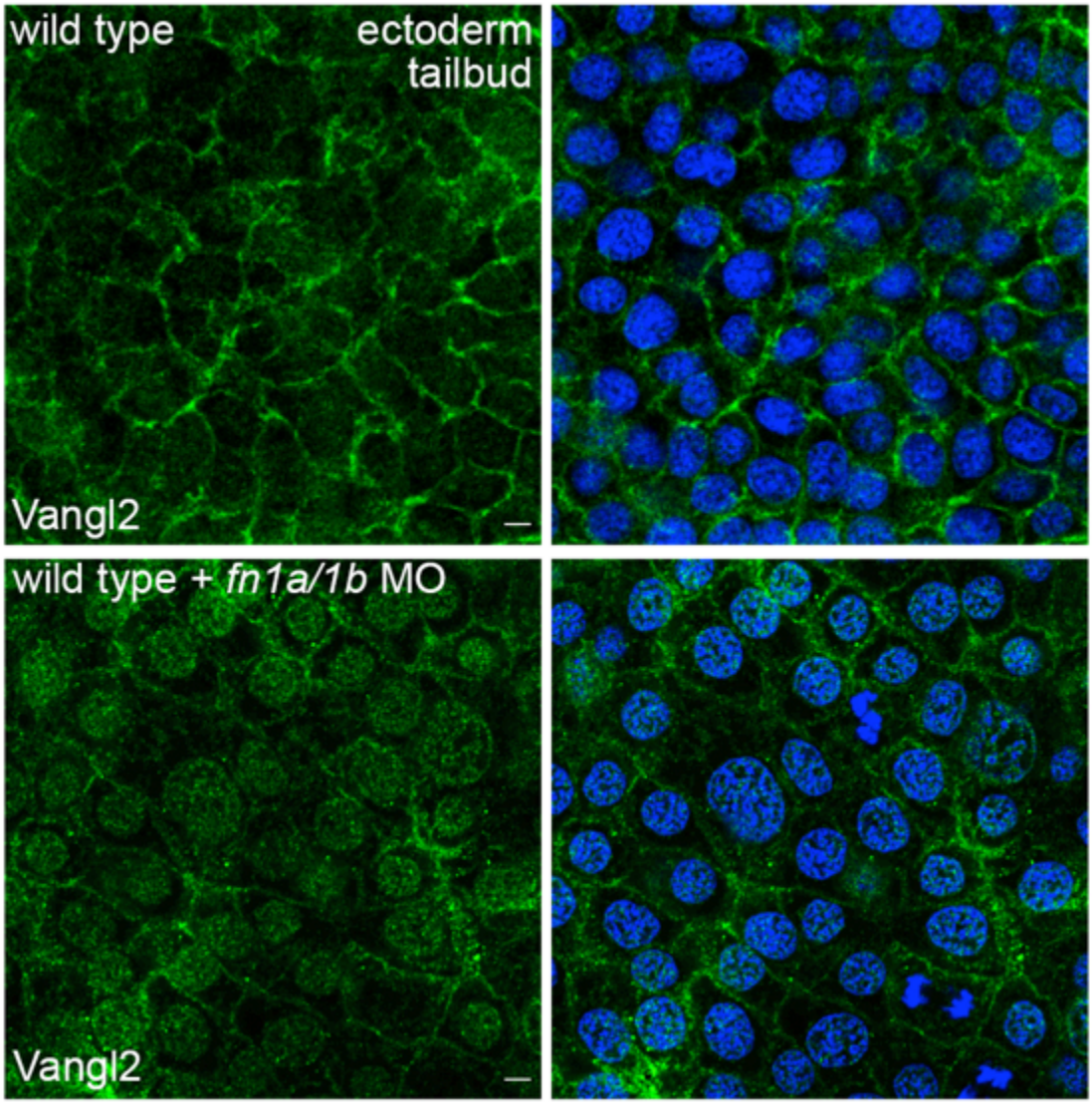

Figure 50 Cell Surface Translocation of Vangl2 Disruption in *fibronectin* (*fn1a/1b*) Morphant Ectodermal Cells: Micrographs of wild-type versus *fn1a/1b* morphant ectodermal cells with Vangl2 immunohistochemistry (Green). Nuclei labeled with DAPI (blue). Scale bar = 5 μm.

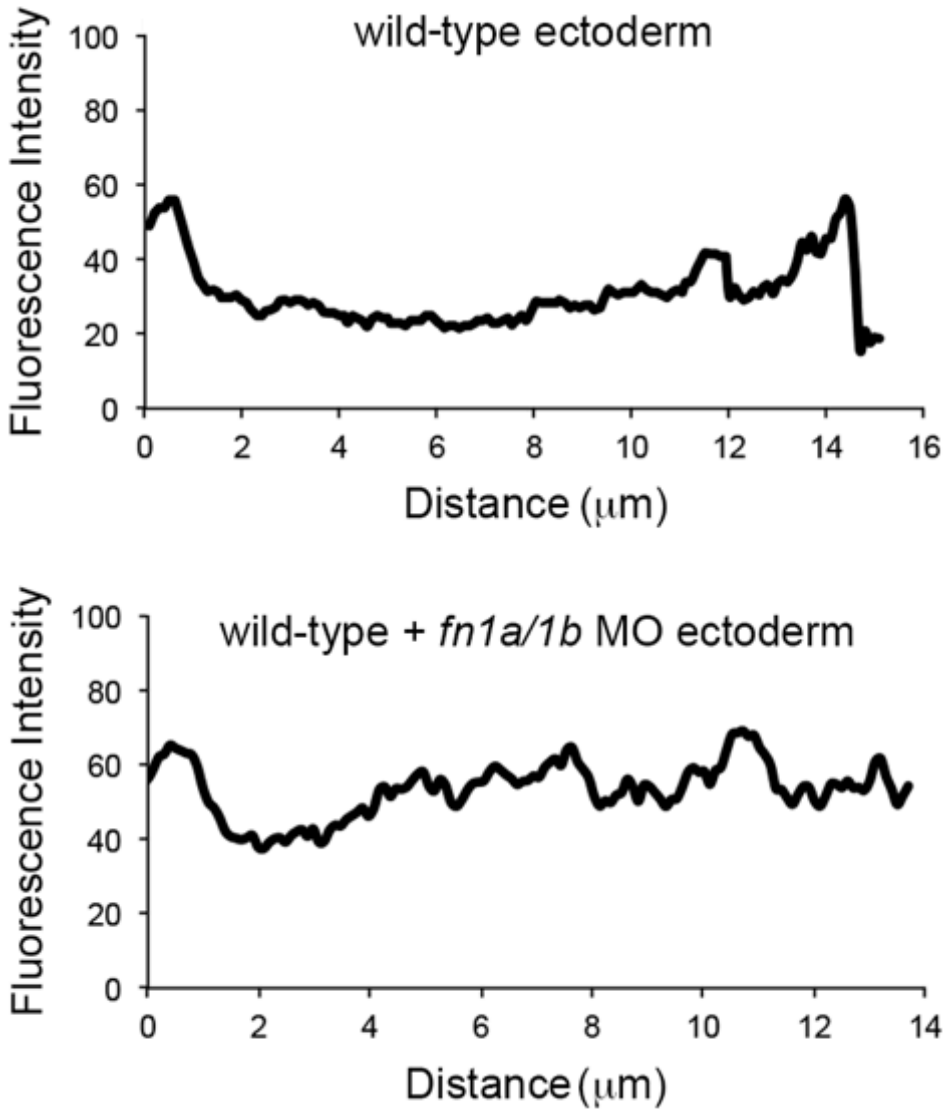

Figure 51 Plot Profiles Illustrating Disrupted Cell Surface Translocation of Vangl2 in *fibronectin* (*fn1a/1b*) Morphant Ectodermal Cells: Fluorescence intensity plot profiles of wild-type versus *fn1a/1b* morphant ectodermal cells. 0 μm distance value corresponds to anterior membrane, and 14 μm value corresponds to posterior membrane.

wild type (n = 30 cells, 10 embryos); *fibronectin* (*fn1a/1b)* morpholino (MO)-injected (n = 30 cells, 10 embryos).

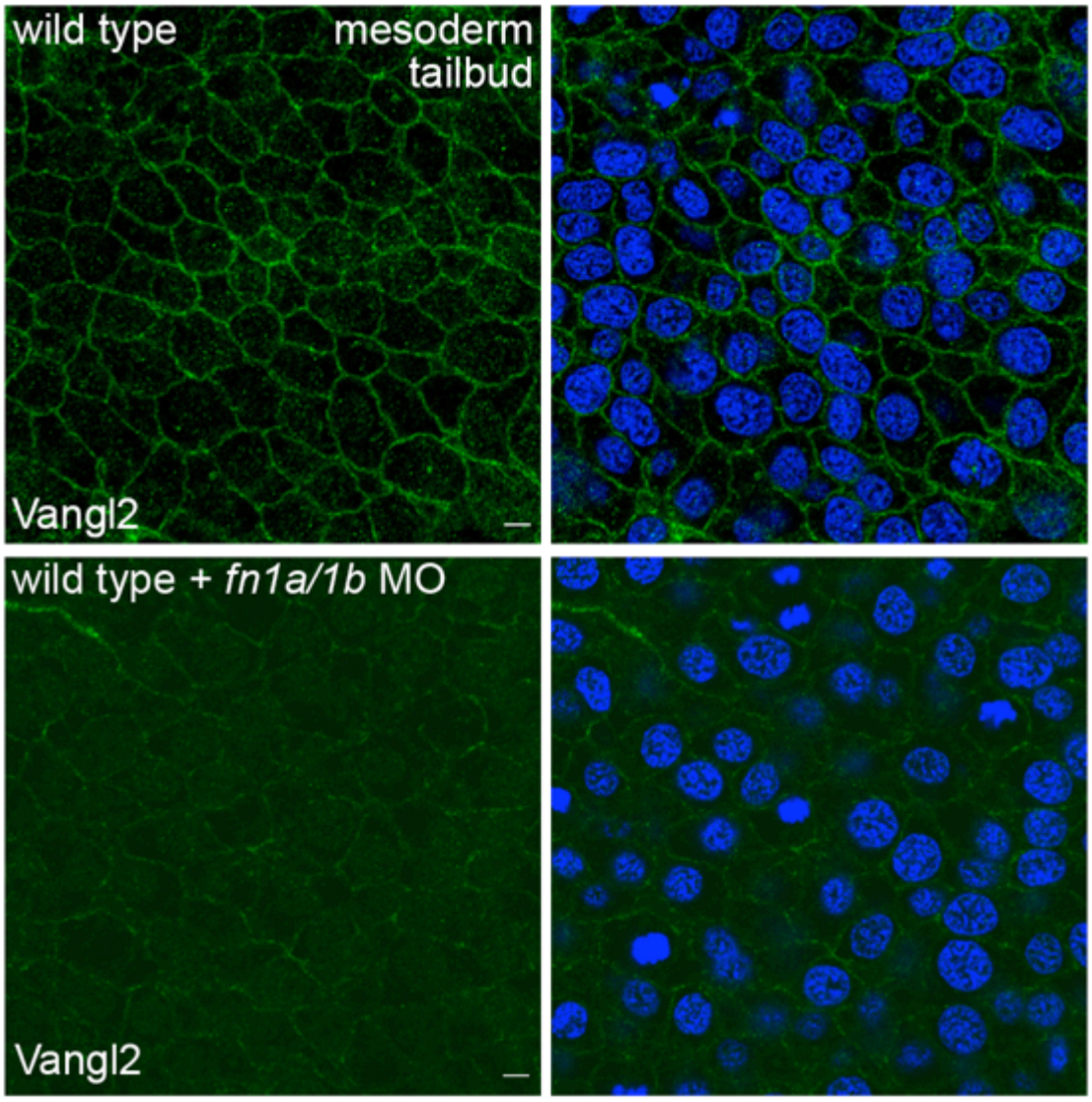

Figure 52 Cell Surface Translocation of Vangl2 Disruption in *fibronectin* (*fn1a/1b*) Morphant Mesodermal Cells: Micrographs of wild-type versus *fn1a/1b* morphant mesodermal cells with Vangl2 immunohistochemistry (Green). Nuclei labeled with DAPI (blue). Scale bar = 5 μm.

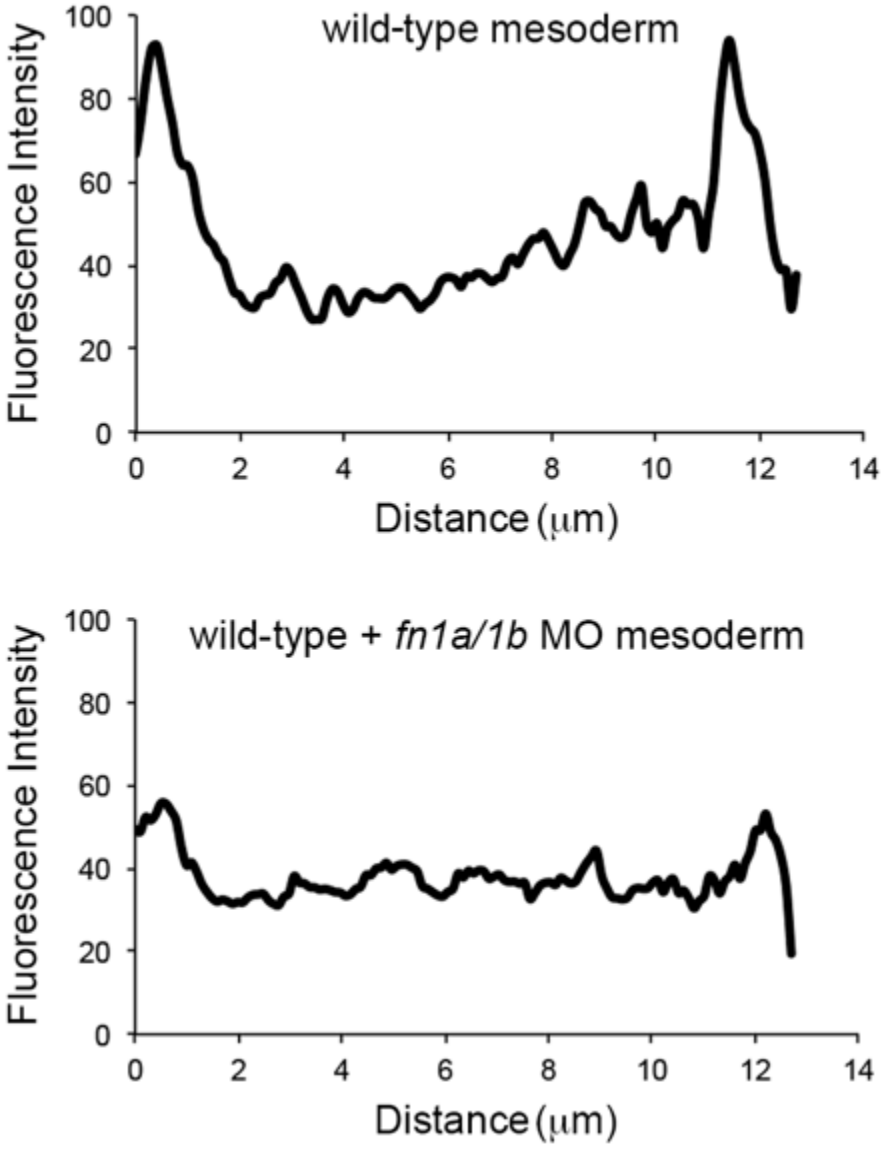

Figure 53 Plot Profiles Illustrating Disrupted Cell Surface Translocation in *fibronectin* (*fn1a/1b*) Morphant Mesodermal Cells: Fluorescence intensity plot profiles of wild-type versus *fn1a/1b* morphant mesodermal cells. 0 μm distance value corresponds to anterior membrane, and 14 μm value corresponds to posterior membrane.

wild type (n = 30 cells, 10 embryos); *fibronectin* (*fn1a/1b*) morpholino (MO)-injected (n = 30 cells, 10 embryos).

ectodermal cells by tailbud stage in wild-type embryos injected with *fibronectin* (*fn1a/1b*) morpholino (Figures 50, 51, 52, 53). Vangl2 fluorescence intensity appears weaker in *fibronectin* (*fn1a/1b*) morphant ectodermal cells. As a result, we verified Vangl2 protein levels using western blot and found no significant change in total Vangl2 protein levels among wild-type and *fibronectin* (*fn1a/1b*) morphant embryos (Data not shown). We propose the weak fluorescence intensity is a result of Vangl2 protein dissemination.

6.3 Conclusion

At mid-gastrulation (80% epiboly), Vangl2 localizes at the cell surface, initiating PCP-dependent activities, while fibronectin fibrillogenesis and deposition appears at approximately the same developmental stage (Dohn et al., 2013; Latimer and Jessen, 2010). Due to the chronology between the onsets of PCP and fibronectin deposition and the f*ibronectin* (*fn1a/1b*) morphant embryo convergence and extension defect, we hypothesized fibronectin may somehow modulate Vangl2 localization at the cell surface (Latimer and Jessen, 2010).

We supported our hypothesis by analyzing Vangl2 fluorescence intensities across gastrula cells at both early gastrulation (60% epiboly) and late gastrulation (tailbud) in wild-type and *fibronectin (fn1a/1b*) morphant embryos. As expected, Vangl2 did not effectively localize at the cell surface of *fibronectin* (*fn1a/1b*) morphant embryos in either ectodermal or mesodermal cell layers. We propose proper cell-matrix interactions are required to initiate Vangl2 translocation to the cell surface and, in turn, complete PCP activation. Vangl2 total protein levels are unaffected in *fibronectin* (*fn1a/1b*) morphant embryos, suggesting cell-matrix interactions may modulate Vangl2 vesicular trafficking

events or stabilization at the cell surface. Our proposal is further supported by the similar *fibronectin* (*fn1a/1b*) morphant and *vangl2* mutant membrane protrusion phenotypes presented in previous chapters.

CHAPTER SEVEN. Fibronectin Knockdown in *vangl2* Mutant Embryos

7.1 Introduction

Due to diminished fibronectin levels in *vangl2* mutant embryos and the results from our membrane protrusion studies on *vangl2* mutant and *fibronectin* (*fn1a/1b*) morphant embryos, we aimed to determine whether these conditions were additive (Latimer and Jessen, 2010; Williams et al., 2012b). We conducted a limited study on *vangl2* mutant embryos with additional loss of fibronectin. Because *vangl2* mutants exhibit decreased fibronectin protein but they do not have total loss of fibronectin, we hypothesized further loss of fibronectin in *vangl2* mutant embryos results in increased membrane-protrusive activity and loss of large protrusion polarity.

7.2 Results

We injected *fibronectin (1a/1b)* morpholino into single cell stage *vangl2* mutant embryos. Once embryos reached the 8-cell stage, we injected membrane-targeted green fluorescent protein (memGFP) for mosaic membrane labeling. Embryos were imaged using a confocal microscope at the end of gastrulation (tailbud). Time-lapse images were collected in 2 min intervals for 20 min (Figure 54). The parameters of this study mirrored the parameters utilized in the previous time-lapse micrograph studies we performed to analyze membrane protrusions.

Manual quantification of membrane protrusions in *vangl2* mutant embryos injected with *fibronectin* (*fn1a/1b*) morpholinos revealed no significant change when we compared *fibronectin* (*fn1a/1b*) morphant embryos, *vangl2* mutant embryos, and *fibronectin (fn1a/1b)* morpholino-injected *vangl2* mutant embryos (Figures 55A, 55B).

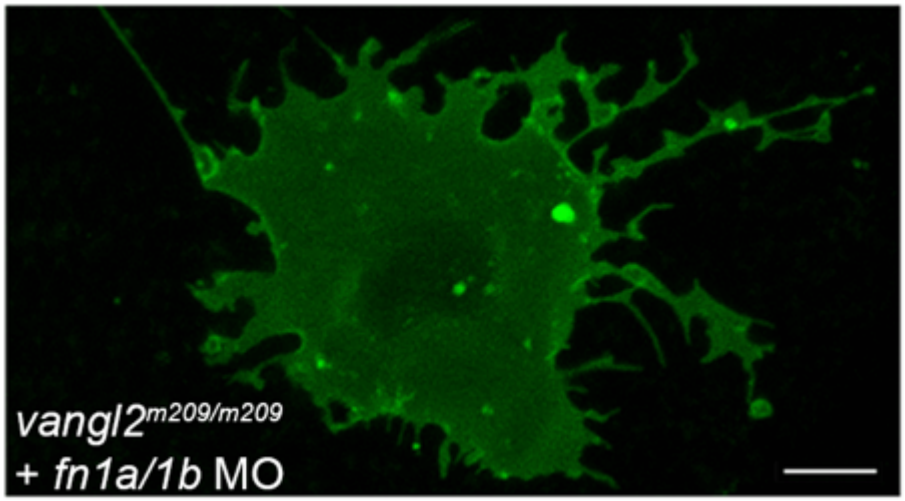

Figure 54 Confocal Micrograph of *fibronectin* (*fn1a/1b*) Morpholino-Injected *vangl2* Mutant Embryo Ectodermal Cell: Confocal micrograph of *fibronectin* (*fn1a*/1b) morpholino (MO)-injected *vangl2* mutant ectodermal cells expressing membrane-targeted green fluorescent protein (memGFP). Scale bar = 5 μm.

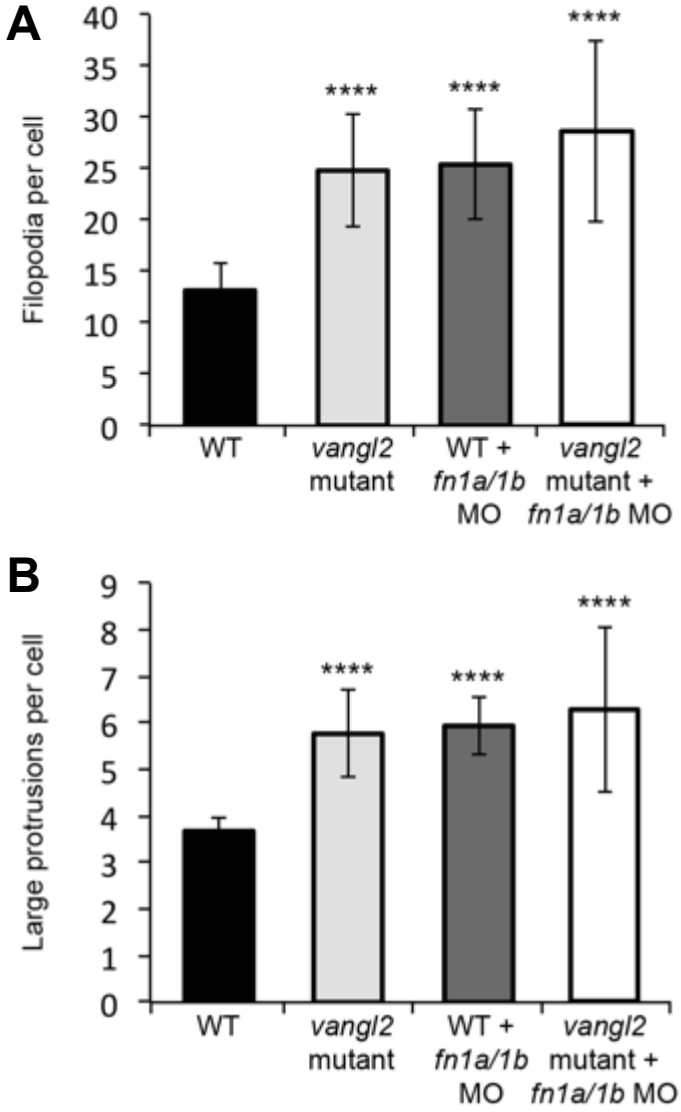

Figure 55 Membrane Protrusions in *fibronectin* (*fn1a/1b*) Morpholino-Injected *vangl2* Mutant Embryos: Graph of average number of filopodia (A) and large membrane protrusions (B) per ectodermal cell in wild-type (WT), *vangl2* mutant, *fibronectin* (*fn1a/1b*) morphant, and *fibronectin* (*fn1a*/1b) morpholino (MO)-injected *vangl2* mutant embryos. Wild-type (n=12 cells, 8 embryos); *vangl2* mutant (n=10 cells, 7 embryos); *fibronectin* (*fn1a/1b*) morphant (n=10 cells, 7 embryos); fibronectin (*fn1a/1b*) MO-injected *vangl2* mutant (n=5 cells, 3 embryos). All values are ± SD. ****$P<0.0001$; P values are versus wild type; one-way ANOVA significance test followed by Tukey HSD post-hoc tests.

Similarly, there was no additional loss of large membrane protrusion polarity. 73.10% +/- 11.28% of large protrusions are polarized along the path of migration in wild-type ectodermal cells (Figure 56). The percentage of polarized large membrane protrusions is reduced to 43.76% +/- 8.24% in *vangl2* mutant ectodermal cells (Figure 56). Wild-type cells injected with fibronectin (fn1a/1b) morpholino produce an average of 46.88% +/- 8.81% of polarized large protrusions (Figure 56). Injecting fibronectin (fn1a/1b) morpholino into *vangl2* mutant embryos to generate further loss of fibronectin did not further reduce the percentage of polarized large membrane protrusions as these ectodermal cells produce an average of 44.26% +/- 5.51% of polarized large membrane protrusions. These results did not support my hypothesis that additional loss of fibronectin in *vangl2* mutant embryos enhances the *vangl2* mutant membrane protrusion phenotype.

7.3 Conclusion

Although *vangl2* mutant embryos produce less fibronectin extracellular matrix than wild-type embryos, some fibronectin remains. Therefore, we hypothesized further diminishing fibronectin levels would enhance membrane protrusion formation and polarity defects (Dohn et al., 2013). Our data illustrate *fibronectin* (*fn1a/1b*) morphlino-injected *vangl2* mutant ectodermal cells produce numbers of membrane protrusions similar to those quantified in *vangl2* mutant and *fibronectin* (*fn1a/1b*) morphant ectodermal cells. Further, we found no significant difference in percentages of polarized large membrane protrusions across *vangl2* mutant, *fibronectin* (*fn1a/1b*) morphant, and *fibronectin* (*fn1a/1b*) morpholino-injected *vangl2* mutant ectodermal cells. These results

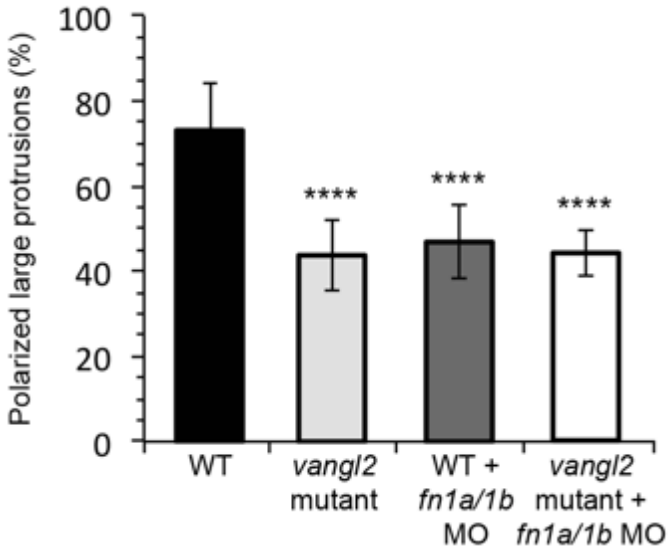

Figure 56 Polarized Membrane Protrusions in *fibronectin* (*fn1a/1b*) Morpholino-Injected *vangl2* Mutant Embryos: Graph of polarized large membrane protrusions per ectodermal cell in wild-type (WT), *vangl2* mutant, *fibronectin* (*fn1a/1b*) morphant, and *fibronectin* (*fn1a*/1b) morpholino (MO)-injected *vangl2* mutant embryos. Wild-type (n=12 cells, 8 embryos); *vangl2* mutant (n=10 cells, 7 embryos); *fibronectin* (*fn1a/1b*) morphant (n=10 cells, 7 embryos); fibronectin (*fn1a/1b*) MO-injected *vangl2* mutant (n=5 cells, 3 embryos). All values are ± SD. ****P<0.0001; P values are versus wild type; one-way ANOVA significance test followed by Tukey HSD post-hoc tests.

indicate the loss of fibronectin and cell-matrix in *vangl2* mutant embryos is substantial enough to disrupt membrane protrusion formation and polarity and further loss of fibronectin in *vangl2* mutant embryos does not compound the membrane protrusion phenotype.

CHAPTER EIGHT. Materials and Methods

8.1 Zebrafish Lines and Husbandry

Adult zebrafish (*Danio rerio*) 1-2 years of age were maintained following standard procedures (Solnica-Krezel et al., 1994). Embryos were collected after natural spawning, grown at 28.5ºC in egg water (purified water with 60 mg/L Instant Ocean), and staged according to morphology (Kimmel et al., 1995). Embryo ages were between 6 and 10.5 hours post-fertilization. Strains used in this study included the following: wild type (AB*, TL, and WIK), *vangl2*/*trilobite*^{m209} (Jessen et al., 2002; Solnica-Krezel et al., 1996), *vangl2*/*trilobite*^{vu7} (Jessen et al., 2002), and *glypican4*/*knypek*^{m119} (Solnica-Krezel et al., 1996; Topczewski et al., 2001). The *vangl2*^{m209} and *glypican4*^{m119} alleles behave like null mutations while the *vangl2*^{vu7} allele is a chromosomal deletion lacking the *vangl2* gene.

The Middle Tennessee State University Institutional Animal Care and Use Committee approved the animal research described in this paper. All procedures were conducted following approved guidelines. The Office of Laboratory Animal Welfare assurance number is A4701-01.

8.2 Morpholinos, Synthetic mRNA, and Embryo Microinjection

Antisense morpholino oligonucleotides were obtained from Gene Tools, LLC. The following previously published morpholinos were used: *fn1a* (5'-tttttttcacaggtgcgattgaacac-3'), *fn1b* (5'-tactgactcacgggtcattttcacc-3' and 5'-gcttctggctttgactgtatttcgg-3'), *prickle1a* (5'-cagctccatcactaacacccccctca-3'), and *vangl2* (5'-agttccaccttactcctgagagaat-3') (Dohn et al., 2013; Julich et al., 2005; Latimer and Jessen, 2010; Trinh and Stainier, 2004; Veeman et al., 2003; Williams et al., 2012). Each

morpholino was injected at a dose of 3-10 ng/embryo. The *fn1a/1b* morpholino combination reduces fibronectin protein expression (Fig. S3) and produces the reported anterior somite defect (Julich et al., 2005; Koshida et al., 2005; Latimer and Jessen, 2010). The *prickle1a* morpholino causes a typical convergence and extension phenotype similar to that produced by other *prickle1a* morpholinos (Carreira-Barbosa et al., 2003; Veeman et al., 2003). The *vangl2* morpholino produces convergence and extension phenotypes (Dohn et al., 2013; Williams et al., 2012) and late gastrulation ectodermal cell protrusion phenotypes similar to the *vangl2*$^{m209/m209}$ mutant (24.60 filopodia and 5.77 large protrusions on average per cell). None of the morpholinos used in this study stimulate obvious p53-dependent cell death.

DNA-encoding full-length Vangl2, the F-actin marker Lifeact-GFP (Riedl et al., 2008) (a gift from A. Diz-Muñoz and M. Bergert), memGFP, memRFP, GFP-VANGL2, Fibronectin 1a, and Fibronectin 1b were cloned in the pCS2 vector and linearized by *NotI* restriction endonuclease. The *fibronectin* clones are not targeted by the *fn1a/1b* morpholinos. Synthetic mRNA was made using the Sp6 mMessage mMachine kit as directed by the manufacturer (Ambion) and purified by G-50 sephadex columns (Roche). Microinjection into single-cell stage or 8-cell stage embryos was performed following standard methods (Gilmour, 2002). Synthetic mRNA was injected at the following doses: *vangl2* (100-300 pg); *Lifeact-GFP* (100 pg), *memGFP* and *memRFP* (100 pg); *GFP-VANGL2* (50 pg); *fn1a* and *fn1b* (200 pg).

8.3 Whole-Mount *in situ* Hybridization, Immunofluorescence, and Antibodies

Staged embryos were fixed overnight in 4% paraformaldehyde in PBS and washed with PBS containing 0.1% Tween-20 before high resolution *in situ* hybridizations were performed as described (Thisse and Thisse, 2008). Antisense RNA probes were generated by *in vitro* transcription and purified following standard methods (Westerfield, 2000).

For immunofluorescence, embryos were fixed in either 4% paraformaldehyde/PBS/sucrose fix buffer (1:1 mixture of 8% paraformaldehyde/PBS and 2X sucrose buffer; 8.0 g Sucrose, 0.15 ml 0.2 M $CaCl_2$, 90 ml 0.2 M Na_2HPO_4 buffer, pH 7.3) overnight or in Prefer fixative (Anatech Ltd.) for 2 h, and then manually dechorionated and permeabilized for 30 min at room temperature (5% normal donkey serum, 0.5% Triton, PBS). Embryos were blocked 2 h at room temperature (5% BSA, 1% DMSO, 0.1% Triton, PBS) with gentle rocking. Primary antibodies diluted in block solution at 1:100 were applied before incubating embryos overnight at 4°C with gentle rocking. Embryos were washed six times, 15 min each, in PBST with DMSO (0.1% Triton, 1% DMSO, PBS). Embryos were treated with secondary antibodies (Jackson ImmunoResearch), diluted 1:500 in 50% block and 50% PBST (0.1% Triton, PBS), and incubated 2 h at room temperature under UV protection with gentle rocking. For nuclei labeling, embryos were washed with PBS prior to 30 min incubation in DAPI (2-(4-amidinophenyl)-1H -indole-6-carboxamidine). Embryos were washed three times with PBS and stored at 4°C. Sections were obtained by embedding fibronectin immunolabeled/DAPI stained embryos in 1.2% agarose in a 5% sucrose solution followed

by cryosectioning (10 mm). Fibronectin was detected using a rabbit polyclonal antibody generated against an epitope within the human protein (F3648, Sigma-Aldrich). An affinity purified rabbit polyclonal antibody capable of recognizing an epitope near the N-terminus (NH_2-RSKSRDSSSRGDKSC-COOH) of zebrafish Vangl2 was generated (ProSci Inc.). This antibody will not bind Vangl1 due to lack of epitope sequence homology and lack of Vangl1 expression during gastrulation (Jessen and Solnica-Krezel, 2004). We validated the antibody by immunolabeling embryos overexpressing *vangl2* mRNA and embryos with a *vangl2* chromosomal deletion (data not shown).

8.4 Embryo Protein Extraction, Western Blot, and Antibodies

For zebrafish embryo whole-cell lysates, pools of approximately 20-50 embryos were manually dechorionated, deyolked, lysed in RIPA (50 mM Tris, pH 7.4, 150 mM NaCl, 1% NP-40, 0.5% DOC, 0.1% SDS, mammalian protease inhibitor cocktail), and clarified by centrifugation. Whole-embryo lysates were boiled 10 min following addition of Laemmli sample buffer (1x final concentration). Protein extracts were separated by 10% SDS-PAGE and transferred to PVDF membrane using a trans-blot turbo transfer system following the manufacturer's instructions (Bio-Rad). Non-specific binding to membranes was blocked with 5% non-fat milk in TBS-Tween (50 mM Tris, pH 7.4, 150 mM NaCl, 0.1% Tween-20), and membranes incubated overnight with rabbit polyclonal Vangl2 antibody (1:1,000) in block at 4°C with gentle rocking. Membranes were incubated with a peroxidase-conjugated secondary antibody (1:5,000; Jackson ImmunoResearch), developed using Clarity ECL substrate (Bio-Rad), and imaged using a UVP GelDoc-It Imaging System (Upland, CA). During each experiment blots were stripped at room

temperature for 15 min using 25 mM glycine and 1% SDS (pH 2.0) and re-probed in a 1:1,000 dilution of beta-actin antibody (#4967, Cell Signaling Technology). Densitometry was performed on western blots with UVP Visionworks software.

8.5 Microscopic Imaging

Staged and dechorionated live or fixed embryos were mounted as previously described (Roszko et al., 2015) and imaged with a Zeiss LSM700 confocal microscope with a 63x oil-immersion objective (N.A. 1.4). Time-lapse images were collected for 20 min at 1-2 min intervals with a 0.39 or 0.50 mm z-axis step size. Embryo orientation was documented for each time-lapse series by taking low-magnification (10x) reference images under transmitted light. Yolk-plug closure-tailbud stage live embryo images were obtained with an Olympus SZX16 stereomicroscope equipped with a Q-Color5 CCD camera. Sectioned embryo images were acquired using an Olympus IX83 inverted microscope equipped with a 20x objective and a Hamamatsu Flash 4.0 CMOS camera.

8.6 Quantitation of Cell Shape, Alignment, Velocity, and Directness

Cell LWRs and MLA analyses were performed using Fiji software (https://fiji.sc/) (Schindelin et al., 2012) as described (Jessen et al., 2002). To obtain cell migration velocity and directionality data, we tracked cell movement during our 20 min time-lapse image series (10 frames) using Fiji's Manual Tracking tool. This tool outputs data points distributed as scaled latitude and longitude values, which were exported to Ibidi's Chemotaxis and Migration Tool standalone software (https://ibidi.com) to generate plot diagrams and directness and velocity statistics (Gerhard Trapp and Elias Horn, 2010).

8.7 Analysis of Membrane Protrusions

We quantified and annotated membrane protrusions using Fiji software (Schindelin et al., 2012). Protrusion number and polarity were quantified as the number formed during a 20 min time interval (10 image frames). A spike-like structure distinguished actin-rich filopodia from other types of protrusions. Large actin-rich protrusions were subjectively classified by their irregular shapes and base widths >2.5 μm and included lamellipodia-like protrusions and filolamellipodia. Characterized by their spherical appearance, blebs were rare in lateral ectodermal cells. Productive protrusions were quantified as the number of large protrusions formed that were associated with cell body translocation during a 20 min time interval (10 image frames). Protrusions were classified as polarized if they had a base to tip orientation within ±45° of the path of migration. Rose diagrams were generated using the angles of individual ectodermal cell large protrusions.

8.8 GFP-VANGL2 and Vangl2 Localization

Time-lapse confocal image series were collected at the tailbud-1-somite stage as described above. Prior to analysis, we subtracted the image background and created sum slice projections. For the GFP-VANGL2 localization studies, we used Fiji's Plot Profile tool to quantify fluorescence intensities along the length of a line and generate an output of distance in mm (x-value) and grey value (y-value) (Schindelin et al., 2012). To test for asymmetric membrane expression bias, we drew a line through each cell from either anterior to posterior or leading edge to trailing edge membranes before producing a plot profile. During our membrane domain fluorescence intensity analysis, we avoided

membrane-protrusive domains. We selected peak values for each membrane domain to generate anterior/posterior and leading edge/trailing edge fluorescence intensity ratios for memRFP and GFP-VANGL2. To assess GFP-VANGL2 expression dynamics in large membrane protrusions, we used Fiji's Plot Profile tool to gather fluorescence intensity data (Schindelin et al., 2012). Drawing a line inward from the plasma membrane at three time points, the Plot Profile tool produced plot profile data similar to that of our Vangl2 asymmetry study. Because membrane protrusion cycles of gastrula cells are highly dynamic in space and time, we examined GFP-VANGL2 expression at subjective time points associated with membrane protrusion preparation, eruption, and extension. We selected the eruption plot apex, and the fluorescence intensity values for the corresponding distance points (x-values) were collected for the preparation and extension phases. These data points produced eruption/preparation and extension/eruption fluorescence intensity ratios for both memRFP and GFP-VANGL2. We used the eruption phase of large protrusion formation for comparison of GFP-VANGL2 expression between protrusive and non-protrusive domains and between polarized and non-polarized protrusions. To analyze endogenous zebrafish Vangl2 expression, we collected confocal z-stack images of epiblast cells at 60% epiboly and ectodermal and mesodermal cells at tailbud stage. We drew a line across the center of each cell from anterior to posterior membranes, and using Fiji's Plot Profile tool we generated a grey value plot profile, representative of fluorescence intensities along the length of the drawn line. Since we used Vangl2 antibody labeling and not mosaic expression, we could not discern adjacent cell membranes. For consistency, we used congruent techniques when

performing plot profile analyses on control and experimental cells. The fluorescence intensities for each distance point along the drawn line were averaged to generate a mean grey value plot profile.

8.9 Statistics

Data were exported to Microsoft Excel for graphing and StatCrunch software was used for statistical analysis. The statistical tests performed and significance values obtained are indicated in each figure legend. The data presented are normally distributed.

CHAPTER NINE. Discussion and Future Directions

Planar cell polarity (PCP) is integral to gastrulation stage convergence and extension movements (Goodrich and Strutt, 2011; Jessen et al., 2002; Wallingford et al., 2002). When the zebrafish gastrula reaches mid-gastrulation (80% epiboly), cells begin meandering dorsally, and by ~95% epiboly PCP-dependent directed migration initiates as the cells elongate, mediolaterally align, and undergo coordinated movement (Sepich et al., 2005). Defective PCP results in directed migration and, in turn, convergence and extension failure, leading to a shortened and broadened dorsal axis. Loss of the core PCP protein Vangl2 disrupts the pathway and causes a severe convergence and extension phenotype that disrupts gastrulation and is associated with neural tube defects in vertebrates, including humans. Data from the fly implicate core PCP proteins, such as Vangl2, are required for actin-rich hair formation and orientation, indicating a potential a role for PCP in actin remodeling (Goodrich and Strutt, 2011; Taylor et al., 1998; Wolff and Rubin, 1998). Early characterization of the zebrafish *vangl2* mutant embryo reported meandering gastrula cells during directed migration processes underlying convergence and extension (Jessen et al., 2002; Sepich et al., 2005). Therefore, we hypothesized PCP, specifically the Vangl2 protein, regulates actin-rich membrane protrusion formation and orientation. To test our hypothesis, we characterized membrane protrusion formation and polarity under a variety of PCP-related conditions. We further aimed to establish Vangl2 localization relative to membrane protrusions and the plasma membrane. We also hypothesized a role for the fibronectin extracellular matrix in membrane protrusion formation and polarization.

9.1 Vangl2 and Glypican4 Differentially Regulate Membrane-Protrusive Activity

First, we quantified the average number of membrane protrusions, both filopodia and large membrane protrusions, in wild-type, *vangl2* mutant, and *glypican4* mutant ectodermal cells. *vangl2* mutant ectodermal cells produce significantly more filopodia and large membrane protrusions than wild-type ectodermal cells, while *glypican4* mutant ectodermal cells have no change in membrane protrusion quantities compared to wild type. Tracking the cell trajectories revealed *vangl2* mutant ectodermal cells have a loss of directness compared to wild type. However, *glypican4* mutant ectodermal cells travel along a much straighter path with a directness value similar to that of wild-type ectodermal cells. Previous work illustrated *vangl2* and *glypican4* mutant embryos exhibit contradicting molecular behaviors, such has fibronectin, cadherin, and matrix metalloproteinase activity, despite their similar embryonic phenotypes (Dohn et al., 2013; Williams et al., 2012a). Glypican4 functions as a Wnt co-receptor and is thought to activate downstream actin effectors. Vangl2 binds Prickle1a and is thought to limit Wnt/Glypican4 signaling. Based on these reports, the contrasting membrane protrusion quantities among *glypican4* and *vangl2* mutant ectodermal cells fit the current model that Vangl2 and Glypican4 differentially regulate cell behaviors underlying convergence and extension movements.

After establishing membrane protrusion quantities, we analyzed membrane protrusion polarity for both filopodia and large membrane protrusions. *vangl2* and *glypican4* mutant ectodermal cells have no change in the percentage of polarized filopodia

compared to wild type. Filopodia can fill multiple roles within the cell, both mechanical and sensory. However, our results indicate a primarily sensory role for filopodia in migrating gastrula cells. To further support the role of filopodia, it would be useful to conduct localization experiments on certain proteins associated with filopodia mechanosensory behaviors, such as Fascin, Plastin, Espin, Myo7, and Myosin (Heckman and Plummer, 2013). Other proteins associated with sensory behaviors include ion channels, while microtubule bridge proteins and focal contact-related integrins localizing within filopodia might suggest a more mechanical role (Heckman and Plummer, 2013). We theorize filopodia extend to sense the extracellular environment and signal to initiate polarized large protrusion formation in this context (Faix and Rottner, 2006).

Both *vangl2* and *glypican4* mutant ectodermal cells have a significant reduction in the percentage of polarized large membrane protrusions. These results indicate the PCP pathway functions to restrict large membrane protrusions to the leading and trailing edges of the cell to promote efficient directed migration. Because *glypican4* ectodermal cells follow a relatively straight path with minimal loss of directness, we suspect non-polarized large protrusion formation is not sufficient enough to disturb directness. The effectual directness of *glypican4* mutant cells may be a result of their enhanced cadherin-mediated cell-cell adhesion, which may work to maintain cell packing and, therefore, straight cell trajectories (Dohn et al., 2013). While *glypican4* mutant ectodermal cells exhibit minimal loss of directness, they still follow aberrant cell trajectories and fail to migrate effectively toward the dorsal body axis. Therefore, loss of large protrusion

polarization is likely a major factor in the cell's ability to participate in efficient dorsal convergence.

In the future, our lab plans to characterize autonomous and non-autonomous functions of PCP protein membrane protrusion defects. Further, we plan to conduct a series of cell-transplantation experiments to explore these features. Using memGFP labeled *vangl2* and *glypican4* mutant donors, we will transplant 20-50 cells from a ~1000 cell stage embryo to wild-type embryos. After recipient embryos reach the end of gastrulation (tailbud), a series of time-lapse confocal micrographs will be collected to perform a membrane protrusion study similar to those mentioned in previous chapters. An examination of the ectodermal cells would allow for an accurate comparison to our existing data to determine if membrane protrusion quantities and large membrane protrusion polarization features of mutant donor cells are propagated to adjacent cells. If adjacent wild-type recipient cells assume the mutant features, *vangl2* membrane protrusion defects will be classified as non-autonomous. However if the membrane protrusion defects of the *vangl2* mutant donor cells are rescued, *vangl2* mutant membrane protrusion defects will be classified as autonomous. We predict a combination of autonomous and non-autonomous effects from these studies.

9.2 Vangl2 Overexpression and *prickle1a* Morphant Ectodermal Cells Exhibit Membrane Protrusion Defects

prickle1a morphant embryos exhibit many of the same molecular features as *vangl2* mutant embryos, including loss of fibronectin (Dohn et al., 2013). Prickle1a is a

known binding partner for Vangl2 and is required for cell surface localization of Vangl2 (Bastock et al., 2003; Carreira-Barbosa et al., 2003; Dohn et al., 2013; Jenny, 2003; Veeman et al., 2003). The current accepted working model of the PCP pathway puts Vangl2 and Prickle1a on the same side of the pathway working cooperatively to regulate downstream effectors. As such, we hypothesized loss of Prickle1a results in a membrane protrusion defect similar to that of *vangl2* mutant ectodermal cells.

A trademark of core PCP proteins, gain and loss of PCP protein function often have comparable phenotypic outcomes (Yang and Mlodzik, 2015). The convergence and extension phenotype associated with Vangl2 overexpression is slightly more severe than the *vangl2* mutant phenotype, and while the embryonic phenotype has been characterized the molecular and membrane protrusion phenotypes were unreported. Because specific levels of Vangl2 are thought to be required for proper convergence and extension, we expected ectodermal cells from wild-type embryos injected with *vangl2* mRNA to have a membrane protrusion defect like that observed in *vangl2* mutants.

Ectodermal cells from embryos with loss of Prickle1a and Vangl2 overexpression produce excess filopodia and large membrane protrusions. We also saw a reduction in the percentage of polarized large membrane protrusions. These results support our hypotheses that Prickle1a and Vangl2 function cooperatively to modulate membrane protrusion formation and polarization and, also, developing gastrulae require a specific quantity of Vangl2 for proper membrane protrusion formation and polarization. Previous work illustrates loss of Vangl2 and Prickle1a compounds the convergence and extension defects seen with loss of the individual proteins, suggesting Vangl2 and

Prickle1a do not function redundantly (Carreira-Barbosa et al., 2003; Veeman et al., 2003). Additional work claims both Vangl2 and Prickle bind to Dishevelled, a protein known to asymmetrically localize at the opposite side of the cell in the fly (Bastock et al., 2003; Carreira-Barbosa et al., 2003; Goodrich and Strutt, 2011; Wallingford and Habas, 2005; Yang and Mlodzik, 2015). The consequences of these interactions are unknown; however, Vangl2 and Prickle may function to inhibit Dishevelled function.

9.3 Vangl2 Asymmetrically Localizes in Erupting Large Membrane Protrusions

In the fly wing, core PCP proteins, Van Gogh, Prickle, Dishevelled, Diego, and Frizzled, localize asymmetrically (Goodrich and Strutt, 2011). However, zebrafish Vangl2 asymmetry has only been reported in highly polarized, non-migrating axial cells, where it localizes with an anterior bias (Roszko et al., 2015). We assessed GFP-VANGL2 localization within migrating gastrula cells, comparing the anterior and posterior membranes and leading edge (dorsal) and trailing edge (ventral) membranes. We found no significant asymmetry among these membranes. These data may be a result of dynamic Vangl2 expression as migrating gastrula cells undergoing directed migration are rapidly changing shape, packing, and membrane protrusion formation. Moreover, previous work reported Wnt5a works to phosphorylate Vangl2 via Ror2 and ties Vangl2 activity to levels of phosphorylated Vangl2 (Gao et al., 2011). As such, post-translational modification, specifically phosphorylation, of Vangl2 may modulate Vangl2 cell-surface localization.

Going forward, we will conduct another analysis of GFP-VANGL2 stability at the cell surface to assess Vangl2 symmetry. Our lab has shown integrin-matrix interactions regulate VANGL2 stability and cell-surface expression in tissue culture studies (T. Jessen and J. Jessen, unpublished data). Therefore, we will perform a fluorescence recovery after photobleaching (FRAP) experiment using the zebrafish model to determine if our tissue culture data is translatable. We will inject GFP-VANGL2 into single cell stage embryos, and at the end of gastrulation (tailbud) we will photobleach with a 488 nm laser to gauge GFP-VANGL2 recovery at the cell surface. Since Glypican4/Frizzled/Dishevelled asymmetry has not been established in the zebrafish model, we will perform micrographic studies to determine their localization within migrating gastrula cells.

We hypothesized Vangl2 functions to suppress inappropriate membrane-protrusive activity or to restrict membrane protrusion formation to specific cellular domains, specifically at the leading and trailing edges along the path of migration. Therefore, we aimed to characterize Vangl2 localization within developing large membrane protrusions. We selected three subjective time points to denote large membrane protrusion formation and development, which we refer to as preparatory, eruption, and extension phases.

An analysis of GFP-VANGL2 localization relative to large membrane protrusions revealed an accumulation of GFP-VANGL2 within large protrusions during their eruption phase, representative of the newly erupted large membrane protrusion. Previous work demonstrated a similar burst of Vangl2 localization within neuronal filopodia just prior to the protrusion collapse (Davey et al., 2016). We supported these data by

examining GFP-VANGL2 localization in non-protrusive domains versus large membrane protrusions in the eruption phase and found a significant increase in GFP-VANGL2 localization in eruption phase large membrane protrusion. Further analysis revealed no significant difference between GFP-VANGL2 localization in polarized and non-polarized large membrane protrusions. Together, these data suggest Vangl2 may function to restrict membrane protrusions to specific functional cellular domains to drive directed migration in lateral ectodermal cells. Vangl2 may also work to initiate large membrane protrusion collapse, thereby limiting protrusion lifespan.

To further characterize Vangl2 localization relative to large protrusions, we will collect another time-lapse series with shorter intervals to follow Vangl2 localization dynamics more precisely. This study will allow us to discern whether Vangl2 functions to trigger large membrane protrusion collapse. A review of our existing time-lapse micrographs indicates a change in GFP-VANGL2 concentration at points of cell-cell contacts within large protrusions and filopodia. It would be useful to also assess Vangl2 localization within filopodia for future studies.

After additional characterization of GFP-VANGL2 localization within large membrane protrusions and filopodia, a similar set of experiments to determine Prickle1a localization within wild-type and *vangl2* mutant ectodermal cell membrane protrusions would be useful. Knocking down Prickle1a and analyzing Vangl2 localization within membrane protrusions will also allow us to expand on the existing knowledge of their functional relationship.

9.4 Fibronectin is Integral to Vangl2-Dependent Membrane-Protrusive Activity

A key component of the zebrafish gastrula extracellular matrix, fibronectin is integral to embryonic development and functions to provide a substrate for migrating cells (Darribère and Schwarzbauer, 2000; Winklbauer and Keller, 1996). More recently, researchers illustrated cell-matrix interactions, specifically fibronectin-integrin interactions, are required for proper membrane protrusion formation and polarization (Davidson et al., 2006). Fibronectin was linked to PCP when scientists manipulated expression of Vangl2, Prickle, and Frizzled and disrupted fibronectin organization in the frog (Goto et al., 2005). Soon after, our lab noticed a reduction of fibronectin in *vangl2* mutants (Dohn et al., 2013). Our lab also found fibronectin fibrillogenesis and deposition coincides with the onset of Vangl2 translocation to the cell surface (Dohn et al., 2013). Additionally, loss of fibronectin results in a mild convergence and extension phenotype, indicating a role for fibronectin in PCP-dependent activities (Dohn et al., 2013).

We hypothesize the diminished levels of fibronectin in *vangl2* mutant embryos contributes to the membrane protrusion defect as migrating cells may be struggling to sense and form meaningful interactions with their migratory substrate and extracellular environment during directed migration. As expected, *fibronectin* (*fn1a/1b*) morphant ectodermal cells produce excess numbers of filopodia and large protrusions, similar to *vangl2* mutant ectodermal cells. *fibronectin* (*fn1a/1b*) morphant ectodermal cells, also, have a significant reduction in the percentage of polarized large membrane protrusions. Despite these membrane protrusion defects, other planar cell polarity features remain

intact, including mediolateral alignment and directness. This data indicates a significant role for fibronectin extracellular matrix in membrane protrusion formation and polarization. We suspect loss of fibronectin within *vangl2* mutant embryos is a major contributing factor to the membrane protrusion phenotype reported here. We were unable to compound the membrane protrusion defect in *vangl2* mutant ectodermal cells by further knocking fibronectin down via *fibronectin* (*fn1a/1b*) morpholino injection. Other unknown mechanisms must drive directed migration movements required for convergence and extension, evidenced by the mild *fibronectin* (*fn1a/1b)* morphant convergence and extension phenotype. Further support for our proposal includes the membrane-protrusion rescue we were able to induce by injecting *fibronectin* (*fn1a/1b*) mRNA into *vangl2* mutant embryos.

We hypothesized a role for fibronectin in Vangl2 translocation to the cell surface due to the chronology of fibronectin fibrillogenesis and the onset of PCP-dependent activities. By injecting *fibronectin (fn1a/1b)* into wild-type embryos and reviewing Vangl2 localization, we determined Vangl2 does not localize at the cell surface without an intact fibronectin extracellular matrix. We propose cell-matrix interactions stimulate Vangl2 translocation as PCP-dependent directed migration requires a fibronectin substrate for effective migration. Our lab previously showed VANGL2 binds integrin heterodimer αvβ3 in tissue culture (Jessen and Jessen, 2017). Because integrin has two conformations, one inactive and the other for extracellular matrix binding, Vangl2 may preferentially bind to integrins in an active, extracellular matrix-binding conformation, which could define the Vangl2/fibronectin relationship (Shimaoka et al., 2002). This relationship may

contribute to Vangl2 localization and/or stability at the cell surface. Alternately, cell-ECM interactions may promote endosomal delivery and fusion with the plasma membrane, thereby, delivering and/or recycling Vangl2. Future studies will address Vangl2 trafficking versus cell-surface stability using both the zebrafish model system and tissue culture. We theorize fibronectin affects membrane protrusion formation and polarization directly and PCP indirectly by initiating Vangl2 translocation.

Future studies could include the use of cell transplantation to assess donor mutant ectodermal cell membrane-protrusive behaviors relative to an intact wild-type fibronectin extracellular matrix. We will also conduct studies to analyze fibronectin fibril orientation and polarization relative to the path of migration and membrane protrusion formation as some previous works suggest a correlation between membrane protrusion and fibronectin fibril orientation (Goto et al., 2005). Lastly, it will critical to identify the integrins involved and the fibronectin-integrin-Vangl2 link.

References

Abercrombie, M., Heaysman, J.E., and Pegrum, S.M. (1970). The locomotion of fibroblasts in culture. II. Exp. Cell Res. *60*, 437–444.

Adler, P.N., Taylor, J., and Charlton, J. (2000). The domineering non-autonomy of frizzled and Van Gogh clones in the Drosophila wing is a consequence of a disruption in local signaling. Mech. Dev. *96*, 197–207.

Banères, J.-L., Roquet, F., Green, M., LeCalvez, H., and Parello, J. (1998). The Cation-binding domain from the α subunit of integrin $\alpha_5\beta_1$ is a minimal domain for fibronectin recognition. J. Biol. Chem. *273*, 24744–24753.

Bastock, R., Strutt, H., and Strutt, D. (2003). Strabismus is asymmetrically localised and binds to Prickle and Dishevelled during Drosophila planar polarity patterning. Dev. Camb. Engl. *130*, 3007–3014.

Boutros, M., and Mlodzik, M. (1999). Dishevelled: at the crossroads of divergent intracellular signaling pathways. Mech. Dev. *83*, 27–37.

Carmany-Rampey, A., and Schier, A.F. (2001). Single-cell internalization during zebrafish gastrulation. Curr. Biol. CB *11*, 1261–1265.

Carreira-Barbosa, F., Concha, M.L., Takeuchi, M., Ueno, N., Wilson, S.W., and Tada, M. (2003). Prickle 1 regulates cell movements during gastrulation and neuronal migration in zebrafish. Dev. Camb. Engl. *130*, 4037–4046.

Chu, Y.-S., Thomas, W.A., Eder, O., Pincet, F., Perez, E., Thiery, J.P., and Dufour, S. (2004). Force measurements in E-cadherin-mediated cell doublets reveal rapid adhesion strengthened by actin cytoskeleton remodeling through Rac and Cdc42. J. Cell Biol. *167*, 1183–1194.

Cirone, P., Lin, S., Griesbach, H.L., Zhang, Y., Slusarski, D.C., and Crews, C.M. (2008). A role for planar cell polarity signaling in angiogenesis. Angiogenesis *11*, 347–360.

Ciruna, B., Jenny, A., Lee, D., Mlodzik, M., and Schier, A.F. (2006). Planar cell polarity signalling couples cell division and morphogenesis during neurulation. Nature *439*, 220–224.

Coyle, R.C., Latimer, A., and Jessen, J.R. (2008). Membrane-type 1 matrix metalloproteinase regulates cell migration during zebrafish gastrulation: Evidence for an interaction with non-canonical Wnt signaling. Exp. Cell Res. *314*, 2150–2162.

Curnis, F., Longhi, R., Crippa, L., Cattaneo, A., Dondossola, E., Bachi, A., and Corti, A. (2006). Spontaneous formation of L-isoaspartate and gain of function in fibronectin. J. Biol. Chem. *281*, 36466–36476.

Darribère, T., and Schwarzbauer, J.E. (2000). Fibronectin matrix composition and organization can regulate cell migration during amphibian development. Mech. Dev. *92*, 239–250.

Davey, C.F., Mathewson, A.W., and Moens, C.B. (2016). PCP signaling between migrating neurons and their planar-polarized neuroepithelial environment controls filopodial dynamics and directional migration. PLOS Genet. *12*, e1005934.

Davidson, L.A., Marsden, M., Keller, R., and DeSimone, D.W. (2006). Integrin α5β1 and fibronectin regulate polarized cell protrusions required for Xenopus convergence and extension. Curr. Biol. *16*, 833–844.

Diz-Muñoz, A., Romanczuk, P., Yu, W., Bergert, M., Ivanovitch, K., Salbreux, G., Heisenberg, C.-P., and Paluch, E.K. (2016). Steering cell migration by alternating blebs and actin-rich protrusions. BMC Biol. *14*.

Dohn, M.R., Mundell, N.A., Sawyer, L.M., Dunlap, J.A., and Jessen, J.R. (2013). Planar cell polarity proteins differentially regulate extracellular matrix organization and assembly during zebrafish gastrulation. Dev. Biol. *383*, 39–51.

Faix, J., and Rottner, K. (2006). The making of filopodia. Curr. Opin. Cell Biol. *18*, 18–25.

Gao, B., Song, H., Bishop, K., Elliot, G., Garrett, L., English, M.A., Andre, P., Robinson, J., Sood, R., Minami, Y., et al. (2011). Wnt signaling gradients establish planar cell polarity by inducing Vangl2 phosphorylation through Ror2. Dev. Cell *20*, 163–176.

Gerhard Trapp, and Elias Horn (2010). Ibidi Chemotaxis and Migration Tool.

Goodrich, L.V., and Strutt, D. (2011). Principles of planar polarity in animal development. Development *138*, 1877–1892.

Goto, T., Davidson, L., Asashima, M., and Keller, R. (2005). Planar cell polarity genes regulate polarized extracellular matrix deposition during frog gastrulation. Curr. Biol. *15*, 787–793.

Gray, R.S., Roszko, I., and Solnica-Krezel, L. (2011). Planar cell polarity: Coordinating morphogenetic cell behaviors with embryonic polarity. Dev. Cell *21*, 120–133.

Gubb, D., and García-Bellido, A. (1982). A genetic analysis of the determination of cuticular polarity during development in Drosophila melanogaster. J. Embryol. Exp. Morphol. *68*, 37.

Hall, A. (2005). Rho GTPases and the control of cell behaviour. Biochem. Soc. Trans. *33*, 891.

He, L., and Wirtz, D. (2014). Switching from protease-independent to protease-dependent cancer cell invasion. Biophys. J. *107*, 2484–2485.

Heckman, C.A., and Plummer, H.K. (2013a). Filopodia as sensors. Cell. Signal. *25*, 2298–2311.

Iwasa, J.H., and Mullins, R.D. (2007). Spatial and temporal relationships between actin-filament nucleation, capping, and disassembly. Curr. Biol. *17*, 395–406.

Jacinto, A., and Wolpert, L. (2001). Filopodia. Curr. Biol. *11*, R634.

Jenny, A. (2003). Prickle and Strabismus form a functional complex to generate a correct axis during planar cell polarity signaling. EMBO J. *22*, 4409–4420.

Jessen, J.R., and Solnica-Krezel, L. (2005). Axis Formation— β-Catenin Catches a Wnt. Cell *120*, 736–737.

Jessen, J.R., and Solnica-Krezel, L. (2005). Morphogenetic cell movements shaping the zebrafish gastrula. In Advances in Developmental Biology, (Elsevier), pp. 131–165.

Jessen, T.N., and Jessen, J.R. (2017). VANGL2 interacts with integrin αv to regulate matrix metalloproteinase activity and cell adhesion to the extracellular matrix. Exp. Cell Res. *361*, 265–276.

Jessen, J.R., Topczewski, J., Bingham, S., Sepich, D.S., Marlow, F., Chandrasekhar, A., and Solnica-Krezel, L. (2002). Zebrafish trilobite identifies new roles for Strabismus in gastrulation and neuronal movements. Nat. Cell Biol.

Kane, D., and Adams, R. (2002). Life at the edge: Epiboly and involution in the zebrafish,, L. Solnica-Krezel, ed. (Berlin, Heidelberg: Springer Berlin Heidelberg), pp. 117–135.

Keller, R., Cooper, M.S., Danilchik, M., Tibbetts, P., and Wilson, P.A. (1989). Cell intercalation during notochord development in Xenopus laevis. J. Exp. Zool. *251*, 134–154.

Keller, R., Davidson, L., Edlund, A., Elul, T., Ezin, M., Shook, D., and Skoglund, P. (2000). Mechanisms of convergence and extension by cell intercalation. Philos. Trans. R. Soc. B Biol. Sci. *355*, 897–922.

Kimmel, C.B., Ballard, W.W., Kimmel, S.R., Ullmann, B., and Schilling, T.F. (1995). Stages of embryonic development of the zebrafish. Dev. Dyn. *203*, 253–310.

Latimer, A., and Jessen, J.R. (2010). Extracellular matrix assembly and organization during zebrafish gastrulation. Matrix Biol. *29*, 89–96.

Lawrence, P. (1966). Gradients in the insect segment: The orientation of hairs in the milkweed bug Oncopeltus fasciatus. J. Exp. Biol. 607–620.

Lee, M., and Vasioukhin, V. (2008). Cell polarity and cancer - cell and tissue polarity as a non-canonical tumor suppressor. J. Cell Sci. *121*, 1141–1150.

Lepage, S.E., and Bruce, A.E.E. (2010). Zebrafish epiboly: mechanics and mechanisms. Int. J. Dev. Biol. *54*, 1213–1228.

Mao, Y., and Schwarzbauer, J.E. (2005). Fibronectin fibrillogenesis, a cell-mediated matrix assembly process. Matrix Biol. J. Int. Soc. Matrix Biol. *24*, 389–399.

Marlow, F., Zwartkruis, F., Malicki, J., Neuhauss, S.C., Abbas, L., Weaver, M., Driever, W., and Solnica-Krezel, L. (1998). Functional interactions of genes mediating convergent extension, knypek and trilobite, during the partitioning of the eye primordium in zebrafish. Dev. Biol. *203*, 382–399.

Marsden, M., and DeSimone, D.W. (2001). Regulation of cell polarity, radial intercalation and epiboly in Xenopus: novel roles for integrin and fibronectin. Dev. Camb. Engl. *128*, 3635–3647.

Martinez-Rico, C., Pincet, F., Thiery, J.-P., and Dufour, S. (2010). Integrins stimulate E-cadherin-mediated intercellular adhesion by regulating Src-kinase activation and actomyosin contractility. J. Cell Sci. *123*, 712–722.

May-Simera, H. (2016). Evaluation of planar-cell-polarity phenotypes in ciliopathy mouse mutant cochlea. J. Vis. Exp.

May-Simera, H., and Chunqiao, L. (2013). Neuronal polarity and neurological disorders. J. Neurol. Transl. Neurosci.

Merte, J., Jensen, D., Wright, K., Sarsfield, S., Wang, Y., Schekman, R., and Ginty, D.D. (2010). Sec24b selectively sorts Vangl2 to regulate planar cell polarity during neural tube closure. Nat. Cell Biol. *12*, 41–46.

Montcouquiol, M. (2006). Asymmetric localization of Vangl2 and Fz3 indicate novel mechanisms for planar cell polarity in mammals. J. Neurosci. *26*, 5265–5275.

Myers, D.C., Sepich, D.S., and Solnica-Krezel, L. (2002). Convergence and extension in vertebrate gastrulae: cell movements according to or in search of identity. Trends Genet. *18*, 447–455.

Ohkawara, B. (2003). Role of glypican 4 in the regulation of convergent extension movements during gastrulation in Xenopus laevis. Development *130*, 2129–2138.

Olson, D.J., and Gibo, D.M. (1998). Antisensewnt-5a mimics wnt-1-mediated C57MG mammary epithelial cell transformation. Exp. Cell Res. *241*, 134–141.

Paluch, E.K., and Raz, E. (2013). The role and regulation of blebs in cell migration. Curr. Opin. Cell Biol. *25*, 582–590.

Parsons, M.J., Pollard, S.M., Saúde, L., Feldman, B., Coutinho, P., Hirst, E.M.A., and Stemple, D.L. (2002). Zebrafish mutants identify an essential role for laminins in notochord formation. Dev. Camb. Engl. *129*, 3137–3146.

Ponti, A. (2004). Two distinct actin networks drive the protrusion of migrating cells. Science *305*, 1782–1786.

Ridley, A.J. (2001). Rho GTPases and cell migration. J. Cell Sci. *114*, 2713–2722.

Ridley, A.J. (2006). Rho GTPases and actin dynamics in membrane protrusions and vesicle trafficking. Trends Cell Biol. *16*, 522–529.

Rørth, P. (2003). Communication by Touch. Cell *112*, 595–598.

Roszko, I., S. Sepich, D., Jessen, J.R., Chandrasekhar, A., and Solnica-Krezel, L. (2015). A dynamic intracellular distribution of Vangl2 accompanies cell polarization during zebrafish gastrulation. Development *142*, 2508–2520.

Schindelin, J., Arganda-Carreras, I., Frise, E., Kaynig, V., Longair, M., Pietzsch, T., Preibisch, S., Rueden, C., Saalfeld, S., Schmid, B., et al. (2012). Fiji: an open-source platform for biological-image analysis. Nat. Methods *9*, 676–682.

Schlessinger, K., Hall, A., and Tolwinski, N. (2009). Wnt signaling pathways meet Rho GTPases. Genes Dev. *23*, 265–277.

Sepich, D.S., Calmelet, C., Kiskowski, M., and Solnica-Krezel, L. (2005). Initiation of convergence and extension movements of lateral mesoderm during zebrafish gastrulation. Dev. Dyn. *234*, 279–292.

Settleman, J. (2001). Rac 'n Rho. Dev. Cell *1*, 321–331.

Shimaoka, M., Takagi, J., and Springer, T.A. (2002). Conformational regulation of integrin structure and function. Annu. Rev. Biophys. Biomol. Struct. *31*, 485–516.

Solnica-Krezel, L., and Driever, W. (1994). Microtubule arrays of the zebrafish yolk cell: organization and function during epiboly. Dev. Camb. Engl. *120*, 2443–2455.

Solnica-Krezel, L., and Sepich, D.S. (2012). Gastrulation: making and shaping germ layers. Annu. Rev. Cell Dev. Biol. *28*, 687–717.

Solnica-Krezel, L., Stemple, D.L., Mountcastle-Shah, E., Rangini, Z., Neuhauss, S.C., Malicki, J., Schier, A.F., Stainier, D.Y., Zwartkruis, F., Abdelilah, S., et al. (1996). Mutations affecting cell fates and cellular rearrangements during gastrulation in zebrafish. Dev. Camb. Engl. *123*, 67–80.

Strutt, H., and Strutt, D. (2002). Nonautonomous planar polarity patterning in Drosophila. Dev. Cell *3*, 851–863.

Strutt, D., Johnson, R., Cooper, K., and Bray, S. (2002). Asymmetric localization of Frizzled and the determination of Notch-dependent cell fate in the Drosophila eye. Curr. Biol. *12*, 813–824.

Svitkina, T.M., and Borisy, G.G. (1999). Arp2/3 complex and actin depolymerizing factor/cofilin in dendritic organization and treadmilling of actin filament array in lamellipodia. J. Cell Biol. *145*, 1009–1026.

Taylor, J., Abramova, N., Charlton, J., and Adler, P.N. (1998). Van Gogh: a new Drosophila tissue polarity gene. Genetics *150*, 199–210.

Theisen, H., Purcell, J., Bennett, M., Kansagara, D., Syed, A., and Marsh, J.L. (1994). dishevelled is required during wingless signaling to establish both cell polarity and cell identity. Dev. Camb. Engl. *120*, 347–360.

Topczewski, J., Sepich, D.S., Myers, D.C., Walker, C., Amores, A., Lele, Z., Hammerschmidt, M., Postlethwait, J., and Solnica-Krezel, L. (2001). The zebrafish Glypican Knypek controls cell polarity during gastrulation movements of convergent extension. Dev. Cell *1*, 251–264.

Trinkhaus, J.P. (1984). Mechanism of Fundulus epiboly - a current view. Integr. Comp. Biol.

Veeman, M.T., Slusarski, D.C., Kaykas, A., Louie, S.H., and Moon, R.T. (2003). Zebrafish Prickle, a modulator of noncanonical Wnt/Fz signaling, regulates gastrulation movements. Curr. Biol. *13*, 680–685.

Vinson, C.R., and Adler, P.N. (1987). Directional non-cell autonomy and the transmission of polarity information by the frizzled gene of Drosophila. Nature *329*, 549.

Wallingford, J.B., and Habas, R. (2005). The developmental biology of Dishevelled: an enigmatic protein governingcell fate and cell polarity. Development *132*, 4421–4436.

Wallingford, J.B., Fraser, S.E., and Harland, R.M. (2002). Convergent extension. Dev. Cell *2*, 695–706.

Warga, R.M., and Kimmel, C.B. (1990). Cell movements during epiboly and gastrulation in zebrafish. Dev. Camb. Engl. *108*, 569–580.

Warga, R.M., and Nüsslein-Volhard, C. (1999). Origin and development of the zebrafish endoderm. Dev. Camb. Engl. *126*, 827–838.

Wei, Q., Zhao, Y., Yang, Z.-Q., Dong, Q.-Z., Dong, X.-J., Han, Y., Zhao, C., and Wang, E.-H. (2008). Dishevelled family proteins are expressed in non-small cell lung cancer and function differentially on tumor progression. Lung Cancer *62*, 181–192.

Williams, B.B., Cantrell, V.A., Mundell, N.A., Bennett, A.C., Quick, R.E., and Jessen, J.R. (2012a). VANGL2 regulates membrane trafficking of MMP14 to control cell polarity and migration. J. Cell Sci. *125*, 2141–2147.

Williams, B.B., Mundell, N., Dunlap, J., and Jessen, J. (2012b). The planar cell polarity protein VANGL2 coordinates remodeling of the extracellular matrix. Commun. Integr. Biol. *5*, 325–328.

Winklbauer, R., and Keller, R.E. (1996). Fibronectin, mesoderm migration, and gastrulation in Xenopus. Dev. Biol. *177*, 413–426.

Wolff, T., and Rubin, G.M. (1998). Strabismus, a novel gene that regulates tissue polarity and cell fate decisions in Drosophila. Dev. Camb. Engl. *125*, 1149–1159.

Wu, G., Huang, X., Hua, Y., and Mu, D. (2011). Roles of planar cell polarity pathways in the development of neutral tube defects. J. Biomed. Sci. *18*, 66.

Xu, J., Maurer, L.M., Hoffmann, B.R., Annis, D.S., and Mosher, D.F. (2010). iso-DGR sequences do not mediate binding of fibronectin N-terminal modules to adherent fibronectin-null fibroblasts. J. Biol. Chem. *285*, 8563–8571.

Yang, Y., and Mlodzik, M. (2015). Wnt-Frizzled/planar cell polarity signaling: cellular orientation by facing the wind (Wnt). Annu. Rev. Cell Dev. Biol. *31*, 623–646.

Yin, C., Kiskowski, M., Pouille, P.-A., Farge, E., and Solnica-Krezel, L. (2008). Cooperation of polarized cell intercalations drives convergence and extension of presomitic mesoderm during zebrafish gastrulation. J. Cell Biol. *180*, 221–232.

Ying, J., Li, H., Chen, Y.-W., Srivastava, G., Gao, Z., and Tao, Q. (2007). WNT5A is epigenetically silenced in hematologic malignancies and inhibits leukemia cell growth as a tumor suppressor. Blood *110*, 4130–4131.

Ying, J., Li, H., Yu, J., Ng, K.M., Poon, F.F., Wong, S.C.C., Chan, A.T.C., Sung, J.J.Y., and Tao, Q. (2008). WNT5A exhibits tumor-suppressive activity through antagonizing the Wnt/ -Catenin signaling, and is frequently methylated in colorectal cancer. Clin. Cancer Res. *14*, 55–61.

Yu, J.S., Koujak, S., Nagase, S., Li, C.-M., Su, T., Wang, X., Keniry, M., Memeo, L., Rojtman, A., Mansukhani, M., et al. (2008). PCDH8, the human homolog of PAPC, is a candidate tumor suppressor of breast cancer. Oncogene *27*, 4657–4665.

Zamir, E., Katz, B.Z., Aota, S., Yamada, K.M., Geiger, B., and Kam, Z. (1999). Molecular diversity of cell-matrix adhesions. J. Cell Sci. *112 (Pt 11)*, 1655–1669.